8-2016

ANTHRAX MODELS INVOLVING IMMUNOLOGY, EPIDEMIOLOGY AND CONTROLS

Buddhi Raj Pantha
University of Tennessee, Knoxville, bpantha@vols.utk.edu

To the Graduate Council:

I am submitting herewith a dissertation written by Buddhi Raj Pantha entitled "ANTHRAX MODELS INVOLVING IMMUNOLOGY, EPIDEMIOLOGY AND CONTROLS." I have examined the final electronic copy of this dissertation for form and content and recommend that it be accepted in partial fulfillment of the requirements for the degree of Doctor of Philosophy, with a major in Mathematics.

Suzanne Lenhart, Major Professor

We have read this dissertation and recommend its acceptance:

Judy Day, Vasilios Alexiades, Shigetoshi Eda

Accepted for the Council:

Carolyn R. Hodges

Vice Provost and Dean of the Graduate School

(Original signatures are on file with official student records.)

ANTHRAX MODELS INVOLVING IMMUNOLOGY, EPIDEMIOLOGY AND CONTROLS

A Dissertation Presented for the

Doctor of Philosophy

Degree

The University of Tennessee, Knoxville

Buddhi Raj Pantha

August 2016

This dissertation is dedicated to my parents ***Krishna Prasad Pantha, Maiya Devi Pantha*** *and my dearest wife* ***Bibina Adhikari Pantha*** *for their continuous support and encouragement.*

Acknowledgments

It is my pleasure to thank the many people who made this dissertation possible. First of all, I want to express my deepest gratitude to my advisers, Dr. Suzanne Lenhart and Dr. Judy Day, for guiding me through this process. I greatly appreciate all their support, advice, encouragement, scientific counsel and enthusiasm. Involvement in outreach activities and participation in conferences and summer research assistantships were made possible due to their support. I would have not accomplished this dissertation without them.

I would like to thank the other members of my doctoral committee, Dr. Vasilios Alexiades and Dr. Shigetoshi Eda, for their time. Their comments, suggestions, feedback and critical review of my work are valuable to better my work. Special thanks to Dr. Tuoc Phan for his advice and support. Also, sincere thanks to my undergraduate adviser, Mr. Jaya Bishnu Pradhan, for his continuous encouragement for my graduate study

I would like to thank the Department of Mathematics at the University of Tennessee, Knoxville, for providing me financial support during my graduate study in the form of a teaching assistantship. I am also grateful to this department and the staff who made it so enjoyable. Many thanks to National Institute of Mathematical and Biological Synthesis (NIMBioS) for providing a research assistantship during my final year and for the wonderful opportunities to participate many conferences and

workshops as well as for mentoring undergraduate research projects.

I am grateful to all my friends in Knoxville and peers in Mathematics Department, in particular: Cody Lorton, Amanda Diegel, Ben Levy, Craig Collins and Eric Numfor. A special and profound gratitude to my parents and brother for continuous support and encouragement and more especially, to my wonderful wife, Bibina Adhikari for her ever-ready and unconditional love and support.

Abstract

This dissertation is divided in two parts. Chapters 2 and 3 consider the use of optimal control theory in anthrax epidemiological models. Models consisting of systems of ordinary differential equations (ODEs) and partial differential differential equations (PDEs) are considered to describe the dynamics of infection spread. Two controls, vaccination of animals and disposal of infected carcasses, are considered and their optimal management strategies are investigated. Chapter 4 involves modeling early host pathogen interaction in an inhalational anthrax infection which consists a system of ODEs that describes early dynamics of bacteria-phagocytic cell interaction associated to an inhalational anthrax infection.

First we consider an anthrax epizootic model with system of ODEs describing the disease dynamics between in an animal population. Stability analysis is performed for our system and basic reproduction number is calculated for our system. Two controls representing vaccination of animals and disposal of infected carcasses are investigated in order to minimize the number of infected animals, number of infected carcasses and the cost of vaccination and carcass disposal. Model parameters are estimated using outbreak data, and some numerical results for the optimal control problem are presented. We extend the model to a system of PDEs coupled with ODEs to include animal movement within a region. Both time and space dependent controls are applied into this hybrid system. Existence and uniqueness results are established for weak solutions of the system. The existence of an optimal control

pair is proven and the characterization of the controls are derived from corresponding adjoint systems. Numerical results are completed to illustrate various scenarios.

The immunological model in Chapter 4 consists of a system of ODEs that consists of the early host pathogen interaction within a lung. The modeling assumptions are derived from an experimental setting and the model parameters are estimated using these experimental data. Our goal is to understand the early processes such as the spore phagocytosis, spore germination, killing of the germinated spores and their replication. Different functional forms for germination and killing are considered and two different models based on bacterial stage are considered to better fit the experimental data.

Table of Contents

List of Tables

List of Figures

Chapter 1

Introduction

1.1 Anthrax

Anthrax is a fatal disease caused by a gram positive, spore forming and rod-shaped bacterium called *Bacillus anthracis* that can persist in soil for long periods of time [20, 49]. Animals, and in particular herbivore mammals, are susceptible to becoming infected by contacting spores in the environment. An infected host sheds vegetative bacteria into the environment and these bacteria form endospores, oval shaped dehydrated cells with thick outer wall and additional layers within the cell membrane that make these cells highly resistant to heat, drying, and many disinfectants [49]. This robustness has enabled anthrax to persist for centuries as a major global threat to livestock and wild animals. In fact, in much of Africa and Asia as well as parts of Europe and North and South America, anthrax is regarded as enzootic in non-humans with occasional outbreaks still occurring even in developed countries. The anthrax outbreak in August of 2012 in the Northwest Territories of Canada is the latest known fatal outbreak observed in wild animals in North America and killed more than half of the bison population [5, 48]. Similarly, about 400 livestock were lost to anthrax infection during the summer of 2005 in South Dakota, Texas, and Minnesota [28], and a heavy loss in the deer population was reported in Texas in 2001 [8].

Based on the portal of entry, *B. anthracis* spores can enter a body through one or more of the three known routes: cutaneous, gastrointestinal and inhalational [49]. Cutaneous anthrax occurs when anthrax spores contact a cut or any opening of the skin. It is the most common type of anthrax infection in animals and considered one of the least fatal. Left untreated, only about one-fifth of infected animals or humans die due to the disease, while almost all cutaneous infections can be saved with timely treatment [50, 20, 49]. The second form of anthrax is gastrointestinal anthrax. Usually, herbivore mammals acquire anthrax by ingestion of spores while grazing or browsing. Humans and other carnivore animals can then acquire infection by ingesting spores through contact with infected animal hides or hairs, meat and bone products. This type of anthrax is more fatal than the cutaneous form. However with proper treatment, more than half of those infected via the gastrointestinal route can be saved [49]. The third and the most fatal form is inhalational or pulmonary anthrax. This form is almost always fatal if left untreated and is typically difficult to treat since early detection is key to successful treatment. However, this is complicated by the fact that the symptoms mimic those of the flu and are often overlooked until it is too late. This deadly form of anthrax starts with the germination of the inhaled spores inside local lung phagocytes (immune cells) which transport their contents to nearby draining lymph nodes [49]. Recently, another route of anthrax infection has been identified in northern Europe with heroin-injecting drug users. Injected heroin laced with anthrax spores releases the spores quickly throughout the body and thus harder to diagnose and treat [23].

In humans, anthrax is primarily seen as the result of exposure to infected animals or animal products such as hides, hairs, bone and wool products. Agriculturally, this occurs following direct contact with anthrax-infected animals or through the handling of carcasses of deceased animals, presenting a risk to farmers, veterinarians, slaughterhouse workers, and butchers [46]. Usually, individuals who work in places such as wool mills, slaughterhouses, and tanneries may breathe in the spores when working with infected animals or animal products; however, deliberate release in cases

of biological warfare or terrorism can also lead to inhalational anthrax infection. The latest incident of deliberate release in the United States of America was in 2001 where letters containing anthrax spores were sent to different political and media personnel, endangering the lives of dozens of people [49].

When anthrax spores enter an individual or animal through any of the above routes, the spores are taken up by phagocytic immune cells such as macrophages, dendritic cells, microfold cells and neutrophills depending on the portal of entry [7, 12, 27, 49]. In the case of inhalational anthrax, alveolar macrophages as well as dendritic cells transport the phagocytosed spores to nearby lymph nodes. While on the way to the lymph nodes, some spores germinate inside the phagocytic cells but some may stay ungerminated for times estimated as long as 100 days [49]. Germinated spores are susceptible to macrophage killing because their protective layers begin to break down through the process, however some germinated spores may still manage to survive. These germinated spores become mature vegetative cells capable of replication and toxin production, which may cripple the body's immune response and lyse the host cell [11, 49]. The extracellular vegetative cells, may eventually enter the blood stream after proliferating extensively in the lymph nodes, release toxin which can lead to tissue damage, vascular collapse and hemorrhage, and finally death of the infected host [33, 49].

The uptake of *B. anthracis* spores from the environment is the major way wild animals contract anthrax, especially from sites where infected carcasses have been lying and also directly from infected animals. Since *B. anthracis* spores can remain in soil for a long time, grazing animals may eventually encounter these spores, making it is predominantly a disease of herbivores [17]. Also, anthrax spores have a high buoyant density and may be ingested while drinking from contaminated water sources [29, 49]. Although anthrax in animals via the pulmonary route is rare, animals in the wild sometimes can get exposed and inhale anthrax spores while grazing over very dry and dusty contaminated areas. For example, wind can blow spore contaminated dust from an infected carcass site into the air and to the surrounding areas. The effects

of this kind of transmission is not clear since only negligible number of spores have been detected downwind of anthrax sites [29, 49]. However, there is some evidence of inhalation of aerosolized spores causing an anthrax, as reported for outbreak among bison in the Northwest Territories of Canada [13]. In the contaminated areas, stamping and wallowing behavior of some animals can also create large dust clouds during hot and dry seasons increasing the risk of inhaling anthrax spores [29].

Animals who die of anthrax are one of the main sources of infection due to the large outgrowth of bacteria that occurs inside their body prior to the host succumbing to the infection. When an infected animal dies and if conditions are no longer favorable to bacterial growth, the bacteria transform into spores and remain dormant in the soil for a long time until a new host is found. Consequently, herbivores that graze on the site where another animal died of anthrax at some point in the past, are likely to ingest anthrax spores [49]. In addition, scavengers that feed on infected carcasses can carry the spores far distances as observed in Kruger National Park, South Africa [51].

Although anthrax cases in domesticated animals is declining in many parts of the world, it remains enzootic in many national parks and wild life reserves around the world and is one of the major reasons for species decline in many national parks and wildlife reserves [5, 49]. These areas then present a continuous risk to surrounding livestock herds as well as to the public. Since the spores can exist in the soil and can be found throughout the world, it is impossible to clear the environmental spores by disinfectants. Thus, any control measures should focus on limiting the environmental contamination as well as immunizing susceptible animals. Since infected carcasses are the main source of spores in the environment, the best ways to control and lower infection are good hygienic disposal practices when animals die regardless of cause, antibiotic treatments when cases do occur, and vaccination of animals in anthrax prone regions. Once the outbreak is observed in a region, close and continuous monitoring of animals, safe disposal of infected carcasses, and vaccinating the susceptible animals are some practices observed to be successful to reduce the

causalities among endangered animal species [49]. Burial, incineration and rendering of infected carcasses are recommended methods for carcass disposal [6, 38, 49, 52]. However, these measures in wildlife are complicated and fairly expensive [49]. One goal of this thesis is to optimize these intervention and mediation efforts, while minimizing cost by using a mathematical model and including control measures to investigate optimal control strategies. Another goal is to better understand the host's immune response to inhalational anthrax during the early stage of an infection.

The dissertation is divided into two parts. Part One consists of the development of epidemiological models for an anthrax outbreak in wild animals and the application of intervention strategies through an optimal control problem. The effectiveness of allocated intervention strategies in an outbreak region is studied. First, the time dependent case is considered through the development and analysis of a system of ordinary differential equations (ODEs) and then, the work is extended to include both time and spatial dependence through a model including partial differential equations (PDEs). This work is in collaboration with Dr. Suzanne Lenhart and Dr. Judy Day.

In Chapter 2, the ODE model for Part One is presented along with linear stability results of the model and the formulation of the basic reproduction number. Two controls representing vaccination in animals and disposal of carcasses are introduced. The optimality system for the model and the characterization of the optimal controls are derived as well. The model parameters are then estimated using available field data, and some simulation results are presented for various scenarios where control strategies are initiated at various time points. In Chapter 3, the model from Chapter 2 is extended to include the animal movement using a diffusion term. The existence and uniqueness of the system of partial differential equations are established, the optimality system is formulated and the existence and uniqueness results of the controls are proven. Some numerical simulations for one spatial dimension for several different scenarios are presented.

Part Two consists of modeling work to investigate early host-pathogen interaction in an inhalational infection. This work is in collaboration with Dr. Judy Day, Dr.

Suzanne Lenhart and Dr. Alan Cross. We developed a mathematical model using ODEs which include early host-pathogen interaction events: phagocytosis of spores by macrophages, germination of spores, and replication and killing of germinated spores. The modeling assumptions are kept as close to a given experimental protocol as possible. Two versions of the model are considered. One model version considers only one homogeneous population of bacteria and another considers bacteria in two distinct stages differed in replication mechanism to test which model version fits the experimental data better. For each model, different functional forms for spore germination and phagocyte killing are also used to acquire a better fit of the model output to the experimental data.

Chapter 2

Optimal Control Applied in an Anthrax Epizootic Model

2.1 Introduction

There are a few mathematical models that describe the disease dynamics in an anthrax outbreak in the animal world. Hahn and Fursniss [26] developed a system of ordinary differential equations (ODEs) based on the hypothesis that environmental spores are the main source of infection. Their model consists of three components: susceptible animals, environmental spores and infected carcasses. Analytical expressions for generation multiplication rate, which is similar to the basic reproduction number, was calculated. The paper also discussed the threshold of the disease, which is defined as the minimum number of susceptible population at the beginning, above which an epidemic will occur if a single infected is introduced into the susceptible population. The total size of the epidemic was also derived. The model output is compared with some weekly carcass data. Friedman and Yakubu [21] extended the Hahn and Fursniss model by considering spatio-temporal dependence that consists of both ODEs and partial differential equations (PDEs) and also added a separate compartment for infected animals. Their work studied the effect of transmission rates, carcass

feeding rates, and migration rates on the disease dynamics. The paper also derived the basic reproduction number for the two models they presented (ODEs only and coupled ODEs and PDEs). They studied the effect of parameter values such as carcass ingestion rates and the environmental contamination rates in the population of the endemic area. Both of these prior studies have a separate compartment for anthrax spores in the environment but estimating parameters related to the environmental spores such as their natural decay in the soil and their initial population in the environment is problematic because of the lack of the data. Moreover, neither of these studies explored optimal intervention strategies as an effort to control the disease [21, 22].

To add to this body of work, this study investigates the effects of intervention strategies to the disease outbreak in wild animals. We modified the mathematical model by Friedman and Yakubu [21] and due to the difficulties of measuring the anthrax spores lying in the environment and their temporal spread and decay, we chose not to include a separate compartment for the anthrax spores in the environment. Instead since anthrax spores in the environment are mainly found in the infected carcass sites, we assume that the number of these spores are proportional to the number of anthrax infected carcasses. Thus in our model, we assume that the infected carcass and infected animals are the main sources of infection. Our model consists of a system of ODEs to describe the dynamics of susceptible and infected animals and of infected carcasses. The disease free equilibrium and the condition for its stability are found. We then use anthrax outbreak data [6] to estimate model parameters for use in the numerical simulations. We formulate an optimal control problem where we apply two controls: vaccination of susceptible animals and disposal of infected carcasses. In this work, we consider model with temporal dependence as we do not have spatio-temporal data. Finally, we present simulation results for an outbreak with optimal controls started at various time of the outbreak.

2.2 Model Formulation and Stability Analysis

Consider an anthrax outbreak in a region where the sources of new infection are infected carcasses and infected animals. Assume that the dynamics of the population growth for the animals in the region follows logistic growth and that there is no recovery from the infection. Also, assume that live animals can feed on carcasses and that there is no immigration or emigration of animals in the region. Let $s(t)$ and $i(t)$ denote the number of susceptible and infected animals and let $c(t)$ denote the number of infected carcasses in the environment due to death from anthrax infection. Based on these assumptions, we formulate the system of ODEs given by equations $(2.1) - (2.3)$

$$\frac{ds}{dt} = rs(1 - \frac{s}{K}) - \theta_c sc - \theta_i si \tag{2.1}$$

$$\frac{di}{dt} = \theta_c sc + \theta_i si - \gamma i \tag{2.2}$$

$$\frac{dc}{dt} = \gamma i - \alpha(s + i)c - (p + u_2)c \tag{2.3}$$

with initial conditions,

$$s(0) = s^0, i(0) = i^0, c(0) = c^0.$$

where r denotes the intrinsic growth rate, K denotes the carrying capacity of the population, θ_c and θ_i denote the transmission rates from infected carcasses and infected animals respectively, and γ denotes the disease induced death rate. In addition, α denotes the rate at which carcasses are eaten by animals, p is the natural decay rate of carcasses and u_2 is the constant carcass removal rate. We assume that the parameter α is non-negative and all other parameters are positive.

The right hand side of the Equation (2.1) describes the rate of change of the susceptible animals due to logistic growth, disease transmission and vaccination. Equation (2.2) describes the rate of change of infected animals from new infections

and disease induced death. Equation (2.3) describes the rate of change of the infected carcasses due to death of infected animals, natural decay, animal feeding on carcasses, and carcass disposal.

2.2.1 The Disease Free Equilibrium and the Basic Reproduction Number

The disease free equilibrium (DFE) of system $(2.1) - (2.3)$ with constant carcass removal rate, u_2, is $(K, 0, 0)$, where K is the carrying capacity of the population. The severity of a disease can be measured by the basic reproductive number, $\mathcal{R}_0$, which is defined as the average number of secondary infections caused by a single infected individual in a completely susceptible population. We use the next generation matrix approach [14] to find $\mathcal{R}_0$.

We begin with those equations of system $(2.1) - (2.3)$ that describe the production of new infections. This subsystem is called infected subsystem. Then, we separate the parts of the subsystem that describe new infectious, denoted by matrix $\mathcal{F}$, and those that involve transfer of the animals, denoted by matrix $\mathcal{V}$ respectively. For our compartmental model, the infected subsystem can then be written in the matrix form as

$$\begin{pmatrix} i' \\ c' \end{pmatrix} = \mathcal{F} - \mathcal{V}$$

where the matrices $\mathcal{F}$ and $\mathcal{V}$ are given by

$$\mathcal{F} = \begin{pmatrix} \theta_c sc + \theta_i si \\ 0 \end{pmatrix}$$

and

$$\mathcal{V} = \begin{pmatrix} \gamma i \\ \alpha(s+i)c + (p+u_2)c - \gamma i \end{pmatrix}.$$

The corresponding Jacobian matrices of $\mathcal{F}$ and $\mathcal{V}$ evaluated at the DFE $x_0 = (K, 0, 0)$ are

$$F = \begin{pmatrix} \theta_i K & \theta_c K \\ 0 & 0 \end{pmatrix}$$

and

$$V = \begin{pmatrix} \gamma & 0 \\ -\gamma & \alpha K + p + u_2 \end{pmatrix}.$$

Consequently, the the next generation matrix is

$$\begin{aligned} \mathcal{K} =& FV^{-1} \\ =& \frac{1}{\gamma(\alpha K + p + u_2)} \begin{pmatrix} \theta_i K & \theta_c K \\ 0 & 0 \end{pmatrix} \begin{pmatrix} p + u_2 + \alpha K & 0 \\ \gamma & \gamma \end{pmatrix} \\ =& \frac{1}{\gamma(\alpha K + p + u_2)} \begin{pmatrix} \theta_i K(p + u_2 + \alpha K) + \theta_c K\gamma & \theta_c K\gamma \\ 0 & 0 \end{pmatrix}. \end{aligned}$$

The matrix $\mathcal{K}$ is an upper triangular matrix with zero determinant and the dominant eigenvalue of $\mathcal{K}$ is

$$\mathcal{R}_0 = \rho(FV^{-1}) = \frac{\theta_i K}{\gamma} + \frac{\theta_c K}{\alpha K + p + u_2}.$$

The first term of $\mathcal{R}_0$ represents the number of new infections produced by an animal in the infected compartment and the second term represents the number of new infections produced by a carcass.

Hence, using Theorem 2 from Van den Driessche and Watmough [14], the DFE is locally asymptotically stable if $\mathcal{R}_0 < 1$ and unstable when $\mathcal{R}_0 > 1$.

2.3 The Optimal Control Problem

As mentioned in the introduction, vaccination of animals and disposal of infected carcasses are the only feasible ways to prevent further anthrax transmission. Vaccinating animals prevents susceptibility to the disease and disposing infected carcasses reduces contact of susceptible animals with spores between spores and susceptible animals. To include vaccination and carcass disposal as two controls, we extend model $(2.1) - (2.3)$. Vaccinated animals are moved to a separate compartment denoted by $v(t)$. The constant carcass disposal rate is now assumed to be time dependent $u_2(t)$ together with the time dependent vaccination rate $u_1(t)$. The extended model is given by $(2.4) - (2.7)$

$$\frac{ds}{dt} = rn(1 - \frac{n}{K}) - \theta_c sc - \theta_i si - u_1(t)s \tag{2.4}$$

$$\frac{di}{dt} = \theta_c sc + \theta_i si - \gamma i \tag{2.5}$$

$$\frac{dv}{dt} = u_1(t)s \tag{2.6}$$

$$\frac{dc}{dt} = \gamma i - \alpha(s + i + v)c - (p + u_2(t))c \tag{2.7}$$

$$n = s + v$$

with initial conditions,

$$s(0) = s^0, i(0) = i^0, v(0) = 0, c(0) = c^0.$$

To make biological sense,we assume $s^0, i^0 > 0 \ \ and \ \ c^0 \geq 0$.

A successful control strategy is one that reduces anthrax related deaths and the number of infected carcasses, while minimizing the costs associated with these efforts. Thus, our goal is to find a pair of controls (u_1^*, u_2^*) that minimize the number of infected

animals and the number of infected carcasses, the cost of vaccination and the cost of carcass disposal. Our objective functional is therefore formulated as Equation (2.8):

$$J(u_1, u_2) = \int_0^T \big[A_1 i(t) + A_2 c(t) + B_1 u_1(t)\big(s(t) + i(t)\big) + B_2 u_2(t) c(t) + C_1 u_1(t)^2 + C_2 u_2(t)^2\big] dt \tag{2.8}$$

subject to the constraints of the ODEs $(2.4) - (2.7)$ and where $A_1, A_2, B_1, B_2, C_1, C_2$ are balancing coefficients (positive) transferring the integrals into monetary quantity over a finite period of T days. The first two terms of (2.8) with coefficients A_1 and A_2 represent the cost (due to the loss of animals) associated with the numbers of anthrax infected animals and carcasses respectively. The terms with coefficients B_1 and B_2 represent the cost associated with the number of animals vaccinated and the number of carcasses removed respectively. The objective functional in (2.8) also includes quadratic terms with coefficients C_1 and C_2 to indicate potential non-linearities in the costs. Note that the vaccination is applied to both susceptible and infected animals, although there is no effect of vaccination on infected animals. We do this since in the wild, vaccination programs vaccinate all animals that are found and can not distinguish whether they are infected or not. We seek the pair $(u_1^*, u_2^*) \in \mathcal{U}$ such that

$$J(u_1^*, u_2^*) = \inf_{(u_1, u_2) \in \mathcal{U}} J(u_1, u_2)$$

for the admissible set $\mathcal{U} = \{(u_1, u_2) \in \big(L^\infty(0, T)\big)^2 : 0 \leq u_i \leq q_i; q_i \in \mathbb{R}^+, i = 1, 2\}$.

The following theorem states the existence of the solution of the system $(2.4) - (2.7)$ as well as their non negativity and boundedness.

Theorem 2.1. *Given $u = (u_1, u_2) \in \mathcal{U}$, there exists a non-negative bounded solution (s, i, v, c) to the state system $(2.4) - (2.7)$ on the finite interval $[0, T]$ with given initial conditions.*

The existence and uniqueness of solutions for the state system $(2.4)-(2.7)$ with a given control pair can be proven by using a result from Lukes [36]. The structure of system $(2.4)-(2.7)$ gives the non-negativity and boundedness of the state solutions.

The following theorem proves the existence of the optimal controls.

Theorem 2.2. *There exists an optimal control pair* $(u_1^*, u_2^*) \in \mathcal{U}$ *with corresponding states* (s^*, i^*, v^*, c^*) *that minimizes the objective functional* $J(u_1, u_2)$.

Proof: Since the controls and the state variables are uniformly bounded and non-negative on the finite interval $[0, T]$, there exists a minimizing sequence (u_1^n, u_2^n) such that

$$\lim_{n\to\infty} J(u_1^n, u_2^n) = \inf_{(u_1,u_2)\in\mathcal{U}} J(u_1, u_2).$$

We denote the corresponding sequence of state variables by (s_n, i_n, v_n, c_n). Since all state and control variables are bounded, then all the derivatives of the state variables are also bounded. This implies that all state variables are Lipschitz continuous with the same Lipschitz constant. Thus the sequence (s_n, i_n, v_n, c_n) is uniformly equicontinuous in $[0, T]$. Thus by the Arzela-Ascoli Theorem [36], the state sequence has a subsequence that converges uniformly to (s^*, i^*, v^*, c^*) in $[0, T]$.
The control sequence $u^n = (u_1^n, u_2^n)$ has a subsequence that converges weakly in $L^2(0, T)$. Let $(u_1^*, u_2^*) \in \mathcal{U}$ be such that $u_i^n \rightharpoonup u_i^*$ weakly in $L^2(0, T)$ for $i = 1, 2$.
Using lower semi-continuity of norms in weak L^2, we get

$$||u_i^*||_{L^2}^2 \leq \lim_{n\to\infty} \inf ||u_i^n||_{L^2}^2 \text{for } i = 1, 2.$$

Hence,

$$\begin{aligned} J(u_1^*, u_2^*) \leq & \underline{\lim}_{n\to\infty} \int_0^T \big[A_1 i^n(t) + A_2 c^n(t) + \{B_1 u_1^n\big(s^n(t) + i^n(t)\big) + B_2 u_2^n c^n(t) \\ & + C_1 u_1^n(t)^2 + C_2 u_2^n(t)^2\}\big] dt \\ = & \underline{\lim}_{n\to\infty} J(u_1^n, u_2^n) \end{aligned}$$

Thus we conclude that there exists a pair of controls (u_1^*, u_2^*) that minimizes the objective functional $J(u_1, u_2)$. ■

Next we characterize an optimal control pair. Pontryagin's Maximum Principle [41] introduces adjoint functions that allow the state system (2.4) – (2.7) to be attached to the objective functional (2.8).

Theorem 2.3. *Given an optimal control $u = (u_1, u_2) \in \mathcal{U}$ and corresponding state solutions s, i, v and c there exist adjoint functions $\lambda_i(t)$, $i = 1, 2, 3, 4$ satisfying*

$$\begin{aligned}
\lambda_1' =& - B_1 u_1 - \lambda_1[r - \frac{2r}{K}(s+v) - \theta_c c - \theta_i i - u_1] \qquad (2.9)\\
& - \lambda_2(\theta_c c + \theta_i i) - \lambda_3 u_1 + \lambda_4 \alpha c \\
\lambda_2' =& - A_1 - B_1 u_1 + \lambda_1 \theta_i s - \lambda_2(\theta_i s - \gamma) - \lambda_4(\gamma - \alpha c) \qquad (2.10)\\
\lambda_3' =& - \lambda_1(r - \frac{2r}{K}(s+v)) + \lambda_4 \alpha c \qquad (2.11)\\
\lambda_4' =& - A_2 - B_2 u_2 + \lambda_1 \theta_c s - \lambda_2 \theta_c s - \lambda_4[-\alpha(s+i+v) - (p+u_2)] \qquad (2.12)
\end{aligned}$$

with transversality condition $\lambda_i(T) = 0$ for $i = 1, 2, 3, 4$.

Furthermore, these optimal controls are characterized by

$$u_1 = \min\left(q_1, \max(\frac{(\lambda_1 - \lambda_3)s - B_1(s+i)}{2C_1}, 0)\right) \qquad (2.13)$$

$$u_2 = \min\left(q_2, \max(\frac{(\lambda_4 - B_2)c}{2C_2}, 0)\right) \qquad (2.14)$$

Proof: To use Pontryagin's Maximum Principle [41], we form the Hamiltonian

$$\begin{aligned}
H =& A_1 i + A_2 c + \{B_1 u_1\big(s+i\big) + B_2 u_2 c + C_1 u_1^2 \\
& + C_2 u_2^2\} + \lambda_1[r(s+v)(1 - \frac{(s+v)}{K}) - \theta_c sc - \theta_i si - u_1 s] \\
& + \lambda_2[\theta_c sc + \theta_i si - \gamma i] + \lambda_3[u_1 s] + \lambda_4[\gamma i - \alpha(s+i+v)c - (p+u_2)c].
\end{aligned}$$

The adjoint equations are found by

$$\lambda_1' = -\frac{\partial H}{\partial s} = -B_1 u_1 - \lambda_1[r - \frac{2r}{K}(s+v) - \theta_c c - \theta_i i - u_1] - \lambda_2(\theta_c c + \theta_i i) - \lambda_3 u_1 + \lambda_4 \alpha c$$
$$\lambda_2' = -\frac{\partial H}{\partial i} = -A_1 - B_1 u_1 + \lambda_1 \theta_i s - \lambda_2(\theta_i s - \gamma) - \lambda_4(\gamma - \alpha c)$$
$$\lambda_3' = -\frac{\partial H}{\partial v} = -\lambda_1(r - \frac{2r}{K}(s+v)) + \lambda_4 \alpha c$$
$$\lambda_4' = -\frac{\partial H}{\partial c} = -A_2 - B_2 u_2 + \lambda_1 \theta_c s - \lambda_2 \theta_c s - \lambda_4[-\alpha(s+i+v) - (p+u_2)].$$

with transversality condition $\lambda_i(T) = 0$ for $i = 1, 2, 3, 4$.

Now, we minimize the Hamiltonian with respect to the controls. Note that we have the required convexity for minimization,

$$\frac{\partial^2 H}{\partial u_1^2} = 2C_1 > 0$$

and

$$\frac{\partial^2 H}{\partial u_2^2} = 2C_2 > 0.$$

On the interior of the control set, we have

$$\frac{\partial H}{\partial u_1} = 0 \implies u_1 = \frac{(\lambda_1 - \lambda_3)s - B_1(s+i)}{2C_1}$$
$$\frac{\partial H}{\partial u_2} = 0 \implies u_2 = \frac{(\lambda_4 - B_2)c}{2C_2}.$$

Using the standard arguments and the bounds for the controls, we obtain the characterization of this optimal pair (2.13) – (2.14).■

The optimality system consists of the state system (2.4)–(2.7), the adjoint system (2.9)–(2.11) and the characterization of the control (2.13) – (2.14). The following theorem states the uniqueness of the optimal controls for small values of T. For the standard technique to prove such a result, see [19].

Theorem 2.4. *For sufficiently small T, the solution of the optimality system is unique, which gives uniqueness of the optimal controls.*

2.4 Estimation of Parameter Values

To estimate some of the model parameters, anthrax outbreak data by Clegg et al. [6] was one of the data sets used. The data were collected in Malilangwe Wildlife Reserve in Zimbabwe, where anthrax related deaths were recorded for 86 days beginning from August 12 to November 4, 2004. Carcass disposal efforts were started one week after the first carcass was found due the time required to collect and analyze the diagnostic samples to confirm anthrax as the cause of death and deploy the disposal team [6]. Almost 20 animal species were affected in the outbreak but five of them: kudu, nyala, waterbuck, bushbuck and roan antelope, were badly affected. These five species made up about 80% of the total deaths recorded. In our numerical simulations, we used data from these species only. The total number of animals from these five species was estimated to be 902 with 709 of those dying due to the disease. Figure 2.1 shows the data representing the number of animal carcasses collected and disposed of each day between August 12 to November 4. To estimate the

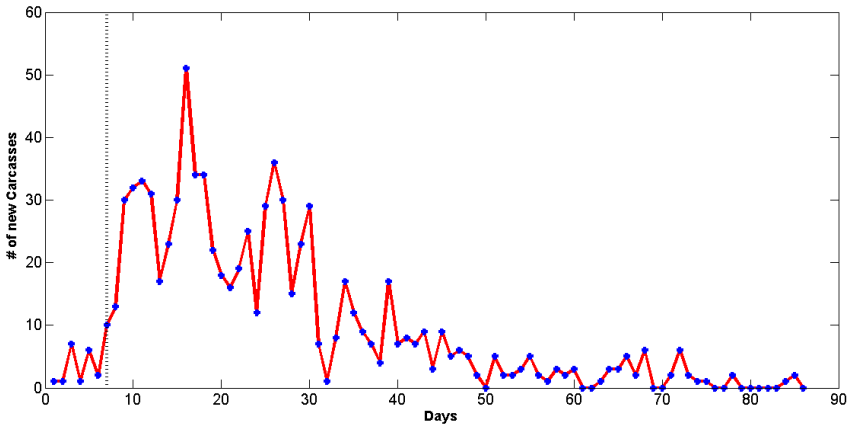

Figure 2.1: Number of anthrax related deaths each day in Malilangwe Wildlife Reserve, Zimbabwe between August 12 and November 4, 2004. The vertical dotted line is the time when carcass disposal efforts were first started.

carcass decay rate, p, we use experimental data by Bellan et al. [3] where soil samples from an infected carcass site were collected at $1, 4, 7, 30, 180$ and 365 days and the number of spores per gram of soil were counted. For instance, the average number of spores per gram of soil in the first day was 15 thus giving $a(0) = 15$ where $a(t)$ represents the environmental spores at time t. While taking soil samples, four different regions of the carcass site were chosen: hemorrhagic blood-stained soil, non-hemorrhagic fluid-stained soil and unstained

soil in a 1 and 3 meters radius from the center of the carcass site. We use an average number of spores per gram of soil from all of these four soil types in our estimation. To estimate p, we formulate a separate system of ODEs $(2.15) - (2.16)$ which describes the rate of change of spores and the carcasses.

$$\frac{da}{dt} = -\lambda a + \beta c \tag{2.15}$$

$$\frac{dc}{dt} = -pc \tag{2.16}$$

with the initial conditions $a(0) = 15$ per gram of soil and $c(0) = 1$; where c is the fraction of the carcass, λ is the natural decay rate of spores per gram of soil per day, β is the spore gain per gram of soil per carcass per day, and p is the decay rate of the carcass per day.

From the above system of ODEs and the data from Bellan et al. [3], we estimate the best fit values of λ, β and p by minimizing the sum of squared errors. From MATLAB's *global optimization toolbox* [31], we implement the *multistart* algorithm, which uses uniformly distributed starting points around which a local solver, $fmincon$, is used in order to better achieve a global minimum. Using this, we estimated the carcass decay rate to be $p = 0.2816$. We incorporate this estimate for p into the full model $(2.4) - (2.7)$ and then estimate the remaining model parameters using Clegg et al. [6] and several other literature as described below.

The parameters r and γ in the model $(2.4)-(2.7)$ are estimated from published literature. The growth rate, r, is estimated as the average growth rates of all five animal species obtained from the literature [39, 40, 45, 1, 52]. Since the average time to death for an anthrax infected animal is about 7.5 days [49], we used the disease induced death rate γ as $\frac{1}{7.5}$ per day. The total number of animals in the wildlife reserve was given as 902 (i.e. $s(0) + i(0) = 902$) and thus we assumed their carrying capacity slightly more then twice of their starting population: $K = 2000$. Also, since all five animal species are herbivores, we assume the carcass feeding rate, α, to be zero. We assume an animal that grazes near or at the carcass sites can come in contact with anthrax spores and therefore has a chance to become infected [49, 52]. From the data [6], the number of carcasses found on the first day is 1, giving $c(0) = 1$, is an initial condition for the carcass equation given by (2.7) . We assume that all 709 carcasses were disposed of during the outbreak. Since the outbreak

lasted for 86 days and the disposal started a week after the first carcass was found, we chose a carcass disposal rate of $u_2 = 0.09$, which would result in a disposal of all 709 carcasses in 79 days without the carcass decay and their feeding from other animals.

Assuming no vaccination ($u_1 = 0$) and a constant carcass disposal rate ($u_2 = 0.09/day$), we find the best fit values for the disease transmission rates θ_c and θ_i from carcass and infected animals, respectively. Also, we estimate the initial number of infected animals I_0. Since the data in [6] represent the rate of change of carcasses, we fit this data to the quantity γI (see Figure 2.2c in Section 2.5), which represents the rate at which the infected animals died due to the disease. While estimating the parameter values of ODE system, the initial conditions used were

$$s(0) = 902 - i_0, i(0) = i_0, c(0) = 1.$$

Table 2.1 shows the estimated values of θ_c, θ_i, and $I(0)$ as well as other parameter values we discussed above together with their corresponding references. With these parameter values, the basic reproduction number is $R_0 \approx 5.67$, which implies that the disease free equilibrium solution $(s^*, i^*, c^*) = (2000, 0, 0)$ is unstable.

Table 2.1: The model parameters, their description, values, units and corresponding references.

Parm.	Description	Values	Units	Ref.
r	Growth rate of animals	3.93×10^{-4}	day^{-1}	[39, 40, 45, 1, 52]
γ	Disease induced death rate of animals rate	$\frac{1}{7.5}$	day^{-1}	[49]
α	Carcass feeding rate	0	$\text{animal}^{-1}\ \text{day}^{-1}$	[6]
K	Carrying capacity	2000	animal	[6]
p	Carcass decay rate	0.2816	day^{-1}	[3]
θ_c	Transmission rate from carcasses	3.47×10^{-5}	$\text{carcass}^{-1}\ \text{day}^{-1}$	[6]
θ_i	Transmission rate from infected animals	3.76×10^{-4}	$\text{animal}^{-1}\ \text{day}^{-1}$	[6]
u_2	Constant carcass disposal rate	0.09	day^{-1}	[6]
$I(0)$	Initial number of inf. animals	39	animals	[6]

2.5 Numerical Simulations

Using the parameter values from Table 1, we find the simulation results under the five different strategies described in Table 2. Note that for Strategies $1-3$, $\tau = 8$ meaning the first 7 days are simulated without any controls ($u_1 = 0, u_2 = 0$ per day) and for the remaining 79 days the carcass disposal (constant or optimal) is considered. For strategies 4 and 5, the simulations include time varying optimal carcass disposal and optimal vaccination rates after 4 days ($\tau = 5$) and 14 days ($\tau = 15$) respectively. For all simulations, we take

$$s(0) = 863, i(0) = 39, v(0) = 0 \text{ and } c(0) = 1.$$

For each strategy, we find the total number of new infections

$$\int_0^{86} (\theta_c sc + \theta_i si)dt,$$

and the total cost associated to infected animals, infected carcasses and the controls, J, which is given by (2.8). One or more controls are initiated τ days after the first carcass was discovered. We present the values of total number of new infections and J for all strategies explored in Table 2.2.

Table 2.2: Control strategies and their descriptions where τ is the day at which one or more controls are initiated after the first carcass was recovered.

Strategy	Description
1	No vaccination and constant carcass disposal rate started after one week ($\tau = 8$ days)
2	No vaccination and optimal carcass disposal rate started after one week ($\tau = 8$ days)
3	Optimal vaccination rate and optimal carcass disposal rate started after one week ($\tau = 8$ days)
4	Optimal vaccination rate and optimal carcass disposal rate started after 4 days ($\tau = 5$ days)
5	Optimal vaccination rate and optimal carcass disposal rate started after two weeks ($\tau = 15$ days)

Figure 2.2 shows the simulation results under Strategy 1 with $u_1 = 0$ and $u_2 = 0.09$ per day. The rate of change of new carcasses per day (γI) and its corresponding data set [6] are plotted in Figure (2c). We see that under Strategy 1, our model closely matches the Zimbabwe outbreak data [6].

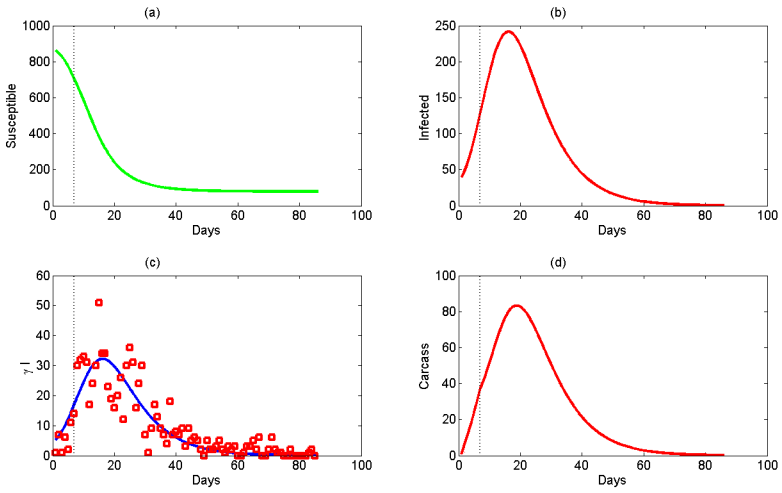

Figure 2.2: Simulation results for Strategy 1: no vaccination and constant carcass removal rate initiated after one week of the first carcass was discovered. The solid line in (a) and (b) represent the number of susceptible and infected animals. In (c), the squares denote the data representing the number of carcasses collected daily and the solid line is the model approximation. The model approximation for the number of carcasses in the environment is plotted in (d). The vertical dotted line present in all figures denotes the time, τ, when carcass disposal was first started ($\tau = 8$ days).

From Figure 2.2, we see that under Strategy 1, most of the animals get infected in the first month of the outbreak. This is reasonable since there were more than 100 infected animals and more than 30 infected carcasses before the carcass disposal formally started (one week after the discovery of the first anthrax related death). The size of the basic reproduction number R_0 may illustrate why the outbreak in the Malilangwe Wildlife Reserve, Zimbabwe, turned into an epidemic although constant carcass disposal was applied. Also, the total number of new infections over 86 days is 760 and the total cost is $J = 37164$ (see Table 2.3).

Next, we determine what optimal control strategies will acheive the objective given in Equation (2.8). To choose the cost coefficients in the objective functional (2.8), we give more weight on the cost associated with infected animals than the cost associated with infected carcasses: $A_1 > A_2$. Also, in the wild, vaccinating animals is very expensive and difficult, as they are hard to catch. Thus, we assume that the vaccination cost is higher than the cost of carcass disposal: $B_1 > B_2$. We take

$$A_1 = 5, A_2 = 3, B_1 = 3, B_2 = 1, C_1 = 1 \text{ and } C_2 = 1.$$

First, we test how well does an optimal carcass disposal rate (Strategy 2) help to reduce the number of infected animals, infected carcasses and the cost of applying these controls. In Figure 2.3, we will show the simulation results for Strategy 2: no vaccination and a time-varying optimal carcass disposal rate. We then compare Strategy 2 with Strategy 1 to determine which is best in terms of the total number of new infections over 86 days and the associated cost J. We solve the optimality system using a forward-backward sweep iterative method with a Runge-Kutta four scheme with $u_1 = 0$. To apply the optimal carcass disposal rate, we set the bounds for u_2 as,

$$0 \leq u_2(t) \leq \ 0.5.$$

The upper bound for the carcass disposal rate, $u_2(t)$, is chosen to allow more carcasses to be disposed per day than the constant carcass disposal rate discussed earlier. Starting with initial guesses for the controls and given initial values for state variables, the state equations $(2.4) - (2.7)$ are solved forward in time. Then, the state values and controls are used to solve the adjoint equations $(2.9) - (2.12)$ backward in time, and the iterations continue until convergence is reached [19]. See Hackbusch [25] and Lenhart and Workman [35] for such iterative algorithms. The initial values for the state variables are $s(0) = 863, i(0) = 39$ and $c(0) = 1$. Figure 2.3 shows the simulation results for implementing Strategy 2.

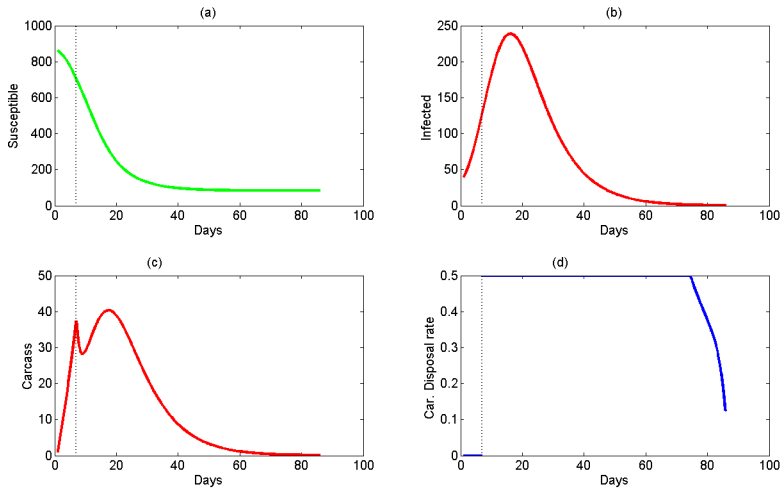

Figure 2.3: Simulation results for Strategy 2: no vaccination and optimal carcass disposal rate initiated after one week since the first carcass was discovered. The solid lines in (a), (b), and (c) represent time courses of the number of susceptible and infected animals and the number of carcasses, respectively. The time-varying optimal carcass disposal rate is plotted in (d). The vertical dotted line present in all figures denotes the time, τ, when carcass disposal was first started ($\tau = 8$ days).

From Figure 2.3, we see that the initial delay in the disease diagnosis causes steady increase in the number of carcasses as well as the number of infected animals. The application of optimal carcass disposal is able to decrease the level of carcasses for a time but due to the high infectivity and the high disease related death, the carcass count begins to rise again before further decrease. Comparing Strategies 1 and 2, in Table 2.3 we see that Strategy 2 saves about 5 more animals from becoming infected than in Strategy 1. Also seen in Table 2.3 is that the total cost J is reduced only by 10% in Strategy 2 than in Strategy 1. In the Strategy 2, we also observe the carcass disposal rate is applied to its maximum capacity nearly until the end. Thus, to lower the number of infected animals, it is evident that carcass disposal alone is not sufficient and that another control method is needed.

Strategy 3 considers two time-varying optimal controls: vaccination and carcass disposal both initiated one week after the first carcass is found. We choose the respective bounds on these controls as

$$0 \leq u_1 \leq 0.1, \text{ and } 0 \leq u_2 \leq 0.5 \tag{2.17}$$

where these same bounds are also used in the optimal control simulations for Strategies 3 - 5. The upper bound for the vaccination rate is chosen to allow approximately 95% of the susceptible animals to be vaccinated in a month if the maximum vaccination rate is applied. The upper bound of the carcass disposal rate is kept at 0.5 per day as in Strategy 2. Figure 2.4 shows the simulation results for Strategy 3. From Table 2.3 we see that under Strategy 3, about 50% less animals get infected compared to Strategy 1. Also, the total cost J is brought down by 46% under Strategy 3 than in Strategy 1(see Table 2.3 for details). From Figure, we see that the vaccination efforts can essentially be ceased after $\sim$ 1 month. Carcass disposal efforts should be continued until the end of the outbreak but can begin to be tapered off after $\sim$ 2 months.

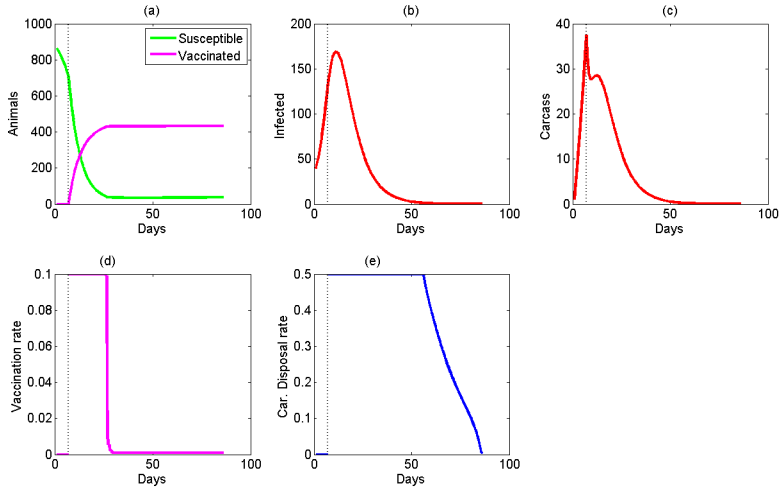

Figure 2.4: Simulation results for Strategy 3: optimal vaccination and optimal carcass disposal rates initiated after one week since the first carcass was discovered. The solid lines in (a) represent the number of susceptible and vaccinated animals, the solid lines in (b) and (c) represent the number of infected animals and the number of carcasses, respectively. The time-varying optimal rates for vaccination and carcass disposal are plotted in (d) and (e), respectively. The vertical dotted line present in all figures denotes the time, τ, when carcass disposal was first started ($\tau = 8$ days).

The next Strategies explored are similar to the Strategy 3 but with different values of τ, the day on which one or more controls are initiated after the first carcass was discovered. Since anthrax infected animals can live about a week after becoming sick

[49], and the disease cannot be diagnosed without a laboratory test, many animals can get infected before the actual control programs are in action as observed in the Malilangwe Wildlife Reserve, Zimbabwe [6]. In general, diseases in the wild may go unnoticed unless several animals die within a short period of time. In the following simulations, we explore whether the starting of optimal vaccination and optimal carcass disposal on 4^{th} day (Strategy 4) or on 14^{th} day (Strategy 5) of the first carcass observed give different results in terms of the number of new infections and the associated costs. Figures 2.5 and 2.6 show the simulation results for Strategies 4 and 5, respectively.

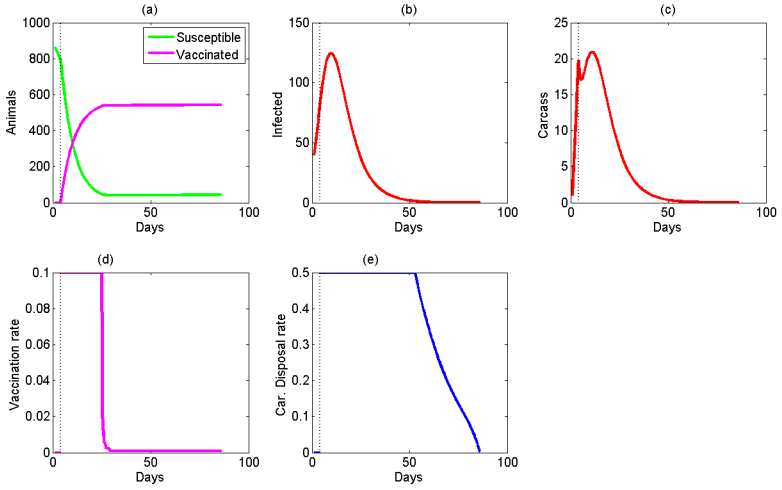

Figure 2.5: Simulation results for Strategy 4: optimal vaccination and optimal carcass disposal rate initiated after 4 days of the first carcass was discovered. The solid lines in (a) represent the number of Susceptible and vaccinated animals, the solid lines in(b) and (c) represent the number of infected animals and number of carcasses respectively. The time varying optimal vaccination and optimal carcass disposal rates are plotted in (d) and (e) respectively. The vertical dotted line present in all figures denotes the time, τ, when carcass disposal was first started ($\tau = 4$ days).

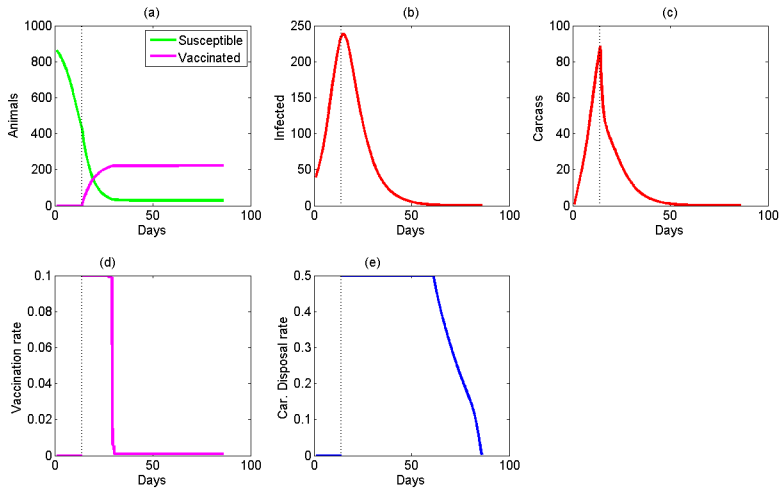

Figure 2.6: Simulation results for Strategy 5: optimal vaccination and optimal carcass disposal rates initiated after two weeks since the first carcass was discovered. The solid lines in (a) represent the number of susceptible and vaccinated animals, the solid lines in (b) and (c) represent the number of infected animals and number of carcasses, respectively. The time-varying optimal rates for vaccination and carcass disposal are plotted in (d) and (e), respectively. The vertical dotted line present in all figures denotes the time, τ, when carcass disposal was first started ($\tau = 14$ days).

From these simulation results, we see that under the Strategy 4, approximately 65% fewer animals get infected than in Strategy 1 while this percentage decreased just by 32% under strategy 5. Also, the total cost compared to Strategy 1 is lowered by 59% and 22%, respectively under Strategy 4 and 5 (see Table 3 for details). This suggests that earliest application of time-varying optimal controls can save more animals from acquiring anthrax infection following an outbreak. Note that in all simulation results, the total number of new infections excludes the initial number of infected animals $i(0) = 39$.

Table 2.3: The total number of new infections animals over 86 days with anthrax and the total cost J with respect to different control strategies. τ represents the day on which one or more controls are initiated.

Strategy	Description	Total # of new infections	J
1	$u_1 = 0,\ u_2 = 0.09, \tau = 8$	760	37164
2	$u_1 = 0, u_2(t), \tau = 8$	755	34013
3	$u_1(t), u_2(t), \tau = 8$	379	20217
4	$u_1(t), u_2(t), \tau = 5$	269	15595
5	$u_1(t), u_2(t), \tau = 15$	586	29057

From Table 2.3, we see that the earliest application of optimal vaccination and carcass disposal is the best strategy in terms of the total cost and the number of

animals avoiding infection. Comparing Strategies 1, 2 and 3 implies that Strategy 3 keeps more animals from becoming infected with the lowest cost suggesting the need for both optimal vaccination and carcass disposal strategies. Also, comparing Strategies 3 and 4 implies that Strategy 4 which is started after 4 days of the first carcass observed, saves about 30% more animals from infection than the Strategy 3 that is started after one week. Also, Strategy 4 is 25% more cost efficient the than Strategy 3. Comparison of Strategies 3, 4, and 5 suggests that an earlier optimal vaccination and optimal carcass disposal strategy is the best in terms of the lowest total number of infected animals and the total cost over 86 days.

2.6 Conclusions

We have formulated a mathematical framework to investigate the effect of intervention strategies for an anthrax outbreak in wild animals. Parameters of our model have been estimated based on available experimental and outbreak data. We calculated the disease free equilibrium solution and found the basic reproduction number $\mathcal{R}_0$. For the outbreak we considered, the value of $\mathcal{R}_0$ is much larger than its epidemic threshold, which may be the reason why the only carcass disposal strategy was not successful in controlling the outbreak in the Malilangwe Wildlife Reserve, Zimbabwe.

An important result of this analysis is that using both vaccination and the carcass disposal would be a cost effective way that will minimize the number of infected animals and the infected carcasses. Although a constant carcass disposal rate can reduce the sources of new infection to some extent, it is not enough to effectively control the outbreak. The intervention strategies that were implemented after 4, 7 and 14 days of the first carcass was found suggest that earlier use of controls help slow the spread of the disease and keep the overall cost minimum. This model with limited data can only approximate what happened in this Zimbabwe anthrax outbreak. Studies like this can be helpful for policy makers and conservationists to preserve endangered animal species in the endemic regions. Any outbreak should be

taken seriously and combination of infected carcass disposal should be implemented as soon as possible.

This work illustrates the value of optimal control theory as a tool to suggest management strategies in disease outbreaks.

Chapter 3

Optimal Control Analysis: The PDE Epidemiological Model

3.1 Introduction

It has been commonly accepted that spatial diffusion and environmental heterogeneity are important factors that should be considered in the spread of any infectious diseases. Movement and the mingling of wildlife species and domesticated animals with infected ones can cause disease spread over a large range of area [18, 49]. Thus understanding these movements and the associated risk can be very important in the application of effective control strategies for curbing animal disease and their spread. In many parts of world, animal movements have resulted in the emergence of new pathogens to previously disease free areas [18]. Intentional movements of animals such as translocation can be one of the major causes for the emergence of new diseases into new regions. On the other hand daily movements of animals within an area in order to graze or browse may cause disease spread when susceptible animals come in contact with infected animals or a contaminated environment. For anthrax, it is highly likely that susceptible animals who come into contact with infected animals or who graze on old carcass sites can ingest anthrax spores that may cause the disease. As seen in the

Malilangwe Wildlife Reserve in Zimbabwe, an anthrax outbreak starting at a point in the region spread miles away within a few weeks [6]. Also, the licking behavior of animals on fresh carcasses or carcass sites, scavenging infected animal carcasses for food, and breathing in dusty air in an infected region can transmit the disease [49].

In order to understand the impact of the movement of individuals on the persistence and extinction of anthrax, Friedman et al. [21] proposed a PDE model for an anthrax epizootic with density-dependent and frequency-dependent transmissions for a population in a continuous spatial habitat. They calculated the basic reproduction number for the model with and without animal migration. Their work is mainly focused on evaluating the effect of parameters that reduce carcass ingestion or environmental contamination in the outbreak.

In this chapter, we extend the ODE model presented in Chapter 2 to include animal movements within a hypothetical a region and consider state variables depending on both space and time. We assume that the animals movement is mainly by diffusion and the diffusion coefficient of infected animals is less than that of susceptible or vaccinated animals under the hypothesis that infected animals have behaviors thats reduce their normal movement. Two space and time dependent controls representing vaccination of susceptible animals and disposing of infected carcasses are considered and a separate compartment of vaccinated animals is added. Our goal is to investigate control strategies that minimize the outbreak (infecteds and carcasses) and the cost of control measures. We establish the existence and uniqueness of the state system and derive the optimality system. The existence and uniqueness results of the optimal controls are presented. At the end of this chapter, we present some numerical results for various parameter sets that illustrate different outbreak scenarios.

3.2 The Model

Let $s(x,t)$, $i(x,t)$ and $v(x,t)$ denote the density of susceptible, infected and vaccinated animals and $c(x,t)$ be the density of infected carcasses at spatial location $x \in \Omega$ and time $t \in [0,T]$. Also, $n(x,t) = s(x,t)+v(x,t)$ denote the sum of non infected animals. The structure of the model is the same as in the ODE model from Chapter 2 except for the movements of the animals. We assume that animals move by diffusion and that infected animals have a smaller diffusivity then healthy animals. We also assume Dirichlet boundary conditions (*i.e.*, no animals move across the boundary $\partial\Omega$). Our PDE/ODE model on domain $Q = \Omega \times (0,T)$ is

$$\frac{\partial s}{\partial t} = d\triangle s + rn(1-\frac{n}{K}) - \theta_c sc - \theta_i si - u_1 s \tag{3.1}$$

$$\frac{\partial i}{\partial t} = d_1\triangle i + \theta_c sc + \theta_i si - \gamma i \tag{3.2}$$

$$\frac{\partial v}{\partial t} = d\triangle v + u_1 s \tag{3.3}$$

$$\frac{dc}{dt} = \gamma i - \alpha(s+i+v)c - (p+u_2)c, \tag{3.4}$$

where $n = s + v$ and

with initial and boundary conditions,

$$s(x,0) = s^0(x),\ i(x,0) = i^0(x),\ v(x,0) = v^0(x),\ c(x,0) = c^0(x), \quad x \in \Omega,$$

$$s(x,t) = i(x,t) = v(x,t) = 0; \qquad (x,t) \in \partial\Omega \times [0,T].$$

The positive constant, d, is the diffusion coefficient for susceptible and vaccinated animals, and the positive constant, d_1, is the diffusion coefficient for infected animals. We assume that the diffusion rate of infected animals, due to their sickness, is less than the diffusion rate of healthy (susceptible or vaccinated) animals. All the state variables and controls are functions of both space and time. The two control functions representing the vaccination rate and the carcass disposal rate are denoted by $u_1(x,t)$

and $u_2(x,t)$, respectively. For simplicity, let us write the above system as

$$\begin{aligned}
\frac{\partial s}{\partial t} - d\frac{\partial^2 s}{\partial x^2} =& \mathcal{F}(s,i,v,c,u_1)\\
\frac{\partial i}{\partial t} - d_1\frac{\partial^2 i}{\partial x^2} =& \mathcal{G}(s,i,v,c)\\
\frac{\partial v}{\partial t} - d\frac{\partial^2 v}{\partial x^2} =& \mathcal{H}(s,u_1)\\
\frac{\partial c}{\partial t} =& \mathcal{N}(s,i,v,c,u_2)
\end{aligned}$$

where

$$\begin{aligned}
\mathcal{F}(s,i,v,c,u_1) =& rn(1-\frac{n}{K}) - \theta_c sc - \theta_i si - u_1 s\\
\mathcal{G}(s,i,v,c) =& \theta_c sc + \theta_i si - \gamma i\\
\mathcal{H}(s,u_1) =& u_1 s\\
\mathcal{N}(s,i,v,c,u_2) =& \gamma i - \alpha(s+i+v)c - (p+u_2)c.
\end{aligned}$$

Our goal is to minimize the number of infected animals and carcasses while also minimizing the total cost associated with vaccination and carcasses disposal. Again, as in the ODE model of Chapter 2, the vaccination is applied to both susceptible and infected animals, although there is no effect of vaccination on infected animals. We do this since in the wild, vaccination programs vaccinate all animals that are found and cannot distinguish whether they are infected or not. The objective functional then becomes

$$\begin{aligned}
J(u_1,u_2) = \int_Q \big[&A_1 i(x,t) + A_2 c(x,t)\\
&+ \{B_1 u_1\big(s(x,t)+i(x,t)\big) + B_2 u_2 c(x,t) + C_1 u_1(x,t)^2 + C_2 u_2(x,t)^2\}\big]dxdt
\end{aligned} \tag{3.5}$$

where the weighting coefficients $A_i, B_i, C_i; i = 1,2$ are positive constants. Here, the first two terms $A_1 i(x,t) + A_2 c(x,t)$ denote cost related to the infected animals and

the infected carcasses and the remaining terms

$$B_1u_1\big(s(x,t)+i(x,t)\big)+B_2u_2c(x,t)+C_1u_1(x,t)^2+C_2u_2(x,t)^2$$

represent the cost of applying the two controls. This cost is assumed to be non-linear and quadratic terms are used here for simplicity. We seek to minimize the functional $J(u_1,u_2)$ over the admissible class of controls. In other words, we want to characterize u_1^* and u_2^* such that

$$J(u_1^*,u_2^*)=\inf_{(u_1,u_2)\in\mathcal{U}}J(u_1,u_2).$$

where the control set $\mathcal{U}=\big\{(u_1,u_2)\in L^2(Q)^2:0\le u_i\le M_i \text{ a.e. for } i=1,2\big\}$.

3.3 Existence and Uniqueness of Weak Solutions

We are interested in a weak solution of the above system (3.1) − (3.4). Let Ω be bounded, smooth domain in $\mathbb{R}^n$. Let $\mathcal{V}=L^2\big(0,T;H_0^1(\Omega)\big)$ and $\mathcal{V}^*=L^2\big(0,T;H^{-1}(\Omega)\big)$ where $H^{-1}(\Omega)$ is the dual of $H_0^1(\Omega)$. For a control pair $(u_1,u_2)\in\mathcal{U}$, we say that the functions $s,i,v\in\mathcal{V}\cap L^\infty(Q)$ and $c\in L^2(Q)$ with time derivatives $s_t,i_t,v_t\in\mathcal{V}^*$ and $c_t\in L^2(Q)$ are weak solutions of our system if for any test functions $\phi_1,\phi_2,\phi_3\in\mathcal{V}\cap L^\infty(Q)$ the following equations (3.6) − (3.9) are satisfied:

$$\int_0^T<s_t,\phi_1>dt+d\int_Q\nabla s\cdot\nabla\phi_1dxdt=\int_Q\mathcal{F}(s,i,c,u_1)\phi_1dxdt; \tag{3.6}$$

$$\int_0^T<i_t,\phi_2>dt+d_1\int_Q\nabla i\cdot\nabla\phi_2dxdt=\int_Q\mathcal{G}(s,i,c)\phi_2dxdt; \tag{3.7}$$

$$\int_0^T<v_t,\phi_3>dt+d\int_Q\nabla v\cdot\nabla\phi_3dxdt=\int_Q\mathcal{H}(s,u_1)\phi_3dxdt; \tag{3.8}$$

$$c(x,t)=c^0(x)+\int_0^t\mathcal{N}(s,i,v,c,u_2)(x,\tau)d\tau \tag{3.9}$$

together with initial and boundary conditions

$$s(x,0) = s^0(x), i(x,0) = i^0(x), v(x,0) = v^0(x), c(x,0) = c^0(x), \ \ for\ x \in \Omega.$$
$$s = i = v = 0; \qquad on \ \ \partial\Omega \times (0,T)$$

where $< \ , \ >$ is the duality between $H_0^1(\Omega)$ and $H^{-1}(\Omega)$.

To derive the weak forms, we formally apply integration by parts and the boundary conditions on the second term of equations $(3.6) - (3.8)$ to obtain:

$$\begin{aligned}
\int_Q (\triangle s)\phi_1 dxdt &= \int_{\partial\Omega\times(0,T)} \phi_1(\frac{\partial s}{\partial \nu})ds - \int_Q \nabla s \cdot \nabla\phi_1 dxdt \\
&= -\int_Q \nabla s \cdot \nabla\phi_1 dxdt; \\
\int_Q (\triangle i)\phi_2 dxdt &= \int_{\partial\Omega\times(0,T)} \phi_2(\frac{\partial i}{\partial \nu})ds - \int_Q \nabla i \cdot \nabla\phi_2 dxdt \\
&= -\int_Q \nabla i \cdot \nabla\phi_2 dxdt;
\end{aligned}$$

and

$$\begin{aligned}
\int_Q (\triangle v)\phi_3 dxdt &= \int_{\partial\Omega\times(0,T)} \phi_3(\frac{\partial v}{\partial \nu})ds - \int_Q \nabla v \cdot \nabla\phi_3 dxdt \\
&= -\int_Q \nabla v \cdot \nabla\phi_3 dxdt.
\end{aligned}$$

Throughout this chapter, we make the following assumptions:

- Ω is smooth bounded domain in $\mathbb{R}^n$;
- $d, d_1, r, K, \theta_c, \theta_i, \gamma, \alpha, p$ are positive constants;
- $s^0, i^0, v^0, c^0 \in L^\infty(\Omega)$;
- $0 \le s^0(x), i^0(x), v^0(x), c^0(x) \le B < \frac{K}{2}$ for some $B \in \mathbb{R}$.

To prove the existence of weak solution of system $(3.1) - (3.4)$, we first note the following fact:

Note: Let $\Omega \subset \mathbb{R}^n$ be open and bounded, $u : \Omega \to \mathbb{R}^n$, and $1 \leq p < \infty$. If $u \in H^1(\Omega)$ then $u^+, u^- \in H^1(\Omega)$ and

$$Du^+ = \begin{cases} \text{Du}, & \text{if } u > 0 \\ 0, & \text{otherwise;} \end{cases}$$

and

$$Du^- = \begin{cases} \text{-Du}, & \text{if } u < 0 \\ 0, & \text{otherwise;} \end{cases}$$

where $u^+ = max\{u, 0\}$ and $u^- = -min\{u, 0\}$ [43].

Theorem 3.1. *For sufficiently small T and given $(u_1, u_2) \in \mathcal{U}$, the state system (3.1)-(3.4) together with initial and boundary conditions admits a unique solution in the corresponding solution space.*

Proof: We use the Banach Fixed Point Theorem to get a fixed point.
Since $s \in \mathcal{V}$ and $s_t \in \mathcal{V}^*$, then $s \in C\big(0, T; L^2(\Omega)\big)$ [16] and similar results hold for state variables i and v. Next, we want to define $L^\infty(\Omega)$ bounds for (s, i, v, c). Let

$$X = C\big(0, T; L^2(\Omega)\big) \cap \{y \in L^\infty(Q) : 0 \leq y \leq M \text{ a.e. in } Q\}$$

for a fixed $M = 2\max\{||s^0(x)||_{L^\infty(\Omega)}, ||i^0(x)||_{L^\infty(\Omega)}, ||v^0(x)||_{L^\infty(\Omega)}, ||c^0(x)||_{L^\infty(\Omega)}\}$ with $K > 2M$. We use the norm

$$||(s, i, v, c)||_{X^4} = (||s||_X + ||i||_X + ||v||_X + ||c||_X)$$

where

$$||w(x,t)||_X = \sup_{0 \leq t \leq T} ||w(x,t)||_{L^2(\Omega)} = \sup_{0 \leq t \leq T} \left(\int_\Omega w(x,t)^2 dx \right)^{\frac{1}{2}}.$$

For $\lambda > 0$, let $s = e^{\lambda t} S$, $i = e^{\lambda t} I$, $v = e^{\lambda t} V$, $c = e^{\lambda t} C$. The equations (3.1)-(3.4) on the domain Q reduce to

$$\frac{\partial S}{\partial t} - d\triangle S = -\lambda S + rN(1 - \frac{N}{K})e^{\lambda t} - \theta_c SCe^{\lambda t} - \theta_i SIe^{\lambda t} - u_1 S \tag{3.10}$$

$$\frac{\partial I}{\partial t} - d_1\triangle I = -\lambda I + \theta_c SCe^{\lambda t} + \theta_i SIe^{\lambda t} - \gamma I \tag{3.11}$$

$$\frac{\partial V}{\partial t} - d\triangle V = -\lambda V + u_1 S \tag{3.12}$$

$$\frac{dC}{dt} = -\lambda C + \gamma I - \alpha(S + I + V)Ce^{\lambda t} - (p + u_2)C \tag{3.13}$$

where N=S+V. The initial and boundary conditions are

$$S(x,0) = s^0(x),\ I(x,0) = i^0(x),\ V(x,0) = v^0(x),\ C(x,0) = c^0(x),\quad x \in \Omega.$$

$$S(x,t) = I(x,t) = V(x,t) = 0; \qquad for\ \ (x,t) \in \partial\Omega \times [0,T].$$

Let $(h_1, h_2, h_3, h_4) \in X^4$. Consider the system of uncoupled linear PDEs

$$\frac{\partial S}{\partial t} - d\triangle S = -\lambda S + r(S + h_3)\big(1 - \frac{(h_1 + h_3)}{K}\big)e^{\lambda t} - \theta_c S h_4 e^{\lambda t} - \theta_i S h_2 e^{\lambda t} - u_1 S \tag{3.14}$$

$$\frac{\partial I}{\partial t} - d_1\triangle I = -\lambda I + \theta_c h_1 h_4 e^{\lambda t} + \theta_i h_1 I e^{\lambda t} - \gamma I \tag{3.15}$$

$$\frac{\partial V}{\partial t} - d\triangle V = -\lambda V + u_1 h_1 \tag{3.16}$$

$$\frac{\partial C}{\partial t} = -\lambda C + \gamma h_2 - \alpha(h_1 + h_2)Ce^{\lambda t} - (p + u_2)C \tag{3.17}$$

with initial and boundary conditions,

$$S(x,0) = s^0(x), I(x,0) = i^0(x), V(x,0) = v^0(x), C(x,0) = c^0(x), x \in \Omega.$$

$$S(x,t) = I(x,t) = V(x,t) = 0; \qquad (x,t) \in \partial\Omega \times [0,T].$$

For fixed $(h_1, h_2, h_3, h_4) \in X^4$, the system of equations (3.14)-(3.16) has a unique weak solutions $(S, I, V) \in \mathcal{V}^3$ with $(S_t, I_t, V_t) \in (V^*)^3$ [16]. Equation (3.17) has a unique solution in $L^2(Q)$ since its right hand side is linear in C. Also, we have $S, I, V, C \in C\big(0, T; L^2(\Omega)\big)$. In order to show that $(S, I, V, C) \in X^4$, we need to show that $0 \le S, I, V, C \le M$. Rearranging

the terms of (3.14) − (3.16) and using the fact that $h_1 + h_2 \leq 2M < K$ we obtain,

$$\begin{aligned}
&\frac{\partial S}{\partial t} - d\triangle S + \lambda S e^{\lambda t} - rS\frac{(h_1+h_3)}{K}e^{\lambda t} + \theta_c S h_4 e^{\lambda t} + \theta_i S h_2 e^{\lambda t} + u_1 S = rh_3(1 - \frac{h_1+h_3}{K})e^{\lambda t} \geq 0,\\
&\frac{\partial I}{\partial t} - d_1\triangle I + \lambda I - \theta_i h_1 I e^{\lambda t} + \gamma I = \theta_c h_1 h_4 e^{\lambda t} \geq 0, \qquad (3.18)\\
&\frac{\partial V}{\partial t} - d\triangle V + \lambda V = u_1 h_1 \geq 0,
\end{aligned}$$

for a.e. $(x,t) \in Q$.

Claim I:
$S(x,t), I(x,t), V(x,t) \geq 0$.
Proof of Claim I: We prove the claim for the variable $S(x,t)$. The claim can be similarly proven for $I(x,t)$ and $V(x,t)$. We have that

$$\frac{\partial S}{\partial t} - d\triangle S + \lambda S e^{\lambda t} - rS\frac{(h_1+h_3)}{K}e^{\lambda t} + \theta_c S h_4 e^{\lambda t} + \theta_i S h_2 e^{\lambda t} + u_1 S \geq 0$$

Let $S^- := -\min\{S, 0\}$ then $S^- \in \mathcal{V}$. Multiply by S^- and use the weak formulation on Ω to arrive

$$\int_\Omega \frac{\partial S}{\partial t} S^- dx + d\int_\Omega \nabla S \cdot \nabla S^- dx + \int_\Omega \big[\lambda - r\frac{(h_1+h_3)}{K}e^{\lambda t} + \theta_c h_4 e^{\lambda t} + \theta_i h_2 e^{\lambda t} + u_1\big] S S^- dx \geq 0$$

$$-\frac{1}{2}\frac{\partial}{\partial t}\int_\Omega (S^-)^2 dx - d\int_\Omega |\nabla S^-|^2 dx - \int_\Omega \big[\lambda - r\frac{(h_1+h_3)}{K}e^{\lambda t} + \theta_c h_4 e^{\lambda t} + \theta_i h_2 e^{\lambda t} + u_1\big](S^-)^2 dx \geq 0.$$

Choose λ sufficiently large ($\lambda > \frac{2rM}{K}$) and then choose T small enough so that

$$\lambda - r\frac{(h_1+h_3)}{K}e^{\lambda t} + \theta_c h_4 e^{\lambda t} + \theta_i h_2 e^{\lambda t} + u_1 \geq 0.$$

This implies that

$$\frac{1}{2}\frac{\partial}{\partial t}\int_\Omega (S^-)^2(x,t)dx \leq 0.$$

Integrating over 0 to t gives

$$\int_\Omega (S^-)^2(x,t)dx \leq \int_\Omega (S^-)^2(x,0)dx.$$

Since $S(x,0) \geq 0$, and $S^-(x,0) = 0$ by definition of S^-, the above inequality implies that $S^-(x,t) = 0$. Hence, $S(x,t) \geq 0$. **End of the Claim I.**

Next, we show that $S(x,t), I(x,t), V(x,t) \leq M$ a.e. in Q. Since $h_1, h_2, h_3 \in X$ and r, λ, K, T are finite, there exists a positive constant C_1 (depending on model parameters, the bounds on the functions in X and the bounds on the controls), such that

$$|rh_3(1-\frac{h_1+h_3}{K})e^{\lambda t}| \leq rMe^{\lambda T} \leq C_1,\ |\theta_c h_1 h_4 e^{\lambda t}| \leq \theta_c M^2 e^{\lambda T} \leq C_1,\ |u_1 h_1| \leq M_1 M \leq C_1$$

a.e. in Q, where $C_1 = max\{rMe^{\lambda T}, \theta_c M^2 e^{\lambda T}, M_1 M\}$. Thus we have bounded RHS of the system (3.18) ,

$$\begin{aligned}
\frac{\partial S}{\partial t} - d\triangle S + \lambda S - rS\frac{(h_1+h_3)}{K}e^{\lambda t} + \theta_c S h_4 e^{\lambda t} + \theta_i S h_2 e^{\lambda t} + u_1 S \leq C_1 \\
\frac{\partial I}{\partial t} - d_1\triangle I + \lambda I - \theta_i h_1 I e^{\lambda t} + \gamma I \leq C_1 \\
\frac{\partial V}{\partial t} - d\triangle V + \lambda V \leq C_1
\end{aligned}$$

for a.e. $(x,t) \in Q$.
Consider $\bar{S}(x,t) = S(x,t) - C_1 t,\ \bar{I}(x,t) = I(x,t) - C_1 t,\ \bar{V}(x,t) = V(x,t) - C_1 t$. Then we have

$$\begin{aligned}
&\frac{\partial \bar{S}}{\partial t} - d\triangle \bar{S} + \lambda \bar{S} - r\bar{S}\frac{(h_1+h_3)}{K}e^{\lambda t} + \theta_c \bar{S} h_4 e^{\lambda t} + \theta_i \bar{S} h_2 e^{\lambda t} + u_1 \bar{S} \\
&\quad = \left(\frac{\partial S}{\partial t} - d\triangle S + \lambda S - rS\frac{(h_1+h_3)}{K}e^{\lambda t} + \theta_c S h_4 e^{\lambda t} + \theta_i S h_2 e^{\lambda t} + u_1 S\right) - C_1 \\
&\qquad - \lambda C_1 t - \left(-r\frac{(h_1+h_3)}{K}e^{\lambda t} + \theta_c h_4 e^{\lambda t} + \theta_i h_2 e^{\lambda t} + u_1\right) C_1 t \\
&\quad \leq -\left(\lambda - r\frac{(h_1+h_3)}{K}e^{\lambda t} + \theta_c h_4 e^{\lambda t} + \theta_i h_2 e^{\lambda t} + u_1\right) C_1 t \\
&\quad \leq 0
\end{aligned} \tag{3.19}$$

where λ and T are chosen exactly as before so that

$$\lambda - r\frac{(h_1+h_3)}{K}e^{\lambda t} + \theta_c h_4 e^{\lambda t} + \theta_i h_2 e^{\lambda t} + u_1 \geq 0.$$

Similarly, we obtain

$$\frac{\partial \bar{I}}{\partial t} - d_1 \triangle \bar{I} + \lambda \bar{I} - \theta_i h_1 \bar{I} e^{\lambda t} + \gamma \bar{I} \leq 0,$$

$$\frac{\partial \bar{V}}{\partial t} - d \triangle \bar{V} + \lambda \bar{V} \leq 0,$$

with initial and boundary conditions

$$\bar{S}(x,0) = s^0(x), \bar{I}(x,0) = i^0(x), \bar{V}(x,0) = v^0(x), \quad x \in \Omega$$

and

$$\bar{S}(x,t) = \bar{I}(x,t) = \bar{V}(x,t) = 0; \qquad for\ (x,t) \in \partial\Omega X[0,T]).$$

Claim II: $\bar{S}, \bar{I}, \bar{V}$ are bounded from above.

Proof of Claim II: As in the Claim I, we prove this claim for $\bar{S}(x,t)$. The claim can be proven for $\bar{I}(x,t)$ and $\bar{V}(x,t)$. Since $||s^0(x)||_{L^\infty} \leq \frac{M}{2}$, let $w(x,t) = (\bar{S} - \frac{M}{2})^+ = \max\{(\bar{S} - \frac{M}{2}), 0\}$ multiply the inequality (3.19) by $w(x,t)$ and integrate over Ω. Then as in Claim I, we get (See the details in A.1)

$$\frac{\partial}{\partial t} \int_\Omega w^2 dx \leq 0$$

Integrating over 0 to t for $t \in (0,T)$, we arrive at

$$\int_\Omega w^2(x,t) dx \leq \int_\Omega w^2(x,0) dx \tag{3.20}$$

Since $w(x,0) = max\{\bar{S}(x,0) - \frac{M}{2}, 0\} = max\{s^0(x) - \frac{M}{2}, 0\} = 0$, then (3.20) gives $w(x,t) = 0$.

This implies from the definition of $w(x,t)$ that $\bar{S} - \frac{M}{2} \leq 0$. Thus, $\bar{S}$ is bounded above by $\frac{M}{2}$. **End of Claim II.**

Now, from the definition of $\bar{S}, \bar{I}, \bar{V}$ we have

$$\begin{aligned}
S(x,t) &\leq ||s^0(x)||_{L^\infty(\Omega)} + C_1 t \leq \frac{M}{2} + C_1 T; \\
I(x,t) &\leq ||i^0(x)||_{L^\infty(\Omega)} + C_1 t \leq \frac{M}{2} + C_1 T; \quad \textit{and} \\
V(x,t) &\leq ||v^0(x)||_{L^\infty(\Omega)} + C_1 t \leq \frac{M}{2} + C_1 T.
\end{aligned}$$

For small T with $C_1 T \leq \frac{M}{2}$ we have

$$\begin{aligned}
S(x,t) &\leq \frac{M}{2} + \frac{M}{2} = M; \\
I(x,t) &\leq \frac{M}{2} + \frac{M}{2} = M; \\
V(x,t) &\leq \frac{M}{2} + \frac{M}{2} = M \ \text{ for a.e. } (x,t) \in Q.
\end{aligned}$$

Also, equation (3.17) can be written as

$$\frac{\partial C}{\partial t} + [\lambda + \alpha(h_1 + h_2 + h_3)e^{\lambda t} + p + u_2]C = \gamma h_2$$

This is a linear ODE with bounded coefficients. Thus its solution is bounded. Moreover, for any $x \in \Omega$,

$$\begin{aligned}
&\frac{\partial C}{\partial t} + [\lambda + \alpha(h_1 + h_2 + h_3)e^{\lambda t} + p + u_2]C = \gamma h_2, \quad \textit{and thus} \\
&C(x,t) = e^{-\int_0^t (\lambda + \alpha(h_1+h_2+h_3)e^{\lambda t} + p + u_2)ds} \Big[c^0(x) + \gamma \int_0^t h_2 e^{\int_0^s (\lambda + \alpha(h_1+h_2+h_3)e^{\lambda t} + p + u_2)d\tau} ds \Big] \geq 0.
\end{aligned}$$

Also, since $\frac{\partial C}{\partial t} \leq \gamma h_2$ then

$$C(x,t) \leq \gamma \int_0^t h_2(x,\tau)d\tau + c^0(x) \leq \gamma M T + \frac{M}{2} \leq M$$

for $T \leq \frac{\gamma}{2}$. Hence, the state variable C is bounded above by M. Thus, we have proven that for $(h_1, h_2, h_3, h_4) \in X^4$, the solution (S, I, V, C) to the system $(3.14) - (3.17)$ is

also in X^4.

Let us define a map, $P : X^4 \to X^4$ such that $P(h_1, h_2, h_3, h_4) = (S, I, V, C)$ and where (S, I, V, C) is the solution of the system $(3.14) - (3.17)$. We want to show that P is a contraction mapping. Let $(h_1, h_2, h_3, h_4), (\bar{h}_1, \bar{h}_2, \bar{h}_3, \bar{h}_4) \in X^4$ and define $P(\bar{h}_1, \bar{h}_2, \bar{h}_3, \bar{h}_4) = (\bar{S}, \bar{I}, \bar{V}, \bar{C})$. Then the equations satisfied by $S - \bar{S}$, $I - \bar{I}, V - \bar{V}$ and $C - \bar{C}$ are given by equations $(3.21) - (3.24)$

$$\frac{\partial(S-\bar{S})}{\partial t} - d\triangle(S-\bar{S}) + \lambda(S-\bar{S}) = r(S-\bar{S}) + r(h_3-\bar{h}_3) - \frac{r}{K}\big[(S+h_3)(h_1+h_3) - (\bar{S}+\bar{h}_3)(\bar{h}_1+\bar{h}_3)\big] - \theta_c e^{\lambda t}(Sh_4 - \bar{S}\bar{h}_4) - \theta_i e^{\lambda t}(Sh_2 - \bar{S}\bar{h}_2) + u_1(S-\bar{S}); \tag{3.21}$$

$$\frac{\partial(I-\bar{I})}{\partial t} - d_1\triangle(I-\bar{I}) + \lambda(I-\bar{I}) = \theta_c e^{\lambda t}(h_1h_4 - \bar{h}_1\bar{h}_4) + \theta_i e^{\lambda t}(h_1 I - \bar{h}_1\bar{I}) - \gamma(I-\bar{I}); \tag{3.22}$$

$$\frac{\partial(V-\bar{V})}{\partial t} - d\triangle(V-\bar{V}) + \lambda(I-\bar{V}) = u_1(h_1-\bar{h}_1); \tag{3.23}$$

$$\frac{\partial(C-\bar{C})}{\partial t} + \lambda(C-\bar{C}) = \gamma(h_2-\bar{h}_2) - \alpha\big[(h_1+h_2+h_3)C - (\bar{h}_1+\bar{h}_2+\bar{h}_3)\bar{C}\big]e^{\lambda t} - (p+u_2)(C-\bar{C}); \tag{3.24}$$

with initial and boundary conditions,

$$(S-\bar{S})(x,0) = (I-\bar{I})(x,0) = (V-\bar{V})(x,0) = (C-\bar{C})(x,0) = 0, \quad \text{for } x \in \Omega.$$
$$(S-\bar{S})(x,t) = (I-\bar{I})(x,t) = (V-\bar{V})(x,t) = 0; \qquad \text{for } (x,t) \in \partial\Omega \times [0,T].$$

Let $\tau \in (0,T)$ and $Q_\tau = \Omega \times (0,\tau)$. Then the weak formulation of equation (3.21) over Q_τ gives,

$$\begin{aligned}\frac{1}{2}\int_\Omega (S-\bar{S})^2(x,\tau)dx + d\int_{Q_\tau} |\nabla(S-\bar{S})|^2 dxdt + \lambda\int_{Q_\tau}(S-\bar{S})^2 dxdt \\ = r\int_{Q_\tau}(S-\bar{S})^2 dxdt - \frac{r}{K}\int_{Q_\tau}\big[(S+h_3)(h_1+h_3) - (\bar{S}+\bar{h}_3)(\bar{h}_1+\bar{h}_3)\big](S-\bar{S})dxdt \\ + r\int_{Q_\tau}(h_3-\bar{h}_3)(S-\bar{S})dxdt - \theta_c\int_{Q_\tau} e^{\lambda t}(Sh_4 - \bar{S}\bar{h}_4)(S-\bar{S})dxdt \\ - \theta_i\int_{Q_\tau} e^{\lambda t}(Sh_2 - \bar{S}\bar{h}_2)(S-\bar{S})dxdt + \int_{Q_\tau} u_1(S-\bar{S})^2 dxdt. \end{aligned} \tag{3.25}$$

Similarly, equations (3.22)-(3.24) become

$$\frac{1}{2}\int_\Omega (I-\bar{I})^2(x,\tau)dx + d_1\int_{Q_\tau}|\nabla(I-\bar{I})|^2dxdt + \lambda\int_{Q_\tau}(I-\bar{I})^2dxdt = \theta_c\int_{Q_\tau}e^{\lambda t}(h_1h_4-\bar{h}_1\bar{h}_4)$$
$$(I-\bar{I})dxdt + \theta_i\int_{Q_\tau}e^{\lambda t}(h_1I-\bar{h}_1\bar{I})(I-\bar{I})dxdt - \int_{Q_\tau}\gamma(I-\bar{I})^2dxdt. \tag{3.26}$$

and

$$\frac{1}{2}\int_\Omega (V-\bar{V})^2(x,\tau)dx + d\int_{Q_\tau}|\nabla(V-\bar{V})|^2dxdt + \lambda\int_{Q_\tau}(V-\bar{V})^2dxdt$$
$$= \int_{Q_\tau}u_1(h_1-\bar{h}_1)(V-\bar{V})dxdt \tag{3.27}$$

$$\frac{1}{2}\int_\Omega (C-\bar{C})^2(x,\tau)dx + \lambda\int_{Q_\tau}(C-\bar{C})^2dxdt = \int_{Q_\tau}\gamma(h_2-\bar{h}_2)(C-\bar{C})dxdt$$
$$-\int_{Q_\tau}\alpha\big[(h_1+h_2+h_3)C-(\bar{h}_1+\bar{h}_2+\bar{h}_3)\bar{C}\big]e^{\lambda t}(C-\bar{C})dxdt - \int_{Q_\tau}p(C-\bar{C})^2dxdt \tag{3.28}$$

where we used the zero initial condition for all 4 equations $(3.25)-(3.28)$ and

$$\int_\Omega\int_0^t w_t(x,\tau)w(x,\tau)dxdt = \frac{1}{2}\int_\Omega w^2(x,t)dx - \frac{1}{2}\int_\Omega w^2(x,0)dx$$

We illustrate the estimates of a few representative terms such as

$$\int_{Q_\tau}\left|\theta_ce^{\lambda t}(h_4S-\bar{h}_4\bar{S})(S-\bar{S})dxdt\right| = \int_{Q_\tau}\left|\theta_ce^{\lambda t}[h_4(S-\bar{S})+\bar{S}(h_4-\bar{h}_4)](S-\bar{S})dxdt\right|$$
$$\le \int_{Q_\tau}\left|\theta_ce^{\lambda t}h_4(S-\bar{S})^2dxdt\right| + \int_{Q_\tau}\left|\theta_ce^{\lambda t}\bar{S}(h_4-\bar{h}_4)(S-\bar{S})dxdt\right|$$
$$\le \int_{Q_\tau}\theta_ce^{\lambda t}h_4(S-\bar{S})^2dxdt + \frac{1}{2}\int_{Q_\tau}(h_4-\bar{h}_4)^2dxdt + \frac{1}{2}\int_Q\theta_c^2e^{2\lambda t}\bar{S}^2(S-\bar{S})^2dxdt$$
$$\le \int_{Q_\tau}[\theta_ce^{2\lambda t}h_4+\theta_c^2e^{2\lambda t}\bar{S}^2](S-\bar{S})^2dxdt + \frac{1}{2}\int_{Q_\tau}(h_4-\bar{h}_4)^2dxdt$$
$$\le D_1(M+M^2)e^{2\lambda T}\int_{Q_\tau}(S-\bar{S})^2dxdt + \frac{1}{2}\int_{Q_\tau}(h_4-\bar{h}_4)^2dxdt,$$

$$\int_{Q_\tau}\left|\theta_i e^{\lambda t}(h_2S-\bar{h}_2\bar{S})(S-\bar{S})dxdt\right|$$
$$\leq D_2(M+M^2)e^{2\lambda T}\int_{Q_\tau}(S-\bar{S})^2dxdt+\frac{1}{2}\int_{Q_\tau}(h_2-\bar{h}_2)^2dxdt;$$
$$\int_{Q_\tau}\left|\theta_i e^{\lambda t}(h_1I-\bar{h}_1\bar{I})(I-\bar{I})dxdt\right|$$
$$\leq D_2(M+M^2)e^{2\lambda T}\int_{Q_\tau}(I-\bar{I})^2dxdt+\frac{1}{2}\int_{Q_\tau}(h_1-\bar{h}_1)^2dxdt;$$

where $D_1=\max\{\theta_c,\theta_c^2\}$ and $D_2=\max\{\theta_i,\theta_i^2\}$.

Similarly,

$$\int_{Q_\tau}\left|\alpha e^{\lambda t}\big[(h_1+h_2+h_3)C-(\bar{h}_1+\bar{h}_2+\bar{h}_3)\bar{C}\big](C-\bar{C})dxdt\right|$$
$$\leq D_3e^{2\lambda T}\int_{Q_\tau}(C-\bar{C})^2dxdt+\frac{1}{2}\int_{Q_\tau}(h_1-\bar{h}_1)^2dxdt+\frac{1}{2}\int_{Q_\tau}(h_2-\bar{h}_2)^2dxdt$$
$$+\frac{1}{2}\int_{Q_\tau}(h_3-\bar{h}_3)^2dxdt;$$

and

$$\int_{Q_\tau}\left|\theta_c e^{\lambda t}(h_1h_4-\bar{h}_1\bar{h}_4)(I-\bar{I})dxdt\right|$$
$$\leq D_4M^2e^{2\lambda T}\int_{Q_\tau}(I-\bar{I})dxdt+\frac{1}{2}\int_{Q_\tau}(h_1-\bar{h}_1)^2dxdt+\frac{1}{2}\int_{Q_\tau}(h_4-\bar{h}_4)^2dxdt;$$

where $D_3=\max\{\alpha,\alpha^2\}$ and $D_4=\theta_c^2$. Finally,

$$\frac{r}{K}\int_{Q_\tau}\left|\big[(S+h_3)(h_1+h_3)-(\bar{S}+\bar{h}_3)(\bar{h}_1+\bar{h}_3)\big](S-\bar{S})dxdt\right|$$
$$=\int_{Q_\tau}\left|\frac{r}{K}\big[S(h_1-\bar{h}_1)+\bar{h}_1(S-\bar{S})+S(h_3-\bar{h}_3)+\bar{h}_3(S-\bar{S})+h_1h_3-\bar{h}_1\bar{h}_3\right.$$
$$\left.+h_3^2-\bar{h}_3^2\big](S-\bar{S})dxdt\right|$$
$$=\int_{Q_\tau}\left|\big[\frac{r}{K}S(h_1-\bar{h}_1)(S-\bar{S})+\frac{r}{K}\bar{h}_1(S-\bar{S})^2+\frac{r}{K}S(h_3-\bar{h}_3)(S-\bar{S})+\frac{r}{K}\bar{h}_3(S-\bar{S})^2\right.$$
$$\left.+\frac{r}{K}(h_1h_3-\bar{h}_1\bar{h}_3)(S-\bar{S})+\frac{r}{K}(h_3-\bar{h}_3)(h_3+\bar{h}_3)(S-\bar{S})\big]dxdt\right|$$

$$
\begin{aligned}
&\leq \frac{1}{2}\int_{Q_\tau}\frac{r^2}{K^2}M^2(S-\bar{S})^2dxdt+\frac{1}{2}\int_{Q_\tau}(h_1-\bar{h}_1)^2dxdt+\frac{r}{K}M\int_{Q_\tau}(S-\bar{S})^2dxdt\\
&\quad+\frac{1}{2}\int_{Q_\tau}\frac{r^2}{K^2}M^2(S-\bar{S})^2dxdt+\frac{1}{2}\int_{Q_\tau}(h_3-\bar{h}_3)^2dxdt+\frac{r}{K}M\int_{Q_\tau}(S-\bar{S})^2dxdt\\
&\quad+\int_{Q_\tau}\frac{r^2}{K^2}M^2(S-\bar{S})^2dxdt+\frac{1}{2}\int_{Q_\tau}(h_1-\bar{h}_1)^2dxdt+\frac{1}{2}\int_{Q_\tau}(h_3-\bar{h}_3)^2dxdt\\
&\quad+\int_{Q_\tau}2\frac{r^2}{K^2}M^2(S-\bar{S})^2dxdt+\frac{1}{2}\int_{Q_\tau}(h_3-\bar{h}_3)^2dxdt\\
&=\int_{Q_\tau}\big[\{5M^2\frac{r^2}{K^2}+2M\frac{r}{K}\}(S-\bar{S})^2+(h_1-\bar{h}_1)^2+\frac{3}{2}(h_3-\bar{h}_3)^2\big]dxdt\\
&\leq\int_{Q_\tau}\big[D_5(M+M^2)(S-\bar{S})^2+(h_1-\bar{h}_1)^2+\frac{3}{2}(h_3-\bar{h}_3)^2\big]dxdt
\end{aligned}
$$

where $D_5=\max\{\frac{5r^2}{K^2},\frac{2r}{K}\}$.

Adding (3.25) − (3.28) and using the above estimates to obtain,

$$
\begin{aligned}
&\frac{1}{2}\int_\Omega\big[(S-\bar{S})^2+(I-\bar{I})^2+(V-\bar{V})^2+(C-\bar{C})^2(x,\tau)\big]dx+\lambda\int_{Q_\tau}\big[(S-\bar{S})^2+(I-\bar{I})^2\\
&+(V-\bar{V})^2+(C-\bar{C})^2\big]dxdt+\int_{Q_\tau}\big[d|\nabla(S-\bar{S})|^2+d_1|\nabla(I-\bar{I})|^2+d|\nabla(V-\bar{V})|^2\big]dxdt\\
&\quad\leq r\int_{Q_\tau}(S-\bar{S})^2dxdt+\frac{1}{2}\int_Q r^2(S-\bar{S})^2dxdt+\frac{1}{2}\int_{Q_\tau}(h_3-\bar{h}_3)^2dxdt\\
&\quad+\int_{Q_\tau}\big[D_5(M+M^2)(S-\bar{S})^2+(h_1-\bar{h}_1)^2+\frac{3}{2}(h_3-\bar{h}_3)^2\big]dxdt\\
&\quad+D_1(M+M^2)e^{2\lambda T}\int_Q(S-\bar{S})^2dxdt+\frac{1}{2}\int_Q(h_4-\bar{h}_4)^2dxdt\\
&\quad+D_2(M+M^2)e^{2\lambda T}\int_{Q_\tau}(S-\bar{S})^2dxdt+\frac{1}{2}\int_{Q_\tau}(h_2-\bar{h}_2)^2dxdt+M\int_{Q_\tau}(S-\bar{S})^2dxdt\\
&\quad+D_4M^2e^{2\lambda T}\int_{Q_\tau}(I-\bar{I})^2dxdt+\frac{1}{2}\int_Q(h_1-\bar{h}_1)^2dxdt+\frac{1}{2}\int_Q(h_4-\bar{h}_4)^2dxdt\\
&\quad+D_2(M+M^2)e^{2\lambda T}\int_{Q_\tau}(I-\bar{I})^2dxdt+\frac{1}{2}\int_{Q_\tau}(h_1-\bar{h}_1)^2dxdt+\int_Q\gamma(I-\bar{I})^2dxdt\\
&\quad+\frac{1}{2}M^2\int_{Q_\tau}(V-\bar{V})^2dxdt+\frac{1}{2}\int_{Q_\tau}(h_1-\bar{h}_1)^2dxdt+D_3e^{2\lambda T}\int_{Q_\tau}(C-\bar{C})^2dxdt\\
&\quad+\frac{1}{2}\int_{Q_\tau}(h_1-\bar{h}_1)^2dxdt+\frac{1}{2}\int_{Q_\tau}(h_2-\bar{h}_2)^2dxdt+\frac{1}{2}\int_{Q_\tau}(h_3-\bar{h}_3)^2dxdt\\
&\quad+\frac{\gamma^2}{2}\int_{Q_\tau}(C-\bar{C})^2dxdt+\frac{1}{2}\int_{Q_\tau}(h_2-\bar{h}_2)^2dxdt+\int_Q p(C-\bar{C})^2dxdt.
\end{aligned}
$$

Thus,

$$\begin{aligned}\frac{1}{2}\int_\Omega \big[(S-\bar{S})^2+(I-\bar{I})^2+(V-\bar{V})^2+(C-\bar{C})^2\big](x,\tau)dx \\ +\int_{Q_\tau}\big[L_1(S-\bar{S})^2+L_2(I-\bar{I})^2+L_3(V-\bar{V})^2+L_5(C-\bar{C})^2]dxdt \\ +\int_{Q_\tau}\big[d|\nabla(S-\bar{S})|^2+d_1|\nabla(I-\bar{I})|^2+d|\nabla(V-\bar{V})|^2\big]dxdt \\ \leq \int_{Q_\tau} 3(h_1-\bar{h}_1)^2+\frac{3}{2}(h_2-\bar{h}_2)^2+\frac{5}{2}(h_3-\bar{h}_3)^2+(h_4-\bar{h}_4)^2dxdt,\end{aligned}$$

where

$$\begin{aligned}L_1 &= \lambda - r - \frac{1}{2}r^2 - [D_5+(D_1+D_2)e^{2\lambda T}](M+M^2) - M \\ L_2 &= \lambda - D_4M^2e^{2\lambda T} - D_2(M+M^2)e^{2\lambda T} - \gamma \\ L_3 &= \lambda - \frac{1}{2}M^2 \\ L_4 &= \lambda - D_3e^{2\lambda T} - \frac{1}{2}\gamma^2 - p.\end{aligned}$$

We choose λ big enough and T sufficiently small so that $L_i \geq 0$ for $i = 1, ..., 4$. Then

$$\begin{aligned}\int_\Omega \big[(S-\bar{S})^2+(I-\bar{I})^2+(V-\bar{V})^2+(C-\bar{C})^2\big](x,\tau)dx \\ \leq 6\int_{Q_\tau}(h_1-\bar{h}_1)^2+(h_2-\bar{h}_2)^2+(h_3-\bar{h}_3)^2+(h_4-\bar{h}_4)^2dx \\ \leq 6T\Big[\sup_{0\leq t\leq T}\int_\Omega(h_1-\bar{h}_1)^2dx+\sup_{0\leq t\leq T}\int_\Omega(h_2-\bar{h}_2)^2dx+\sup_{0\leq t\leq T}\int_\Omega(h_3-\bar{h}_3)^2dx \\ +\sup_{0\leq t\leq T}\int_\Omega(h_4-\bar{h}_4)^2dx\Big] \\ = 6T(H_1+H_2+H_3+H_4)\end{aligned}$$

where $H_i = \sup_{0\leq t\leq T}\int_\Omega(h_i-\bar{h}_i)^2dx = ||h_i-\bar{h}_i||^2_X$; for i=1,..., 4.

This implies that,

$\int_\Omega (S-\bar{S})^2(x,\tau)dx \leq 6T(H_1+H_2+H_3+H_4)$. In other words

$$||S-\bar{S}||_{L^2(\Omega)} \leq \big(6T\big)^{\frac{1}{2}}\bigg(H_1+H_2+H_3+H_4\bigg)^{\frac{1}{2}} \leq \big(6T\big)^{\frac{1}{2}}\bigg(H_1^{\frac{1}{2}}+H_2^{\frac{1}{2}}+H_3^{\frac{1}{2}}+H_4^{\frac{1}{2}}\bigg)$$

We then take the supremum over the interval (0,T) to obtain

$$||S-\bar{S}||_X = \sup_{0\leq t\leq T}||S-\bar{S}||_{L^2(\Omega)} \leq \big(6T\big)^{\frac{1}{2}}\sum_{i=1}^{4}||h_i-\bar{h}_i||_X$$

Similar expressions for $||I-\bar{I}||_X,\ ||V-\bar{V}||_X$ *and* $||C-\bar{C}||_X$. Adding these estimates yields

$$||S-\bar{S}||_X+||I-\bar{I}||_X+||V-\bar{V}||_X+||C-\bar{C}||_X \leq 4\big(6T\big)^{\frac{1}{2}}\sum_{i=1}^{4}||h_i-\bar{h}_i||_X.$$

Choose T small enough so that $4\big(6T\big)^{\frac{1}{2}}<1$, hence

$$\begin{aligned}||P(h_1,h_2,h_3,h_4)-P(\bar{h}_1,\bar{h}_2,\bar{h}_3,\bar{h}_4)||_{X^4}&\\ &= ||S-\bar{S}||_X+||I-\bar{I}||_X+||V-\bar{V}||_X+||C-\bar{C}||_X\\ &\leq 4\big(6T\big)^{\frac{1}{2}}\big(||h_1-\bar{h}_1||_X+||h_2-\bar{h}_2||_X+||h_3-\bar{h}_3||_X+||h_4-\bar{h}_4||_X\big).\end{aligned}$$

Thus, the mapping P is a contraction mapping. By the Banach Fixed Point theorem, the mapping P has an unique fixed point (h_1,h_2,h_3,h_4):

$$P(h_1,h_2,h_3,h_4)=(S,I,V,C)=(h_1,h_2,h_3,h_4).$$

Hence a unique solution to the system (3.10) - (3.13) exists. It follows that for sufficiently small T, there exists an unique non-negative solutions for (3.1)-(3.4) that are bounded by $Me^{\lambda T}$ for a.e. $(x,t)\in Q$. ■

Next, we state an *a priori* estimate theorem for the state solutions and their derivative. As in the Theorem 3.1, standard techniques of Hölder's Inequality, Young's Inequality and Gronwall's Inequality can be used to prove the following theorem.

Theorem 3.2 (*A Priori* Estimates)**.** *Suppose* $(s,i,v) \in \mathcal{V}^3$ *with* $(s_t,i_t,v_t) \in (\mathcal{V}^*)^3$ *and* $c, c_t \in L^2(Q)$ *is a weak solution of the system (3.1)-(3.4) corresponding to control* $(u_1,u_2) \in \mathcal{U}$*. Then there exists a positive constants* K_1 *such that* $\forall (u_1,u_2) \in \mathcal{U}$*,*

$$||s(u_1,u_2)||_{\mathcal{V}}, ||i(u_1,u_2)||_{\mathcal{V}}, ||i(u_1,u_2)||_{\mathcal{V}}, ||c(u_1,u_2)||_{L^2(Q)} \leq K_1 \quad \textit{and}$$
$$||s_t(u_1,u_2)||_{\mathcal{V}^*}, ||i_t(u_1,u_2)||_{\mathcal{V}^*}, ||v_t(u_1,u_2)||_{\mathcal{V}^*}, ||c_t(u_1,u_2)||_{L^2(Q)} \leq K_1. \quad \blacksquare$$

We next show that there exists an unique optimal control (u_1^*, u_2^*) and corresponding state solution $(s^*, i^*, v^*, c^*) = (s,i,v,c)(u_1^*, u_2^*)$ to the optimal control problem (3.1)-(3.4).

3.4 Existence and Uniqueness of Optimal Control

First, we show that there exists an optimal control pair that minimizes the objective functional given in (3.5). Let $(s,i,v,c)(u_1,u_2)$ be the state solution of the system (3.1)-(3.4) corresponding to the controls $(u_1,u_2) \in \mathcal{U}$ where

$$\mathcal{U} = \left\{(u_1,u_2) \in L^2(Q)^2 : 0 \leq u_i \leq M_i \text{ a.e. for } i = 1,2\right\}.$$

3.4.1 Existence of the Optimal Controls

Theorem 3.3. *There exists* $(u_1^*, u_2^*) \in \mathcal{U}$ *such that*

$$J(u_1^*, u_2^*) = \inf_{(u_1,u_2)\in\mathcal{U}} J(u_1,u_2).$$

Proof: Since the controls and the state variables are uniformly bounded and non-negative,

$$\inf_{(u_1,u_2)\in\mathcal{U}} J(u_1,u_2) \geq 0$$

and thus there exists a minimizing sequence (u_1^n, u_2^n) such that

$$\lim_{n\to\infty} J(u_1^n, u_2^n) = \inf\{J(u_1,u_2)|u_1,u_2 \in \mathcal{U}\}$$

Using Theorem 3.1, let us define for each n,

$$(s_n, i_n, v_n, c_n) = \big(s(u_1^n, u_2^n), i(u_1^n, u_2^n), v(u_1^n, u_2^n), c(u_1^n, u_2^n)\big)$$

Using Theorem 3.2, we have $||s^n||$, $||i^n||$ and $||v^n||$ are uniformly bounded (independent of n) in the space $\mathcal{V}$ and $||s_t^n||$, $||i_t^n||$ and $||v_t^n||$ are uniformly bounded in $\mathcal{V}^*$. Also $||c^n||$ and $||c_t^n||$ are uniformly bounded in $L^2(Q)$. Then, from equation (3.4) and the L^∞ bounds on state variables and controls, the sequence $\{c_n'\}$ is uniformly bounded in $L^\infty(Q)$. Hence the sequence $\{c_n\}$ is uniformly equicontinuous. Then by the Arzela-Ascoli Theorem, the sequence has subsequence that is uniformly convergent in $L^2(Q)$. Thus for each x, $c_n(x,t) \to c^*(x,t)$ uniformly.
Now, from the boundedness of state variables and the fact that $u_1^n, u_2^n \in L^\infty(Q)$, there exist $(s^*, i^*, v^*, c^*, u_1^*, u_2^*)$ and subsequences $(s^n, i^n, v^n, u_1^n, u_2^n)$ such that

$$s_n \rightharpoonup s^*, i_n \rightharpoonup i^* \text{ and } v_n \rightharpoonup v^* \quad \textit{weakly in } \mathcal{V}$$

and

$$u_1^n \rightharpoonup u_1^* \text{ and } u_2^n \rightharpoonup u_2^* \quad \textit{weakly in } L^2(Q).$$

Again, from the above weak convergences, the uniform bounds and the PDE's, we can extract weakly convergent subsequences

$$(s_n)_t \rightharpoonup s_t^*, (i_n)_t \rightharpoonup i_t^* \text{ and } (v_n)_t \rightharpoonup v_t^* \quad \textit{weakly in } \mathcal{V}^*.$$

Next, we show that (s^*, i^*, v^*, c^*) are the states associated with the control (u_1^*, u_2^*). The weak formulation of the system (3.1)-(3.3) satisfied by s^n, i^n, v^n with test functions $\phi_1, \phi_2, \phi_3 \in \mathcal{V}$ is

$$\int_0^T < s_t^n, \phi_1 > dt + d \int_Q \nabla s^n \cdot \nabla \phi_1 dxdt = \int_Q \mathcal{F}(s^n, i^n, c^n, u_1^n)\phi_1 dxdt; \tag{3.29}$$

$$\int_0^T < i_t^n, \phi_2 > dt + d_1 \int_Q \nabla i^n \cdot \nabla \phi_2 dxdt = \int_Q \mathcal{G}(s^n, i^n, c^n)\phi_2 dxdts; \tag{3.30}$$

$$\int_0^T < v_t^n, \phi_3 > dt + d \int_Q \nabla v \cdot \nabla \phi_3 dxdt = \int_Q \mathcal{H}(s^n, u_1^n)\phi_3 dxdt; \tag{3.31}$$

together with initial and boundary conditions

$$s^n(x,0) = s^0(x), i^n(x,0) = i^0(x), v^n(x,0) = v^0(x) \quad \text{for } x \in \Omega.$$
$$s^n(x,t) = i^n(x,t) = v^n(x,t) = 0 \qquad \text{for } (x,t) \in \partial\Omega \times [0,T].$$

Also, the differential equation satisfied by c^n is

$$c^n(x,t) = c_0(x) + \int_0^T \mathcal{N}(s^n, i^n, v^n, c^n, u_2^n)(x,t)dt; \tag{3.32}$$

with $c^n(x,0) = c^0(x)$ for $x \in \Omega$ and $c^n(x,t) = 0$ on $\Omega \times [0,T]$

To pass the limit in the above system $(3.29) - (3.32)$, we need stronger convergence results. Since $\{s^n\}$ is uniformly bounded in $\mathcal{V}$ with $\{(s^n)_t\}$ uniformly bounded in $\mathcal{V}^*$, then by a compactness theorem [47], there exists a subsequence $\{s_n\}$ converging strongly to s^* in $L^2(Q)$. Similarly on subsequences,

$$i_n \to i^* \text{ strongly in } L^2(Q) \text{ and}$$
$$v_n \to v^* \text{ strongly in } L^2(Q).$$

Now, using the weak convergences on the controls, the L^∞ bounds on the corresponding state sequences as well as strong convergence of the sequences of the state

variables, we illustrate the convergence of several terms:

$$\begin{aligned}\left|\int_Q s^n u_1^n \phi_1 - s^* u_1^* \phi_1 dxdt\right| &= \left|\int_Q s^n u_1^n \phi_1 - s^* u_1^n \phi_1 + s^* u_1^n \phi_1 - s^* u_1^* \phi_1 dxdt\right| \\ &\leq \left|\int_Q u_1^n (s^n - s^*)\phi_1 dxdt\right| + \left|\int_Q (u_1^n - u_1^*) s^* \phi_1 dxdt\right| \\ &\leq \int_Q |u_1^n||s^n - s^*||\phi_1| dxdt + \left|\int_Q (u_1^n - u_1^*) s^* \phi_1 dxdt\right| \to 0 \; as \; n \to \infty.\end{aligned}$$

Since the first integral converges to zero as u_1^n is uniformly bounded and the Hölder inequality and the strong convergence $s^n \to s^*$ in $L^2(Q)$ implies

$$\int_Q |u_1^n||s^n - s^*||\phi_1| dxdt \leq M\bigg(\int_Q |s^n - s^*|^2\bigg)^{\frac{1}{2}}\bigg(\int_Q |\phi|^2\bigg)^{\frac{1}{2}} \to 0 \; as \; n \to \infty.$$

The second integral converges to zero as the state variable, s^*, is L^∞ bounded and $\phi \in \mathcal{V} \subset L^2(Q)$ implies $s^*\phi_1 \in L^2(Q)$ and the weak convergence of $u_1^n \to u_1^*$ in $L^2(Q)$ implies

$$\left|\int_Q (u_1^n - u_1^*) s^* \phi_1 dxdt\right| \to 0 \; as \; n \to \infty.$$

Similarly,

$$\begin{aligned}\left|\lim_{n\to\infty}\int_Q s^n i^n \phi_1 - s^* i^* \phi_1 dxdt\right| &= \lim_{n\to\infty}\left|\int_Q s^n i^n \phi_1 - s^n i^* \phi_1 + s^n i^* \phi_1 - s^* i^* \phi_1 dxdt\right| \\ &\leq ||s^n||_{L^\infty} \lim_{n\to\infty}\int_Q |i^n - i^*|^2 dxdt)^{\frac{1}{2}}(\int_Q |\phi_1|^2 dxdt)^{\frac{1}{2}} \\ &+ ||i^*||_{L^\infty} \lim_{n\to\infty}\int_Q |s^n - s^*|^2 dxdt)^{\frac{1}{2}}(\int_Q |\phi_1|^2 dxdt)^{\frac{1}{2}} \to 0;\end{aligned}$$

$$\begin{aligned}&\lim_{n\to\infty}\left|\int_Q [s_n^2 - (s^*)^2]\phi_1 dxdt\right| \\ &\qquad \leq 2M \lim_{n\to\infty}\bigg(\int_Q |s^n - s^*|^2 dxdt\bigg)^{\frac{1}{2}}\bigg(\int_Q |\phi_1|^2 dxdt\bigg)^{\frac{1}{2}} dxdt \to 0;\end{aligned}$$

$$\lim_{n\to\infty}\int_0^T < s_t^n - s_t^*, \phi_1 > dt = 0;$$

and

$$\lim_{n\to\infty}\int_Q d\nabla(s^n - s^*)\cdot\nabla\phi_1 dxdt = 0.$$

All the other limits follow similarly.

With above strong convergence results, we can now pass the limit in the system (3.29) − (3.32) to get a PDE system for the variables (s^*, i^*, v^*, c^*) with controls (u_1^*, u_2^*). Hence, we conclude that

$$(s^*, i^*, v^*, c^*) = (s, i, v, c)(u_1^*, u_2^*).$$

Thus,

$$\begin{aligned}
J(u_1^*, u_2^*) &= \int_0^T\int_\Omega \big[A_1 i^*(x,t) + A_2 c^*(x,t) + \{B_1 u_1^*\big(s^*(x,t) + i^*(x,t)\big) \\
&\qquad + B_2 u_2^* c^*(x,t) + C_1 u_1^*(x,t)^2 + C_2 u_2^*(x,t)^2\}\big]dxdt \\
&\le \liminf_{n\to\infty}\int_0^T\int_\Omega \big[A_1 i^n(x,t) + A_2 c^n(x,t) + \{B_1 u_1^n\big(s^n(x,t) + i^n(x,t)\big) \\
&\qquad + B_2 u_2^n c^n(x,t) + C_1 u_1^n(x,t)^2 + C_2 u_2^n(x,t)^2\}\big]dxdt \\
&= \inf\{J(u_1,u_2)|(u_1,u_2)\in\mathcal{U}\},
\end{aligned}$$

which implies that (u_1^*, u_2^*) is an optimal control for the problem (3.5).■

3.4.2 Derivation of the Optimality System

We derive the optimality system which consists of the state system coupled with the adjoint system and optimal control characterization. To charecterize the optimal control, we have to differentiate the mapping $(u_1, u_2) \to J(u_1, u_2)$ with respect to the controls u_1 and u_2. But since (s, i, v, c) are all functions of (u_1, u_2), we also need to differentiate the mapping $(u_1, u_2) \to (s, i, v, c)(u_1, u_2)$ with respect to the controls u_1

and u_2. These derivatives states with respect to the controls are called sensitivity functions.

Lemma 3.3.1. *Let $(u_1, u_2) \in \mathcal{U}$ with the corresponding state solution $(s, i, v, c)(u_1, u_2)$. Let $(u_1^\epsilon, u_2^\epsilon)$ be another control pair corresponding to the state solution $(s^\epsilon, i^\epsilon, v^\epsilon, c^\epsilon) = (s, i, v, c)(u_1^\epsilon, u_2^\epsilon)$ with*

$$(u_1^\epsilon, u_2^\epsilon) = (u_1 + \epsilon k_1, u_2 + \epsilon k_2),$$

where $(u_1^\epsilon, u_2^\epsilon) \in \mathcal{U}$ for all sufficiently small $\epsilon > 0$ with $k_1, k_2 \in L^\infty(Q)$. Then for any $(u_1, u_2) \in \mathcal{U}$, the mapping $(u_1, u_2) \to \big(s, i, v, c\big)(u_1, u_2)$ is weakly differentiable in the directional derivative sense and there exists $\psi_i \in \mathcal{V}$ with $(\psi_i)_t \in \mathcal{V}^*$ for $i = 1, 2, 3$ and $\psi_4, (\psi_4)_t \in L^2(Q)$ such that as $\epsilon \to 0^+$ we have that,

$$\frac{s^\epsilon - s}{\epsilon} \rightharpoonup \psi_1,$$

$$\frac{i^\epsilon - i}{\epsilon} \rightharpoonup \psi_2,$$

$$\frac{v^\epsilon - v}{\epsilon} \rightharpoonup \psi_3$$

weakly in $\mathcal{V}$ and

$$\frac{c^\epsilon - c}{\epsilon} \rightharpoonup \psi_4$$

weakly in $L^2(Q)$. Also, for each x, $\frac{c^\epsilon - c}{\epsilon} \to \psi_4$ pointwise in t. Furthermore, the sensitivity functions $(\psi_1, \psi_2, \psi_3, \psi_4)$ satisfy the weak form of $\mathcal{L}\psi = K$, where

$$\mathcal{L}\psi = \begin{pmatrix} (\psi_1)_t - d\triangle\psi_1 \\ (\psi_2)_t - d_1\triangle\psi_2 \\ (\psi_3)_t - d\triangle\psi_3 \\ (\psi_4)_t \end{pmatrix} + M \begin{pmatrix} \psi_1 \\ \psi_2 \\ \psi_3 \\ \psi_4 \end{pmatrix}, \; K = \begin{pmatrix} -k_1 s \\ 0 \\ k_1 s \\ -k_2 c \end{pmatrix},$$

where $M = (m_{i,j})$ *is a* 4×4 *coefficient matrix with*

$$m_{1,1} = -r + \frac{2r}{K}(s+v) + \theta_c c + \theta_i i + u_1;\ m_{1,2} = +\theta_i s;\ m_{1,3} = -r + \frac{2r}{K}(s+v);$$
$$m_{1,4} = \theta_c s;$$
$$m_{2,1} = -\theta_c c - \theta_i i;\ m_{2,2} = -\theta_i s + \gamma;\ m_{2,3} = 0;\ m_{2,4} = -\theta_c s;$$
$$m_{3,1} = -u_1;\ m_{3,2} = 0;\ m_{3,3} = 0;\ m_{3,4} = 0;$$
$$m_{4,1} = \alpha c;\ m_{4,2} = -\gamma + \alpha c;\ m_{4,3} = \alpha c;\ m_{4,4} = \alpha(s+i+v) + (u_2 + p);$$

and where the initial and boundary conditions for ψ_i *are* $\psi_i(x,0) = 0$ *for* $i = 1, ..., 4$ *and,* $\psi_1 = \psi_2 = \psi_3 = 0$ *on* $\partial\Omega \times (0,T)$.

Proof: Since $(s^\epsilon, i^\epsilon, v^\epsilon, c^\epsilon)$ is the state corresponding to the control pair $(u_1^\epsilon, u_2^\epsilon)$, the system $(3.6) - (3.9)$ with control pair $(u_1^\epsilon, u_2^\epsilon)$ is written as

$$\int_0^T < s_t^\epsilon, \phi_1 > dt + d\int_Q \nabla s^\epsilon \cdot \nabla \phi_1 dxdt = \int_Q \mathcal{F}(s^\epsilon, i^\epsilon, v^\epsilon, c^\epsilon, u_1^\epsilon)\phi_1 dxdt;$$
$$\int_0^T < i_t^\epsilon, \phi_2 > dt + d_1\int_Q \nabla i^\epsilon \cdot \nabla \phi_2 dxdt = \int_Q \mathcal{G}(s^\epsilon, i^\epsilon, c^\epsilon)\phi_2 dxdt;$$
$$\int_0^T < v_t^\epsilon, \phi_3 > dt + d\int_Q \nabla v^\epsilon \cdot \nabla \phi_3 dxdt = \int_Q \mathcal{H}(s^\epsilon, u_1^\epsilon)\phi_3 dxdt;$$
$$c_t^\epsilon = c^0(x) + \int_0^t \mathcal{N}(s^\epsilon, i^\epsilon, v^\epsilon, c^\epsilon, u_2^\epsilon)ds; \qquad for\ x \in \Omega$$

for any test functions $\phi_1, \phi_2, \phi_3 \in \mathcal{V}$ and $\phi_4 \in L^2(Q)$.
The initial and boundary conditions are

$$s^\epsilon(x,0) = s^0(x), i^\epsilon(x,0) = i^0(x), v^\epsilon(x,0) = v^0(x), c^\epsilon(x,0) = c^0(x),\ \text{for } x \in \Omega.$$
$$s^\epsilon(x,t) = i^\epsilon(x,t) = v^\epsilon(x,t) = 0; \qquad \text{for } \ (x,t) \in \partial\Omega \times (0,T).$$

The weak form of the equations satisfied by $(\frac{s^\epsilon - s}{\epsilon}, \frac{i^\epsilon - i}{\epsilon}, \frac{v^\epsilon - v}{\epsilon}, \frac{c^\epsilon - c}{\epsilon})$ are,

$$\int_0^T < (\frac{s^\epsilon - s}{\epsilon})_t, \phi_1 > dt + d \int_Q \nabla(\frac{s^\epsilon - s}{\epsilon}) \cdot \nabla \phi_1 dxdt = \int_Q \frac{\mathcal{F}(s^\epsilon, i^\epsilon, c^\epsilon, u_1^\epsilon) - \mathcal{F}(s, i, c, u_1)}{\epsilon} \phi_1 dxdt; \tag{3.33}$$

$$\int_0^T < (\frac{i^\epsilon - i}{\epsilon})_t, \phi_2 > dt + d_1 \int_Q \nabla(\frac{i^\epsilon - i}{\epsilon}) \cdot \nabla \phi_2 dxdt = \int_Q \frac{\mathcal{G}(s^\epsilon, i^\epsilon, c^\epsilon) - \mathcal{G}(s, i, c)}{\epsilon} \phi_2 dxdt; \tag{3.34}$$

$$\int_0^T < (\frac{v^\epsilon - v}{\epsilon})_t, \phi_3 > dt + d \int_Q \nabla(\frac{v^\epsilon - v}{\epsilon}) \cdot \nabla \phi_3 dxdt = \int_Q \frac{\mathcal{H}(s^\epsilon, u_1^\epsilon) - \mathcal{H}(s, u_1)}{\epsilon} \phi_2 dxdt; \tag{3.35}$$

$$(\frac{c^\epsilon - c}{\epsilon})_t = \int_Q \frac{\mathcal{N}(s^\epsilon, i^\epsilon, c^\epsilon, v^\epsilon, u_2^\epsilon) - \mathcal{N}(s, i, c, v, u_2)}{\epsilon} \phi_2 dxdt; \tag{3.36}$$

for any test functions $\phi_1, \phi_2, \phi_3 \in \mathcal{V}$ and $\phi_4 \in L^2(Q)$ and together with initial and boundary conditions

$$\frac{s^\epsilon - s}{\epsilon}(x,0) = 0, \ \frac{i^\epsilon - i}{\epsilon}(x,0) = 0, \ \frac{v^\epsilon - v}{\epsilon}(x,0) = 0, \ \frac{c^\epsilon - c}{\epsilon}(x,0) = 0; \qquad \text{for } x \in \Omega$$
$$\frac{s^\epsilon - s}{\epsilon}(x,t) = \frac{i^\epsilon - i}{\epsilon}(x,t) = \frac{v^\epsilon - v}{\epsilon}(x,t) = 0 \qquad \text{for } (x,t) \in \partial\Omega \times (0,T).$$

Similar to the proof of Theorem 3.1, we multiply each of the equations of the system (3.1)-(3.4) by appropriate test functions and integrate over $Q_\tau = \Omega \times (0, \tau)$ for $\tau \in (0, T)$ and add the equations

$$\begin{aligned} \sup_{\tau \in [0,T]} \Bigg(\int_\Omega [(\frac{s^\epsilon - s}{\epsilon})^2(x,\tau) + (\frac{i^\epsilon - i}{\epsilon})^2(x,\tau) + (\frac{v^\epsilon - v}{\epsilon})^2(x,\tau) + (\frac{c^\epsilon - c}{\epsilon})^2(x,\tau)] dx \Bigg) \\ + d_0 \int_{Q_\tau} \big[|\nabla \frac{s^\epsilon - s}{\epsilon}|^2 + |\nabla \frac{i^\epsilon - i}{\epsilon}|^2 + |\nabla \frac{v^\epsilon - v}{\epsilon}|^2 \big] dxdt \\ \leq \tilde{C} \int_Q (k_1^2 + k_2^2) dxdt. \end{aligned} \tag{3.37}$$

where $d_0, \tilde{C}$ depends on the bounds of the states, controls, and coefficients. After using Gronwall's Inequality and taking the supremum over [0,T] we get that, $||\frac{s^\epsilon - s}{\epsilon}||$, $||\frac{i^\epsilon - i}{\epsilon}||$, $||\frac{v^\epsilon - v}{\epsilon}||$ are uniformly bounded in $\mathcal{V}$ and similarly as before $||\big(\frac{s^\epsilon - s}{\epsilon}\big)_t||$, $||\big(\frac{i^\epsilon - i}{\epsilon}\big)_t||$, $||\big(\frac{v^\epsilon - v}{\epsilon}\big)_t||$ are uniformly bounded in $\mathcal{V}^*$. Also, $||\frac{c^\epsilon - c}{\epsilon}||$ and $||\big(\frac{c^\epsilon - c}{\epsilon}\big)_t||$ are uniformly bounded in $L^2(Q)$. Hence, the quotients $\{\frac{s^\epsilon - s}{\epsilon}, \frac{i^\epsilon - i}{\epsilon}, \frac{v^\epsilon - v}{\epsilon}\}$ converge weakly in $\mathcal{V}$ and $\{(\frac{s^\epsilon - s}{\epsilon})_t, (\frac{i^\epsilon - i}{\epsilon})_t, (\frac{v^\epsilon - v}{\epsilon})_t\}$ converge weakly in $\mathcal{V}^*$. Also, the

quotients $\{\frac{c^\epsilon - c}{\epsilon}, (\frac{c^\epsilon - c}{\epsilon})_t\}$ converges weakly in $L^2(Q)$. Then by using Simon's result [47], we get the quotients $\{\frac{s^\epsilon - s}{\epsilon}, \frac{i^\epsilon - i}{\epsilon}, \frac{v^\epsilon - v}{\epsilon}, \frac{c^\epsilon - c}{\epsilon}\}$ converge strongly to $\{\psi_1, \psi_2, \psi_3, \psi_4\}$ in $L^2(Q)$ Thus,

$$
\begin{aligned}
&\mathcal{F}(s^\epsilon, i^\epsilon, v^\epsilon, c^\epsilon, u_1^\epsilon) - \mathcal{F}(s, i, v, c, u_1) \\
&\quad = rn^\epsilon(1 - \frac{n^\epsilon}{K}) - \theta_c s^\epsilon c^\epsilon - \theta_i s^\epsilon i^\epsilon - u_1^\epsilon s^\epsilon - rn(1 - \frac{n}{K}) + \theta_c sc + \theta_i si + u_1 s \\
&\quad = r(n^\epsilon - n) - \frac{r}{K}[(n^\epsilon)^2 - n^2] - \theta_c[s^\epsilon c^\epsilon - sc] - \theta_i\big[s^\epsilon i^\epsilon - si\big] - [u_1^\epsilon s^\epsilon - u_1 s] \\
&\quad = r\big[(s^\epsilon - s) + (v^\epsilon - v)\big] - \frac{r}{K}\big[\{(s^\epsilon + s + v^\epsilon + v)\}\{(s^\epsilon - s) + (v^\epsilon - v)\}\big] \\
&\qquad - \theta_c\big[(s^\epsilon - s)c^\epsilon + s(c^\epsilon - c)\big] - \theta_i\big[(s^\epsilon - s)i^\epsilon + (i^\epsilon - i)s\big] - [u_1(s^\epsilon - s) + \epsilon k_1 s^\epsilon].
\end{aligned}
$$

Similarly,

$$
\begin{aligned}
&\mathcal{G}(s^\epsilon, i^\epsilon, c^\epsilon) - \mathcal{G}(s, i, c) \\
&\qquad = \theta_c s^\epsilon c^\epsilon + \theta_i s^\epsilon i^\epsilon - \gamma i^\epsilon - \theta_c sc - \theta_i si + \gamma i \\
&\qquad = \theta_c[s^\epsilon c^\epsilon - sc] + \theta_i\big[s^\epsilon i^\epsilon - si\big] - \gamma(i^\epsilon - i) \\
&\qquad = \theta_c\big[(s^\epsilon - s)c^\epsilon + s(c^\epsilon - c)\big] + \theta_i\big[(s^\epsilon - s)i^\epsilon + (i^\epsilon - i)s\big] - \gamma(i^\epsilon - i).
\end{aligned}
$$

Also, $\mathcal{H}(s^\epsilon, u_1^\epsilon) - \mathcal{H}(s, u_1) = u_1^\epsilon s^\epsilon - u_1 s = u_1(s^\epsilon - s) + \epsilon k_1 s^\epsilon$. and

$$
\begin{aligned}
&\mathcal{N}(s^\epsilon, i^\epsilon, v^\epsilon, c^\epsilon, u_2^\epsilon) - \mathcal{N}(s, i, v, c, u_2) \\
&\quad = \gamma i^\epsilon - \alpha(s^\epsilon + i^\epsilon + v^\epsilon)c^\epsilon - u_2^\epsilon c^\epsilon - \gamma i + \alpha(s + i + v)c + u_2 c \\
&\quad = \gamma(i^\epsilon - i) - \alpha[(s^\epsilon - s)c^\epsilon + s(c^\epsilon - c) + (i^\epsilon - i)c^\epsilon + i(c^\epsilon - c) + (v^\epsilon - v)c^\epsilon + v(c^\epsilon - c)] \\
&\quad - [(u_2 + p)(c^\epsilon - c) + \epsilon k_2 c^\epsilon]
\end{aligned}
$$

Thus as $\epsilon \to 0^+$,

$$
\begin{aligned}
&\frac{1}{\epsilon}[\mathcal{F}(s^\epsilon, i^\epsilon, v^\epsilon, c^\epsilon, u_1^\epsilon) - \mathcal{F}(s, i, v, a, c, u_1)] \\
&\implies r(\psi_1 + \psi_3) - \frac{2r}{K}(s + v)(\psi_1 + \psi_3) - \theta_c(\psi_1 c + \psi_4 s) - \theta_i(\psi_1 i + \psi_2 s) - u_1\psi_1 - k_1 s \\
&\quad = -(-r + \frac{2r}{K}(s + v) + \theta_c c + \theta_i i + u_1)\psi_1 - (\theta_i s)\psi_2 - (-r + \frac{2r}{K}(s + v))\psi_3 - (\theta_c s)\psi_4 - k_1 s.
\end{aligned}
$$

Similarly,

$$\frac{1}{\epsilon}[\mathcal{G}(s^\epsilon, i^\epsilon, a^\epsilon, c^\epsilon) - \mathcal{G}(s, i, a, c)]$$

$$\implies \theta_c(\psi_1 c + \psi_4 s) + \theta_i(\psi_1 i + \psi_2 s) - \gamma\psi_2$$

$$= -(-\theta_c s - \theta_i i)\psi_1 - (-\theta_i s + \gamma)\psi_2 - (-\theta_c s)\psi_4;$$

$$\frac{1}{\epsilon}[\mathcal{H}(s^\epsilon, u_1^\epsilon) - \mathcal{H}(s, u_1)] \implies u_1\psi_1 + k_1 s;$$

and

$$\frac{1}{\epsilon}[\mathcal{N}(s^\epsilon, i^\epsilon, v^\epsilon, c^\epsilon, u_2^\epsilon) - \mathcal{N}(s, i, v, c, u_2)]$$

$$\implies \gamma\psi_2 - \alpha[(\psi_1 + \psi_2 + \psi_3)c + (s + i + v)\psi_4] - (u_2 + p)\psi_4 - k_2 c$$

$$= -(\alpha c)\psi_1 - (-\gamma + \alpha c)\psi_2 - (\alpha c)\psi_3 - (\alpha(s + i + v) + u_2 + p)\psi_4 - k_2 c.$$

Hence, the limit of the system (3.33)-(3.36) becomes

$$\int_0^T < (\psi_1)_t, \phi_1 > dt + d\int_Q \nabla\psi_1 \cdot \nabla\phi_1 dxdt = \int_Q \mathcal{F}_1(s, i, v, c, u_1, \psi_1, \psi_2, \psi_3, \psi_4)\phi_1 dxdt;$$

$$\int_0^T < (\psi_2)_t, \phi_2 > dt + d_1\int_Q \nabla\psi_2 \cdot \nabla\phi_2 dxdt = \int_Q \mathcal{G}_1(s, i, c, \psi_1, \psi_2, \psi_4)\phi_2 dxdt;$$

$$\int_0^T < (\psi_3)_t, \phi_3 > dt + d\int_Q \nabla\psi_3 \cdot \nabla\phi_3 dxdt = \int_Q \mathcal{H}_1(s, u_1, \psi_1)\phi_3 dxdt;$$

$$\psi_4(x, t) = \int_0^t \mathcal{N}_1(s, i, v, c, u_2, \psi_1, \psi_2, \psi_3, \psi_4)ds;$$

where,

$$\mathcal{F}_1 = -(-r + \frac{2r}{K}(s + v) + \theta_c c + \theta_i i + u_1)\psi_1 - (\theta_i s)\psi_2 - (-r + \frac{2r}{K}(s + v))\psi_3 - (\theta_c s)\psi_4 - k_1 s;$$

$$\mathcal{G}_1 = -(-\theta_c s - \theta_i i)\psi_1 - (-\theta_i s + \gamma)\psi_2 - (-\theta_c s)\psi_4;$$

$$\mathcal{H}_1 = u_1\psi_1 + k_1 s; \ \textit{and}$$

$$\mathcal{N}_1 = -(\alpha c)\psi_1 - (-\gamma + \alpha c)\psi_2 - (\alpha c)\psi_3 - (\alpha(s + i + v) + u_2 + p)\psi_4 - k_2 c.$$

Thus, our sensitivity system is,

$$(\psi_1)_t - d\triangle\psi_1 + (-r + \frac{2r}{K}(s+v) + \theta_c c + \theta_i i + u_1)\psi_1 + (\theta_i s)\psi_2 + (-r + \frac{2r}{K}(s+v))\psi_3 + (\theta_c s)\psi_4 = -k_1 s; \tag{3.38}$$

$$(\psi_2)_t - d_1\triangle\psi_2 + (-\theta_c s - \theta_i i)\psi_1 + (-\theta_i s + \gamma)\psi_2 + (-\theta_c s)\psi_4 = 0; \tag{3.39}$$

$$(\psi_3)_t - d\triangle\psi_3 - u_1\psi_1 = k_1 s; \tag{3.40}$$

$$(\psi_4)_t + (\alpha c)\psi_1 + (-\gamma + \alpha c)\psi_2 + (\alpha c)\psi_3 + (\alpha(s+i+v) + u_2 + p)\psi_4 = -k_2 c. \tag{3.41}$$

together with the initial and boundary conditions

$\psi_i(x,0) = 0$ for $x \in \Omega$, $i = 1, ..., 4$ and,

$\psi_1 = \psi_2 = \psi_3 = 0$ for $(x,t) \in \partial\Omega \times (0,T)$.■

To derive the optimality system and to characterize the optimal control, we need adjoint variables and the adjoint of the operators associated with sensitivities $(\psi_1, \psi_2, \psi_3, \psi_4)$. The sensitivity $(\psi_i)_{i=1}^4$ PDE system $(3.37) - (3.40)$ can be written as,

$$\mathcal{L}\begin{pmatrix}\psi_1\\ \psi_2\\ \psi_3\\ \psi_4\end{pmatrix} = \begin{pmatrix}-k_1 s\\ 0\\ k_1 s\\ -k_2 c\end{pmatrix} \tag{3.42}$$

where the linear operator $\mathcal{L}$ is defined as

$$\mathcal{L}\begin{pmatrix}\psi_1\\ \psi_2\\ \psi_3\\ \psi_4\end{pmatrix} = \begin{pmatrix}\mathcal{L}_1\psi_1\\ \mathcal{L}_2\psi_2\\ \mathcal{L}_3\psi_3\\ \mathcal{L}_4\psi_4\end{pmatrix} + M\begin{pmatrix}\psi_1\\ \psi_2\\ \psi_3\\ \psi_4\end{pmatrix},$$

for

$$\begin{pmatrix} \mathcal{L}_1\psi_1 \\ \mathcal{L}_2\psi_2 \\ \mathcal{L}_3\psi_3 \\ \mathcal{L}_4\psi_4 \end{pmatrix} = \begin{pmatrix} (\psi_1)_t - d\triangle\psi_1 \\ (\psi_2)_t - d_1\triangle\psi_2 \\ (\psi_3)_t - d\triangle\psi_3 \\ (\psi_4)_t \end{pmatrix}$$

and M is defined in Lemma 3.3.1.

We now find the equations for the adjoint functions which will be used to characterize our optimal control. The adjoint operator $\mathcal{L}^*$ is related to the operator $\mathcal{L}$ using weak formulation on both sides;

$$\int_0^T \int_\Omega \vec{\lambda}\mathcal{L}\vec{\psi}dxdt = \int_0^T \int_\Omega \vec{\psi}\mathcal{L}^*\vec{\lambda}dxdt, \tag{3.43}$$

where the sensitivity vector $\vec{\psi} = (\psi_1, \psi_2, \psi_3, \psi_4)^T$ is given in Theorem 3.3.1 and $\vec{\lambda} = (\lambda_1, \lambda_2, \lambda_3, \lambda_4) \in \mathcal{V}^3 \times L^2(Q)$ with $\big((\lambda_1)_t, (\lambda_2)_t, (\lambda_3)_t, (\lambda_4)_t\big) \in (\mathcal{V}^*)^3 \times L^2(Q)$ is called the adjoint vector.

Using (3.42) we have formally

$$\begin{aligned} \lambda\mathcal{L}\psi = (\lambda_1, \lambda_2, \lambda_3, \lambda_4) \begin{pmatrix} \mathcal{L}_1\psi_1 \\ \mathcal{L}_2\psi_2 \\ \mathcal{L}_3\psi_3 \\ \mathcal{L}_4\psi_4 \end{pmatrix} + (\lambda_1, \lambda_2, \lambda_3, \lambda_4) \begin{pmatrix} m_{1,1} & m_{1,2} & m_{1,3} & m_{1,4} \\ m_{2,1} & m_{2,2} & m_{2,3} & m_{2,4} \\ m_{3,1} & m_{3,2} & m_{3,3} & m_{3,4} \\ m_{4,1} & m_{4,2} & m_{4,3} & m_{4,4} \end{pmatrix} \begin{pmatrix} \psi_1 \\ \psi_2 \\ \psi_3 \\ \psi_4 \end{pmatrix}, \\ = \sum_{i=1}^4 \lambda_i\mathcal{L}_i\psi_i + \sum_{i=1}^4 \sum_{j=1}^4 \lambda_i m_{i,j}\psi_j. \end{aligned}$$

To find the specific expression of $\mathcal{L}^*$, we use integration by parts. For example,

$$\int_0^T \int_\Omega \lambda_1(\mathcal{L}_1\psi_1)dxdt = \int_0^T \int_\Omega \lambda_1\big[\{(\psi_1)_t - d\triangle\psi_1\}\big]dxdt \tag{3.44}$$

The first integral in the RHS of (3.44) is

$$\begin{aligned}\int_0^T \int_\Omega \lambda_1(\psi_1)_t &= \int_\Omega \lambda_1\psi_1\big|_0^T dS - \int_0^T \int_\Omega (\lambda_1)_t\psi_1 dxdt \\ &= \int_\Omega \lambda_1(x,T)\psi_1(x,T)dx - \int_0^T \int_\Omega (\lambda_1)_t\psi_1 dxdt. \\ &= -\int_0^T \int_\Omega (\lambda_1)_t\psi_1 dxdt\end{aligned}$$

if $\lambda_1(x,T) = 0, x \in \Omega$. Also, the second integral in the RHS of (3.44) is

$$\begin{aligned}\int_0^T \int_\Omega \lambda_1(d\triangle\psi_1) &= d\int_0^T \int_{\partial\Omega} \lambda_1(\nabla\psi_1\cdot\nu)dxdt - d\int_0^T \int_\Omega \nabla\lambda_1\cdot\nabla\psi_1 dxdt \\ &= d\int_0^T \int_{\partial\Omega} \lambda_1(\nabla\psi_1\cdot\nu)dSdt - d\int_0^T \int_{\partial\Omega} (\nabla\lambda_1\cdot\nu)\psi_1 dSdt + d\int_0^T \int_\Omega (\triangle\lambda_1)\psi_1 dxdt \\ &= d\int_0^T \int_\Omega (\triangle\lambda_1)\psi_1 dxdt\end{aligned}$$

if $\lambda(x,t) = 0$ on $\partial\Omega \times (0,T)$. Thus,

$$\begin{aligned}\int_0^T \int_\Omega \lambda_1(\mathcal{L}_1\psi_1)dxdt &= -\int_0^T \int_\Omega (\lambda_1)_t\psi_1 dxdt - d\int_0^T \int_\Omega (\triangle\lambda_1)\psi_1 dxdt \\ &= \int_0^T \int_\Omega [-(\lambda_1)_t - d(\triangle\lambda_1)]\psi_1 dxdt \\ &= \int_0^T \int_\Omega \psi_1(\mathcal{L}_1^*\lambda_1).\end{aligned}$$

Similar expressions can be generated for other integrals $\int_0^T \int_\Omega \lambda_i(\mathcal{L}_i\psi_i)dxdt$ for i=2,3,4.

Thus, we have formally

$$\begin{aligned}&\int_0^T \int_\Omega \Big[\lambda\mathcal{L}\psi\Big]dxdt \\ &= \int_0^T \int_\Omega \Big[(\lambda_1,\lambda_2,\lambda_3\lambda_4)\begin{pmatrix}\mathcal{L}_1\psi_1 \\ \mathcal{L}_2\psi_2 \\ \mathcal{L}_3\psi_3 \\ \mathcal{L}_4\psi_4 4\end{pmatrix} + (\lambda_1,\lambda_2,\lambda_3,\lambda_4)\begin{pmatrix}m_{1,1} & m_{1,2} & m_{1,3} & m_{1,4} \\ m_{2,1} & m_{2,2} & m_{2,3} & m_{2,4} \\ m_{3,1} & m_{3,2} & m_{3,3} & m_{3,4} \\ m_{4,1} & m_{4,2} & m_{4,3} & m_{4,4}\end{pmatrix}\begin{pmatrix}\psi_1 \\ \psi_2 \\ \psi_3 \\ \psi_4\end{pmatrix}\Big]dxdt\end{aligned}$$

$$
\begin{aligned}
&= \int_0^T \int_\Omega \left[(\psi_1, \psi_2, \psi_3, \psi_4) \begin{pmatrix} \mathcal{L}_1^* \lambda_1 \\ \mathcal{L}_2^* \lambda_2 \\ \mathcal{L}_3^* \lambda_3 \\ \mathcal{L}_4^* \lambda_4 \end{pmatrix} + (\psi_1, \psi_2, \psi_3, \psi_4) \begin{pmatrix} m_{1,1} & m_{2,1} & m_{3,1} & m_{4,1} \\ m_{1,2} & m_{2,2} & m_{3,2} & m_{4,2} \\ m_{1,3} & m_{2,3} & m_{3,3} & m_{4,3} \\ m_{1,4} & m_{2,4} & m_{3,4} & m_{4,4} \end{pmatrix} \begin{pmatrix} \lambda_1 \\ \lambda_2 \\ \lambda_3 \\ \lambda_4 \end{pmatrix} \right] dxdt \\
&= \int_0^T \int_\Omega \left[(\psi_1, \psi_2, \psi_3, \psi_4) \left[\begin{pmatrix} \mathcal{L}_1^* \lambda_1 \\ \mathcal{L}_2^* \lambda_2 \\ \mathcal{L}_3^* \lambda_3 \\ \mathcal{L}_4^* \lambda_4 \end{pmatrix} + M^\tau \begin{pmatrix} \lambda_1 \\ \lambda_2 \\ \lambda_3 \\ \lambda_4 \end{pmatrix} \right] \right] dxdt \\
&= \int_0^T \int_\Omega \Big[\psi \mathcal{L}^* \lambda \Big] dxdt
\end{aligned}
$$

where we used the Dirishlet boundary conditions and assumed the final time condition $\lambda_i(x, T) = 0$ for $i = 1, 2, 3, 4$ called as Transversality Condition. Here we used

$$
\mathcal{L}^* \begin{pmatrix} \lambda_1 \\ \lambda_2 \\ \lambda_3 \\ \lambda_4 \end{pmatrix} = \begin{pmatrix} \mathcal{L}_1^* \lambda_1 \\ \mathcal{L}_2^* \lambda_2 \\ \mathcal{L}_3^* \lambda_3 \\ \mathcal{L}_4^* \lambda_4 \end{pmatrix} + M^\tau \begin{pmatrix} \lambda_1 \\ \lambda_2 \\ \lambda_3 \\ \lambda_4 \end{pmatrix} = \begin{pmatrix} -(\lambda_1)_t - d(\triangle \lambda_1) \\ -(\lambda_2)_t - d_1(\triangle \lambda_2) \\ -(\lambda_3)_t - d(\triangle \lambda_3) \\ -(\lambda_4)_t \end{pmatrix} + M^\tau \begin{pmatrix} \lambda_1 \\ \lambda_2 \\ \lambda_3 \\ \lambda_4 \end{pmatrix}.
$$

Now for the adjoint system, we use source term from the derivative of the integrand in equation (3.5) with respect to the state variable:

$$
\mathcal{L}^* \vec{\lambda} = \begin{pmatrix} B_1 u_1 \\ A_1 + B_1 u_1 \\ 0 \\ A_2 + B_2 u_2 \end{pmatrix}
$$

where the rows in the right hand side of the above matrix are the derivative of the integrand in equation (3.5) with respect to s, i, v, c respectively. Thus the adjoint

system is

$$\begin{pmatrix} -(\lambda_1)_t - d(\triangle\lambda_1) \\ -(\lambda_2)_t - d_1(\triangle\lambda_2) \\ -(\lambda_3)_t - d(\triangle\lambda_3) \\ -(\lambda_4)_t \end{pmatrix} + M^\tau \begin{pmatrix} \lambda_1 \\ \lambda_2 \\ \lambda_3 \\ \lambda_4 \end{pmatrix} = \begin{pmatrix} B_1 u_1 \\ A_1 + B_1 u_1 \\ 0 \\ A_2 + B_2 u_2 \end{pmatrix}$$

with the final time conditions $\lambda_i(x,T) = 0$ *and* $i = 1,2,3,4$ for $x \in \Omega$ and the boundary conditions $\lambda_i(x,t) = 0$ for $i = 1,2,3$ and $(x,t) \in \partial\Omega \times (0,T)$.

Theorem 3.4. *Given an optimal control* $u = (u_1, u_2) \in \mathcal{U}$*, there exists a solution* $(\lambda_1, \lambda_2, \lambda_3, \lambda_4) \in \mathcal{V}^3 \times L^2(Q)$ *to the adjoint system*

$$\begin{pmatrix} -(\lambda_1)_t - d(\triangle\lambda_1) \\ -(\lambda_2)_t - d_1(\triangle\lambda_2) \\ -(\lambda_3)_t - d(\triangle\lambda_3) \\ -(\lambda_4)_t \end{pmatrix} + M^\tau \begin{pmatrix} \lambda_1 \\ \lambda_2 \\ \lambda_3 \\ \lambda_4 \end{pmatrix} = \begin{pmatrix} B_1 u_1^* \\ A_1 + B_1 u_1^* \\ 0 \\ A_2 + B_2 u_2^* \end{pmatrix} \tag{3.45}$$

with the final time conditions $\lambda_i(x,T) = 0$ *for* $i = 1,2,3,4$ *and* $x \in \Omega$ *and the boundary conditions*

$\lambda_i(x,t) = 0$ *for* $i = 1,2,3$ *and* $(x,t) \in \partial\Omega \times (0,T)$*, where the matrix* M^τ *is the transpose of matrix* M *given in the Lemma* (3.3.1)*. evaluated at the corresponding optimal states. Furthermore,*

$$u_1^*(x,t) = \min\left(M_1, max\big(-\frac{(\lambda_3 - \lambda_1 + B_1)s^* + B_1 i^*}{2C_1}, 0\big)\right) \tag{3.46}$$

$$u_2^*(x,t) = \min\left(M_2, max\big(-\frac{(B_2 - \lambda_4)c^*}{2C_2}, 0\big)\right) \tag{3.47}$$

Proof: Since the adjoint system (3.43) is linear in its variables, the solution exists by standard results. For the optimal control characterization, we compute the directional derivative of $J(u_1^*, u_2^*)$ with respect to (u_1^*, u_2^*) in the direction of (k_1, k_2) at (s^*, i^*, v^*, c^*).

Since $J(u_1^*, u_2^*)$ is the minimum, then for $(u_1^\epsilon, u_2^\epsilon) = (u_1^*, u_2^*) + \epsilon(k_1, k_2)$ with corresponding state solution $(s^\epsilon, i^\epsilon, v^\epsilon, c^\epsilon) = (s, i, v, c)(u_1^\epsilon, u_2^\epsilon)$,

$$
\begin{aligned}
0 &\leq \lim_{\epsilon \to 0^+} \frac{J(u_1^* + \epsilon k_1, u_2^* + \epsilon k_2) - J(u_1^*, u_2^*)}{\epsilon} \\
&= \lim_{\epsilon \to 0} \frac{1}{\epsilon} \int_Q \Big(A_1 i^\epsilon + A_2 c^\epsilon + \{B_1(u_1^* + \epsilon k_1)(s^\epsilon + i^\epsilon) + B_2(u_2^* + \epsilon k_2)c^\epsilon + C_1(u_1^* + \epsilon k_1)^2 \\
&\quad + C_2(u_2 + \epsilon k_2)^2)\}\big] - [A_1 i^* + A_2 c^* + \{B_1 u_1^*(s^* + i^*) + B_2 u_2^* c^* + C_1(u_1^*)^2 + C_2(u_2^*)^2\} \Big) dxdt. \\
&= \int_Q (A_1\psi_2 + A_2\psi_4 + B_1 u_1^*(\psi_1 + \psi_2) + B_1 k_1(s^* + i^*) + B_2 u_2^* \psi_4 + B_2 k_2 c^* \\
&\qquad + 2C_1 u_1^* k_1 + 2C_2 u_2^* k_2) dxdt \\
&= \int_Q (\psi_1, \psi_2, \psi_3, \psi_4) \begin{pmatrix} B_1 u_1^* \\ A_1 + B_1 u_1^* \\ 0 \\ A_2 + B_2 u_2^* \end{pmatrix} dxdt + \int_Q \big(B_1 k_1(s^* + i^*) + B_2 k_2 c^* + 2C_1 k_1 u_1^* \\
&\qquad + 2C_2 k_2 u_2^* \big) dxdt \\
&= \int_Q (\psi_1, \psi_2, \psi_3, \psi_4) \mathcal{L}^* \begin{pmatrix} \lambda_1 \\ \lambda_2 \\ \lambda_3 \\ \lambda_4 \end{pmatrix} dxdt + \int_Q \big(B_1 k_1(s^* + i^*) + B_2 k_2 c^* + 2C_1 k_1 u_1^* \\
&\qquad + 2C_2 k_2 u_2^* \big) dxdt \\
&= \int_Q (\lambda_1, \lambda_2, \lambda_3, \lambda_4) \mathcal{L} \begin{pmatrix} \psi_1 \\ \psi_2 \\ \psi_3 \\ \psi_4 \end{pmatrix} dxdt + \int_Q \big(B_1 k_1(s^* + i^*) + B_2 k_2 c^* + 2C_1 k_1 u_1^* + 2C_2 k_2 u_2^* \big) dxdt \\
&= \int_Q (\lambda_1, \lambda_2, \lambda_3, \lambda_4) \begin{pmatrix} -k_1 s \\ 0 \\ k_1 s \\ -k_2 c \end{pmatrix} dxdt + \int_Q \big(B_1 k_1(s^* + i^*) + B_2 k_2 c^* + 2C_1 k_1 u_1^* + 2C_2 k_2 u_2^* \big) dxdt
\end{aligned}
$$

$$= \int_Q k_1\big[(\lambda_3 - \lambda_1 + B_1)s^* + B_1 i^* + 2C_1 u_1^*\big] + k_2\big[(B_2 - \lambda_4)c^* + 2C_2 u_2^*\big]dxdt,$$

where we used sensitivities and adjoint equations in the weak sense. Now consider the following cases:

Case I: $k_2 = 0$

- For $\{(x,t)\big|0 < u_1^*(x,t) < M_1\}$, with a small ϵ and arbitrary k_1 with support on this set we have

$$\int_Q k_1\big[(\lambda_3 - \lambda_1 + B_1)s + B_1 i + 2C_1 u_1^*\big] \geq 0,$$

and then

$$(\lambda_3 - \lambda_1 + B_1)s^* + B_1 i^* + 2C_1 u_1^* = 0,$$

which implies

$$u_1^* = -\frac{(\lambda_3 - \lambda_1 + B_1)s^* + B_1 i^*}{2C_1}.$$

- For $\{(x,t)\big|u_1(x,t)^* = 0\}$, we can choose non-negative k_1 with support in this set, then

$$\int_Q k_1\big[(\lambda_3 - \lambda_1 + B_1)s^* + B_1 i^* + 2C_1 u_1^*\big] \geq 0,$$

which implies

$$(\lambda_3 - \lambda_1 + B_1)s^* + B_1 i^* + 2C_1 u_1^* \geq 0.$$

In other words,

$$0 = u_1^* \geq -\frac{(\lambda_3 - \lambda_1 + B_1)s^* + B_1 i^*}{2C_1}.$$

Hence

$$u_1^* = max\big(-\frac{(\lambda_3 - \lambda_1 + B_1)s^* + B_1 i^*}{2C_1}, 0\big)$$

- Finally, for $\{(x,t)\big|u_1^*(x,t) = M_1\}$, we can choose a non-positive k_1 with support in this set, then

$$\int_Q k_1\big[(\lambda_3 - \lambda_1 + B_1)s^* + B_1 i^* + 2C_1 u_1^*\big] \geq 0,$$

which implies

$$(\lambda_3 - \lambda_1 + B_1)s^* + B_1 i^* + 2C_1 u_1^* \leq 0.$$

In other words,

$$M_1 = u_1^* \leq -\frac{(\lambda_3 - \lambda_1 + B_1)s^* + B_1 i^*}{2C_1}.$$

Thus

$$u_1^* = min\big(-\frac{(\lambda_3 - \lambda_1 + B_1)s^* + B_1 i^*}{2C_1}, M_1\big)$$

Combining above three cases we get,

$$u_1^*(x) = min\bigg(M_1, max\big(-\frac{(\lambda_3 - \lambda_1 + B_1)s + B_1 i}{2C_1}, 0\big)\bigg)$$

Case II: $k_1 = 0$

We follow a method similar to above to get

$$u_2^*(x) = min\bigg(M_2, max\big(-\frac{(B_2 - \lambda_4)c}{2C_2}, 0\big)\bigg). \quad \blacksquare$$

3.4.3 Uniqueness of Optimal Controls

Next, we prove the uniqueness of the optimal controls. Our optimality system consists of the system of state PDE (3.1) − (3.4), the adjoint system (3.45), and the charecterization of controls (3.46) − (3.47).

Theorem 3.5. *For sufficiently small T, the solution to the optimality system is unique, which implies the uniqueness of the optimal control.*

Proof: Suppose $(s,i,v,c),(\lambda_1,\lambda_2,\lambda_3,\lambda_4)$ and $(\bar{s},\bar{i},\bar{v},\bar{c}),(\bar{\lambda}_1,\bar{\lambda}_2,\bar{\lambda}_3,\bar{\lambda}_4)$ are the two pairs each representing a solution of the state system $(3.1)-(3.4)$, adjoint system (3.45), and with the corresponding optimal controls $(3.46)-(3.47)$. Then

$$u_1(x,t) = min\bigg(M_1, max\big(-\frac{(\lambda_3-\lambda_1+B_1)s+B_1 i}{2C_1}, 0\big)\bigg)$$
$$u_2(x,t) = min\bigg(M_2, max\big(-\frac{(B_2-\lambda_4)c}{2C_2}, 0\big)\bigg).$$

and

$$\bar{u}_1(x,t) = min\bigg(M_1, max\big(-\frac{(\bar{\lambda}_3-\bar{\lambda}_1+B_1)\bar{s}+B_1\bar{i}}{2C_1}, 0\big)\bigg)$$
$$\bar{u}_2(x,t) = min\bigg(M_2, max\big(-\frac{(B_2-\bar{\lambda}_4)\bar{c}}{2C_2}, 0\big)\bigg).$$

Consider the change of variables

$$s = e^{at}k, i = e^{at}l, v = e^{at}m, c = e^{at}n, \lambda_1 = e^{-at}\zeta_1, \lambda_2 = e^{-at}\zeta_2, \lambda_3 = e^{-at}\zeta_3, \lambda_4 = e^{-at}\zeta_4,$$

and

$$\bar{s} = e^{at}\bar{k}, \bar{i} = e^{at}\bar{l}, \bar{v} = e^{at}\bar{m}, \bar{c} = e^{at}\bar{n}, \bar{\lambda}_1 = e^{-at}\bar{\zeta}_1, \bar{\lambda}_2 = e^{-at}\bar{\zeta}_2, \bar{\lambda}_3 = e^{-at}\bar{\zeta}_3, \bar{\lambda}_4 = e^{-at}\bar{\zeta}_4,$$

where $a > 0$ is to be chosen. Substituting k,l,m,n and $\bar{k},\bar{l},\bar{m},\bar{n}$ in the system $(3.1)-(3.4)$ and subtracting the equations from one another we get

$$a(k-\bar{k})+(k-\bar{k})_t = d\triangle(k-\bar{k})+r[(k-\bar{k})+(m-\bar{m})]-\frac{r}{K}e^{at}[(k+m)^2 - (\bar{k}+\bar{m})^2]-\theta_c e^{at}(kn-\bar{k}\bar{n})-\theta_i e^{at}(kl-\bar{k}\bar{l})-(u_1 k-\bar{u}_1\bar{k}); \tag{3.48}$$

$$a(l-\bar{l})+(l-\bar{l})_t = d_1\triangle(l-\bar{l})+\theta_c e^{at}(kn-\bar{k}\bar{n})+\theta_i e^{at}(kl-\bar{k}\bar{l})-\gamma(l-\bar{l}); \tag{3.49}$$

$$a(m-\bar{m})+(m-\bar{m})_t = d\triangle(m-\bar{m})+u_1k-\bar{u}_1\bar{k}; \tag{3.50}$$

$$\begin{aligned} a(n-\bar{n})+(n-\bar{n})_t =&\gamma(l-\bar{l})+\alpha e^{at}[(k+l+m)n-(\bar{k}+\bar{l}+\bar{m})\bar{n}] \\ &-p(n-\bar{n})-(u_2n-\bar{u}_2\bar{n}); \end{aligned} \tag{3.51}$$

with initial and boundary conditions

$$(k-\bar{k})(x,0)=(l-\bar{l})(x,0)=(m-\bar{m})(x,0)=(n-\bar{n})(x,0)=0 \text{ for } x\in\Omega$$

$$(k-\bar{k})=(l-\bar{l})=(m-\bar{m})=0 \text{ for } (x,t)\in\partial\Omega\times[0,T].$$

Also, the adjoint system (3.45) satisfied by $(\zeta_i-\bar{\zeta}_i)$ for $i=1,2,3,4$ has the form

$$\begin{aligned} &a(\zeta_1-\bar{\zeta_1})-(\zeta_1-\bar{\zeta_1})_t-d\triangle(\zeta_1-\bar{\zeta_1})-r(\zeta_1-\bar{\zeta_1})+\theta_ce^{at}(n\zeta_1-\bar{n}\bar{\zeta_1}) \\ &\quad+\frac{2r}{K}e^{at}\big[(k+m)\zeta_1-(\bar{k}+\bar{m})\bar{\zeta_1}\big]+\theta_ie^{at}(l\zeta_1-\bar{l}\bar{\zeta_1})+(u_1\zeta_1-\bar{u}_1\bar{\zeta_1}) \\ &\quad-\theta_ce^{at}(n\zeta_2-\bar{n}\bar{\zeta_2})-\theta_ie^{at}(l\zeta_2-\bar{l}\bar{\zeta_2})-(u_1\zeta_3-\bar{u}_1\bar{\zeta_3})+\alpha e^{at}(n\zeta_4-\bar{n}\bar{\zeta_4}) \\ &\quad=B_1(u_1-\bar{u}_1); \end{aligned} \tag{3.52}$$

$$\begin{aligned} &a(\zeta_2-\bar{\zeta_2})-(\zeta_2-\bar{\zeta_2})_t-d_1\triangle(\zeta_2-\bar{\zeta_2})+\theta_ie^{at}(k\zeta_1-\bar{k}\bar{\zeta_1})-\theta_ie^{at}(k\zeta_2-\bar{k}\bar{\zeta_2}) \\ &\quad-\gamma(\zeta_4-\bar{\zeta_4})+\alpha e^{at}(n\zeta_4-\bar{n}\bar{\zeta_4})=B_1(u_1-\bar{u}_1); \end{aligned} \tag{3.53}$$

$$\begin{aligned} &a(\zeta_3-\bar{\zeta_3})-(\zeta_3-\bar{\zeta_3})_t-d\triangle(\zeta_3-\bar{\zeta_3})-r(\zeta_1-\bar{\zeta_1})+\alpha e^{at}(n\zeta_4-\bar{n}\bar{\zeta_4}) \\ &\quad+\frac{2r}{K}e^{at}\big[(k+m)\zeta_1-(\bar{k}+\bar{m})\bar{\zeta_1}\big]=0; \end{aligned} \tag{3.54}$$

$$\begin{aligned} &a(\zeta_4-\bar{\zeta_4})-(\zeta_4-\bar{\zeta_4})_t+\theta_ce^{at}(k\zeta_1-\bar{k}\bar{\zeta_1})-\theta_ce^{at}(k\zeta_2-\bar{k}\bar{\zeta_2})+p(\zeta_4-\bar{\zeta_4}) \\ &\quad+\alpha e^{at}\big[(k+l+m)\zeta_4-(k+\bar{l}+\bar{m})\bar{\zeta_4}\big]+(u_2\zeta_4-\bar{u}_2\bar{\zeta_4})=B_2(u_2-\bar{u}_2); \end{aligned} \tag{3.55}$$

together with the final time conditions and the boundary conditions

$(\zeta_i-\bar{\zeta}_i)(x,T)=0;$ for $x\in\Omega$ and $i=1,2,3,4.$ and
$(\zeta_i-\bar{\zeta}_i)(x,t)=0$ for $(x,t)\in\partial\Omega\times(0,\infty)$ and $i=1,2,3,4$ respectively.

The weak formulation of the system (3.46) − (3.49) and (3.50) − (3.53) with appropriate test functions in $\mathcal{V}$ is

$$
\begin{aligned}
&a\int_Q (k-\bar{k})^2 dxdt + \frac{1}{2}\int_\Omega (k-\bar{k})^2(x,T)dx = -d\int_Q |\nabla(k-\bar{k})|^2 dxdt + r\int_Q (k-\bar{k})^2 dxdt \\
&+ r\int_\Omega (m-\bar{m})(k-\bar{k})dxdt - \frac{r}{K}\int_Q e^{at}[(k+m)^2 - (\bar{k}+\bar{m})^2](k-\bar{k})dxdt \\
&- \theta_c \int_Q e^{at}[k(n-\bar{n}) + \bar{n}(k-\bar{k})](k-\bar{k})dxdt - \int_Q (u_1 k - \bar{u}_1\bar{k})(k-\bar{k})dxdt \\
&- \theta_i e^{at}\int_Q [k(l-\bar{l}) + \bar{l}(k-\bar{k})](k-\bar{k})dxdt; \qquad (3.56)
\end{aligned}
$$

$$
\begin{aligned}
&a\int_Q (l-\bar{l})^2 dxdt + \frac{1}{2}\int_\Omega (l-\bar{l})^2(x,T)dx = -d_1\int_Q |\nabla(l-\bar{l})|^2 dxdt - \gamma\int_Q (l-\bar{l})^2 dxdt \\
&+ \theta_c \int_Q e^{at}(kn - \bar{k}\bar{n})(l-\bar{l})dxdt + \theta_i \int_Q e^{at}(kl - \bar{k}\bar{l})(l-\bar{l})dxdt; \qquad (3.57)
\end{aligned}
$$

$$
\begin{aligned}
&a\int_Q (m-\bar{m})^2 dxdt + \frac{1}{2}\int_\Omega (m-\bar{m})^2(x,T)dx = -d\int_Q |\nabla(m-\bar{m})|^2 dxdt \\
&\qquad + \int_Q (u_1 k - \bar{u}_1\bar{k})(m-\bar{m})dxdt; \qquad (3.58)
\end{aligned}
$$

$$
\begin{aligned}
&a\int_Q (n-\bar{n})^2 dxdt + \frac{1}{2}\int_\Omega (n-\bar{n})^2(x,T)dx = \gamma\int_Q (l-\bar{l})(n-\bar{n})dxdt \\
&+ \alpha\int_Q e^{at}[(k+l+m)n - (\bar{k}+\bar{l}+\bar{m})\bar{n}](n-\bar{n})dxdt - \int_Q (u_2 n - \bar{u}_2\bar{n})(n-\bar{n})dxdt; \qquad (3.59)
\end{aligned}
$$

$$
\begin{aligned}
&a\int_Q (\zeta_1-\bar{\zeta}_1)^2 dxdt + \frac{1}{2}\int_\Omega (\zeta_1-\bar{\zeta}_1)^2(x,0)dx + d\int_Q |\nabla(\zeta_1-\bar{\zeta}_1)|^2 dxdt - r\int_Q (\zeta_1-\bar{\zeta}_1)^2 dxdt \\
&+ \theta_c \int_Q e^{at}(n\zeta_1 - \bar{n}\bar{\zeta}_1)(\zeta_1-\bar{\zeta}_1)dxdt + \frac{2r}{K}\int_Q e^{at}\big[(k+m)\zeta_1 - (\bar{k}+\bar{m})\bar{\zeta}_1\big](\zeta_1-\bar{\zeta}_1)dxdt \\
&+ \theta_i e^{at}(l\zeta_1 - \bar{l}\bar{\zeta}_1)(\zeta_1-\bar{\zeta}_1)dxdt + \int_Q (u_1\zeta_1 - \bar{u}_1\bar{\zeta}_1)(\zeta_1-\bar{\zeta}_1)dxdt \\
&- \theta_c \int_Q e^{at}(n\zeta_2 - \bar{n}\bar{\zeta}_2)(\zeta_1-\bar{\zeta}_1)dxdt - \theta_i \int_Q e^{at}(l\zeta_2 - \bar{l}\bar{\zeta}_2)(\zeta_1-\bar{\zeta}_1)dxdt \\
&- \int_Q (u_1\zeta_3 - \bar{u}_1\bar{\zeta}_3)(\zeta_1-\bar{\zeta}_1)dxdt + \alpha\int_Q e^{at}(n\zeta_4 - \bar{n}\bar{\zeta}_4)(\zeta_1-\bar{\zeta}_1)dxdt \\
&- B_1\int_Q (u_1-\bar{u}_1)(\zeta_1-\bar{\zeta}_1)dxdt = 0; \qquad (3.60)
\end{aligned}
$$

$$
\begin{aligned}
&a\int_Q(\zeta_2-\bar{\zeta}_2)^2dxdt+\frac{1}{2}\int_\Omega(\zeta_2-\bar{\zeta}_2)^2(x,0)dx+d_1\int_\Omega|\nabla(\zeta_2-\bar{\zeta}_2)|^2dxdt\\
&+\theta_i\int_Q e^{at}(k\zeta_1-\bar{k}\bar{\zeta}_1)(\zeta_2-\bar{\zeta}_2)dxdt-\theta_i\int_Q e^{at}(k\zeta_2-\bar{k}\bar{\zeta}_2)(\zeta_2-\bar{\zeta}_2)dxdt\\
&-\gamma\int_Q(\zeta_4-\bar{\zeta}_4)(\zeta_2-\bar{\zeta}_2)dxdt+\alpha\int_Q e^{at}(n\zeta_4-\bar{n}\bar{\zeta}_4)(\zeta_2-\bar{\zeta}_2)dxdt\\
&-B_1\int_Q(u_1-\bar{u}_1)(\zeta_2-\bar{\zeta}_2)dxdt=0; \qquad (3.61)\\
&a\int_Q(\zeta_3-\bar{\zeta}_3)^2dxdt+\frac{1}{2}\int_\Omega(\zeta_3-\bar{\zeta}_3)^2(x,0)dx+d\int_Q|\nabla(\zeta_3-\bar{\zeta}_3)|^2dxdt\\
&-r\int_Q(\zeta_1-\bar{\zeta}_1)(\zeta_3-\bar{\zeta}_3)dxdt+\alpha\int_Q e^{at}(n\zeta_4-\bar{n}\bar{\zeta}_4)(\zeta_3-\bar{\zeta}_3)dxdt\\
&+\frac{2r}{K}\int_Q|e^{at}\big[(k+m)\zeta_1-(\bar{k}+\bar{m})\bar{\zeta}_1\big](\zeta_3-\bar{\zeta}_3)dxdt=0; \qquad (3.62)\\
&a\int_Q(\zeta_4-\bar{\zeta}_4)^2dxdt+\frac{1}{2}\int_\Omega(\zeta_4-\bar{\zeta}_4)^2(x,0)dx+\theta_c\int_Q e^{at}(k\zeta_1-\bar{k}\bar{\zeta}_1)(\zeta_4-\bar{\zeta}_4)dxdt\\
&+p\int_Q(\zeta_4-\bar{\zeta}_4)^2dxdt-\theta_c\int_Q e^{at}(k\zeta_2-\bar{k}\bar{\zeta}_2)(\zeta_4-\bar{\zeta}_4)dxdt\\
&+\alpha\int_Q e^{at}\big[(k+l+m)\zeta_4-(k+\bar{l}+\bar{m})\bar{\zeta}_4\big](\zeta_4-\bar{\zeta}_4)dxdt\\
&+\int_Q(u_2\zeta_4-\bar{u}_2\bar{\zeta}_4)(\zeta_4-\bar{\zeta}_4)dxdt-B_2\int_Q(u_2-\bar{u}_2)\big](\zeta_4-\bar{\zeta}_4)dxdt=0; \qquad (3.63)
\end{aligned}
$$

Next, adding the system $(3.56)-(3.63)$ and using the boundedness of the coefficients, state variables, controls and adjoint variables and using Hölder Inequality as in Theorem 3.1 we obtain

$$
\begin{aligned}
&\frac{1}{2}\int_\Omega\big[(k-\bar{k})^2(x,T)+(l-\bar{l})^2(x,T)+(m-\bar{m})^2(x,T)+(n-\bar{n})^2(x,T)\\
&\quad+(\zeta_1-\bar{\zeta}_1)^2(x,0)+(\zeta_2-\bar{\zeta}_2)^2(x,0)+(\zeta_3-\bar{\zeta}_3)^2(x,0)+(\zeta_4-\bar{\zeta}_4)^2(x,0)\big]dx\\
&\quad+(a-R_1-R_2e^{aT})\int_Q\big[(k-\bar{k})^2+(l-\bar{l})^2+(m-\bar{m})^2+(n-\bar{n})^2+(\zeta_1-\bar{\zeta}_1)^2\\
&\quad+(\zeta_2-\bar{\zeta}_2)^2+(\zeta_3-\bar{\zeta}_3)^2+(\zeta_4-\bar{\zeta}_4)^2\big]dxdt+d\int_Q\big[|\nabla(k-\bar{k})|^2+|\nabla(l-\bar{l})|^2\\
&\quad+|\nabla(m-\bar{m})|^2+|\nabla(\zeta_1-\bar{\zeta}_1)|^2+|\nabla(\zeta_2-\bar{\zeta}_2)|^2+|\nabla(\zeta_3-\bar{\zeta}_3)|^2\big]dxdt\\
&\quad\leq 0 \qquad (3.64)
\end{aligned}
$$

If we choose $a > R_1 + R_2$ and then T sufficiently small so that $a - R_1 - R_2 e^{aT} > 0$, then from inequality (3.64) we must have $k = \bar{k},\ l = \bar{l},\ m = \bar{m}, n = \bar{n},\ \zeta_1 = \bar{\zeta}_1,\ \zeta_2 = \bar{\zeta}_2,\ \zeta_3 = \bar{\zeta}_3,\ and\ \zeta_4 = \bar{\zeta}_4$. Hence, $s = \bar{s},\ i = \bar{i},\ v = \bar{v},\ and\ c = \bar{c}$. Also, $\lambda_1 = \bar{\lambda}_1,\ \lambda_2 = \bar{\lambda}_2,\ \lambda_3 = \bar{\lambda}_3,\ and\ \lambda_4 = \bar{\lambda}_4$. Also, since the optimal controls are characterized in terms of state and adjoint variables, then $u_1 = \bar{u}_1,\ and\ u_2 = \bar{u}_2$. ■

3.5 Numerical Results

In this section we provide some numerical results of our spatio-temporal anthrax model with control strategies for various parameter sets. We consider a one dimensional domain, $\Omega = [0, 1]$, (representing 1 kilometer) and the time interval [0,1](representing 1 month). Hence, in our model (3.1) – (3.4), the Laplacian operator is represented by

$$\triangle = \frac{\partial^2}{\partial x^2}.$$

Thus the state system will have the form

$$\begin{aligned}
\frac{\partial s}{\partial t} &= d\frac{\partial^2 s}{\partial x^2} + rn(1 - \frac{n}{K}) - \theta_c sc - \theta_i si - u_1 s \\
\frac{\partial i}{\partial t} &= d_1\frac{\partial^2 i}{\partial x^2} + \theta_c sc + \theta_i si - \gamma i \\
\frac{\partial v}{\partial t} &= d\frac{\partial^2 v}{\partial x^2} + u_1 s \\
\frac{dc}{dt} &= \gamma i - \alpha(s + i + v)c - (p + u_2)c,
\end{aligned}$$

where n=s+v. The initial and boundary conditions are,

$$\begin{aligned}
&s(x, 0) = s^0(x), i(x, 0) = i^0(x), v(x, 0) = v^0(x), c(x, 0) = c^0(x),\ x \in \Omega, \\
&s(x, t) = i(x, t) = v(x, t) = 0; \qquad for\ (x, t) \in \partial\Omega \times [0, T].
\end{aligned}$$

and the similar expression for the adjoint system (3.45). Also, the optimal controls

$$u_1(x,t) = min\Big(M_1, max\big(-\frac{(\lambda_3-\lambda_1+B_1)s+B_1 i}{2C_1}, 0\big)\Big),$$
$$u_2(x,t) = min\Big(M_2, max\big(-\frac{(B_2-\lambda_4)c}{2C_2}, 0\big)\Big).$$

We assume that the initial population of susceptible animals is approximately normally distributed around the middle of the domain, $x = 0.5$, and the initial populations of the infected and carcasses are also approximately normally distributed near the right corner of the domain say, near $x = 0.7$. To keep the simulation close to the data used in chapter 2, we assume that the initial number of susceptible animals is 863. Similarly, the initial number of infected animals and infected carcasses are assumed to be 39 and 1, respectively. The initial value functions $s^0(x), i^0(x),$ and $v^0(x)$ are chosen in such a way that the areas under these curves are approximately equal to the initial numbers of susceptible animals, infected animals, and infected carcasses, respectively. Thus, we take,

$$s(x,0) = 3744e^{\frac{-(x-0.5)^2}{0.017}},\ i(x,0) = 172e^{\frac{-(x-0.7)^2}{0.017}},\ \text{and}\ c(x,0) = 4.6e^{\frac{-(x-0.7)^2}{0.017}},$$

which are approximately 0 on $\partial\Omega$. Some of the model parameters such as the population growth rate, r, disease induced death rate, γ, carcass decay rate, p, environmental carrying capacity, K, are taken from the ODE model estimates made in Chapter 2 (See Table 2.1 for details). Anthrax incidence is formulated as the mass action terms $\theta_c si$ and $\theta_c sc$ with rate of infections $\theta_c i$ and $\theta_c C$. Also, since we do not have experimental data for transmission with spatial dependence, we take values for the transmission rates to be $\theta_c = 1\times10^{-3}, \theta_c = 3\times10^{-3}$.

In our model, the animal movement is only by diffusion and for simplicity, we consider constant diffusion rates. Also, we consider two values for the diffusion coefficient. For slower diffusion, we assume $d = 0.02$ and for faster diffusion, we assume $d = 0.1$. Also we assume separate diffusion coefficients for healthy and infected animals: diffusion coefficient for healthy animals (susceptible and vaccinated), d, and diffusion coefficient for infected animals, d_1. As mentioned in Section 3.2, the infected animals are too sick to move normally. thus we assume $d_1 < d$. Table 3.1 displays all parameters values used in our simulations.

Table 3.1: The model parameters, their description, values and units.

Parm.	Description	Values	Units
r	Logistic growth rate of healthy animals	3.93×10^{-4}	day^{-1}
γ	Disease induced death rate of infecteds	$\frac{1}{7.5}$	day^{-1}
α	Carcass feeding rate by scavengers	10^{-4}	$\text{animal}^{-1}\ \text{day}^{-1}$
K	Carrying capacity of animals	2000	animal
p	Carcass decay rate	0.01	day^{-1}
d	Diffusion rate of healthy animals	0.1, 0.02	$km^2\ \text{day}^{-1}$
d_1	Diffusion rate of infected animals	$d_1/5$	$km^2\ \text{day}^{-1}$
θ_c	Disease transmission rate from carcasses	1×10^{-3}	$\text{carcass}^{-1}\ \text{day}^{-1}$
θ_i	Disease transmission rate from infected animals	3×10^{-3}	$\text{animal}^{-1}\ \text{day}^{-1}$

The set of admissible controls, denoted by $\mathcal{U}$, consists of all measurable function pairs $(u_1, u_2)(x,t)$ with $0 \leq u_i \leq M_i$, for $i = \{1,2\}$ and $(x,t) \in \Omega \times [0,T]$. In our problem the vaccination rate is denoted by $u_1(x,t)$ and the the carcass disposal rate is denoted by $u_2(x,t)$. As in chapter 2, the optimal control problem under consideration is finding the optimal control pair $(u_1^*, u_2^*) \in \mathcal{U}$ that minimizes the objective functional (3.5), where the cost of applying the controls are considered to be non-linear functions of u_1 and u_2. For simplicity, we choose quadratic functions for the cost of vaccination and of carcass disposal. For all numerical simulations we used a finite difference method with backward-forward sweep scheme. See appendix A.3 for details.

In Figures 3.1-3.2, we simulate system (3.1) − (3.4) without control strategies (i.e., $u_1 = 0, u_2 = 0$) and with slow and fast diffusion rates. Figure 3.1 shows the simulation results for the slow diffusion rate ($d = 0.02$) scenario. We see that without any control strategies and with the slower diffusion rate, the region where most of the susceptible animals are concentrated at the beginning will have more infected animals present over time. This is due to the slow movement of the animals which imply that susceptible animals will have more time to contact with infected animals. Also as expected, more carcasses are observed in the region with more infected animals, as these animals move even slower then their susceptible counterparts. The number of susceptible animals is decreasing over time and this population is also moving slowly throughout the whole region. The fast expanding waves of infected animals and infected carcasses are seen over time while, on the other hand, the animals are moving slowly toward the boundary. The high transmission in the region

of high concentration of animals can also be observed in the Figure 3.1. In the objective functional (3.5), we choose the parameters

$$A_1 = 1,\ A_2 = 0.1,\ B_1 = 0.1,\ B_2 = 0.05,\ C_1 = 0.1,\ C_2 = 0.1.$$

Note that similar to Section 2.5, we assign more weights to A_1 then A_2 and more weights to B_1 than B_2. The total cost associated with the infected animals and infected carcasses as well as the cost of applying the controls in this case is $J = 250.32$.

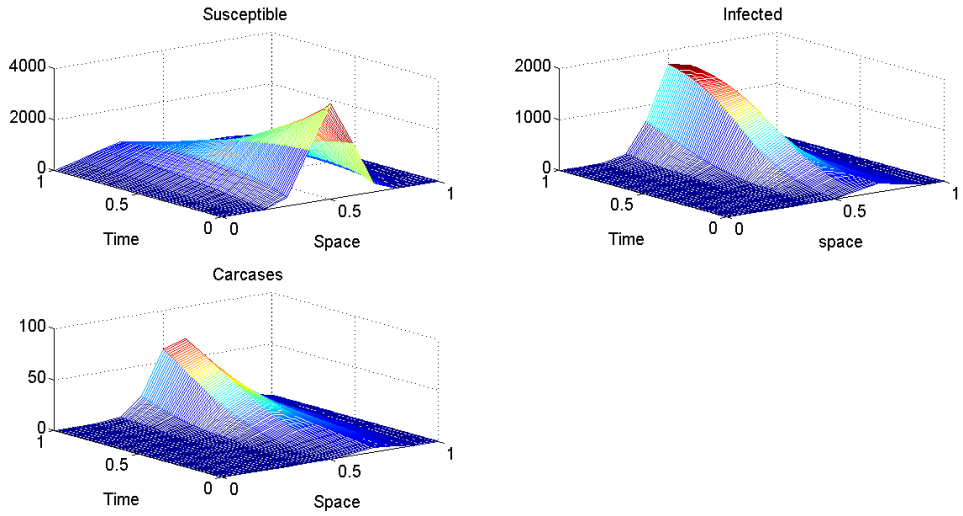

Figure 3.1: Simulation results for model (3.1) – (3.4) with slow diffusion rate (d=0.02) and without control. The figures in the first row show the plots for susceptible (left) and infected (right) animals; and the figure in the second row represents the carcasses.

Figure 3.2 presents the simulation results for the fast diffusion rate ($d = 0.1$) and no control scenario. We see that without control strategies and with the faster diffusion rate, the number of susceptible animals move to the low concentration region quickly. This may help most of the susceptible animals from becoming infected by reducing their chance of contact with infected animals or infected carcasses. However on the other hand, the high movement of infected animals increase the chance of incidence with susceptible animals. As in the previous case, the expanding wave of infected animals and infected carcasses can be seen over time. Over the time, the animals seem to diffuse in the regions where animals concentration is low. The cost associated with the infected animals and infected carcasses as well as the cost of applying the controls in this case is $J = 146.19$. Comparing this with

the value $J = 250.32$ in the previous case with the slower diffusion rate and no control, we see a smaller J value with the fast diffusion and without control due to the smaller number of infected animals and carcasses.

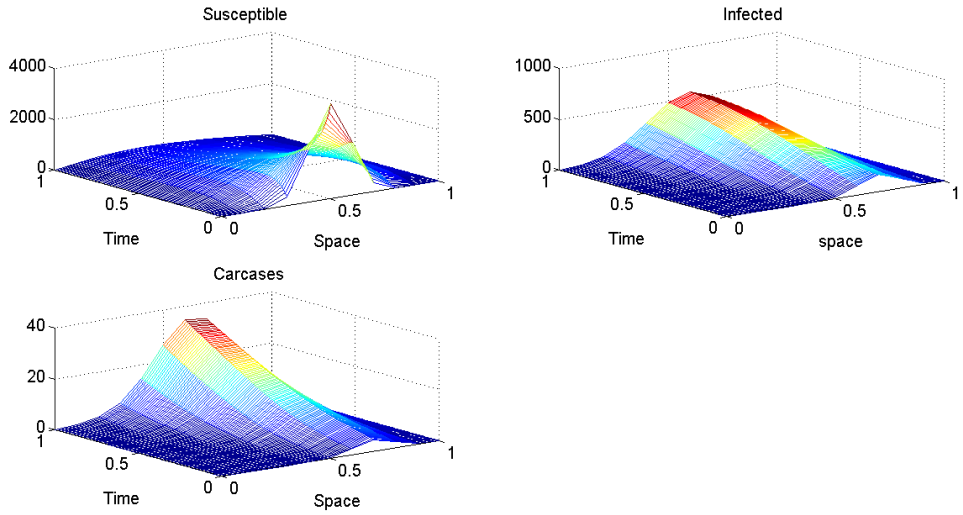

Figure 3.2: Simulation results for model (3.1) – (3.4) with fast diffusion rate (d=0.1) and without control. The figures in the first row show the plots for susceptible and infected animals and the figure in the second row represents the carcasses.

Next, we apply the optimal vaccination strategy and optimal carcass disposal strategy to our model (3.1) – (3.4). We took

$$0 \leq u_1(x,t) \leq 0.8, \quad \text{and} \quad 0 \leq u_2(x,t) \leq 1.5.$$

Here, a higher weight is given to infected animals than to infected carcasses because the infected animals may cause more infection as they move. Also, a higher weight is given to the vaccination rate because of the higher cost assumed to be associated with the vaccination process for wild animals. Figure 3.3 shows the simulation results for the optimal rates of the carcass disposal and vaccination using the slower diffusion coefficient, $d = 0.02$. From the figure, we see that the wave of infected animals and infected carcasses are increasing with time; however, the concentration of infected animals and infected carcasses appears smaller compared to the case with the slow diffusion and no controls (Figure 3.1). The concentration of vaccinated animals are increasing over time and also diffusing throughout the entire region. This implies that for optimal results, the vaccination and carcass disposal

strategies should be mostly applied to the regions where infected animals and infected carcasses were observed in the beginning. The cost associated with the infected animals, infected carcasses and the cost of applying both controls in this case is $J = 198.73$.

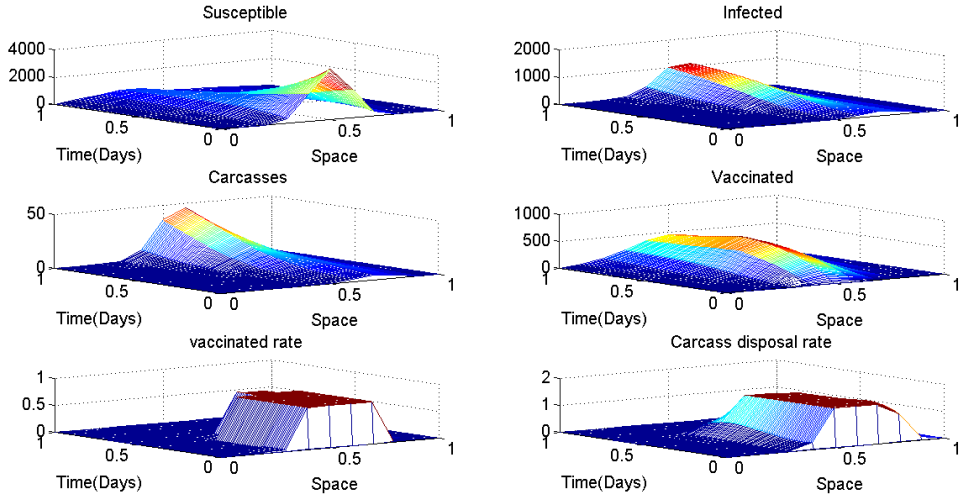

Figure 3.3: Simulation results for model (3.1) − (3.4) with optimal rates of vaccination and optimal carcass disposal using a slow diffusion rate, ($d = 0.02$). The two plots in the first row represent the concentrations of susceptible(left) and infected (right) animals. The plots in the second row represents the concentrations of the infected carcasses(left) and the vaccinated animals(right). The last row represents the vaccination (left) and carcass disposal(right) rates.

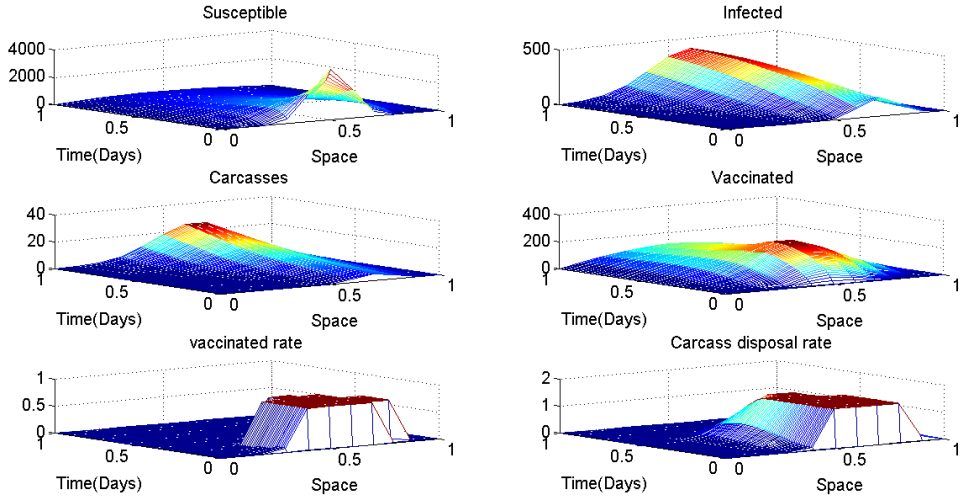

Figure 3.4: Simulation results for model (3.1) − (3.4) with optimal rates of vaccination and optimal carcass disposal using a slow diffusion rate, ($d = 0.1$). The two plots in the first row represent the concentrations of susceptible(left) and infected (right) animals. The plots in the second row represents the concentrations of the infected carcasses(left) and the vaccinated animals(right). The last row represents the vaccination (left) and carcass disposal(right) rates.

Figure 3.4 shows the simulation results for model (3.1)-(3.4) with optimal rates of vaccination and carcass disposal using a faster diffusion coefficient, $d = 0.1$. From this figure, we see that the wave of infected animals and infected carcasses are increasing with time. As in the previous case, the concentration of infected animals and infected carcasses seems smaller as compared to the case (see Figure 3.3) when there is no controls. The reason for this difference is that the cost associated with the infected animals and infected carcasses is smaller in this latter case due to the low disease incidence. Since the animals move faster from the highly populated region that contains some infected animals toward the less populated region, they mostly escape being infected. The population of vaccinated animals is increasing over time and also diffusing throughout the region. This implies that to achieve optimal results in this case, the vaccination and carcass disposal strategies should be applied mostly in the region where infected animals and infected carcasses were observed at the beginning of the outbreak. Also, the cost associated with the infected animals, infected carcasses, and the cost of applying both controls in this case is $J = 134.47$, which is smaller than the case of no control with fast diffusion.

3.6 Conclusions and Discussion

This chapter extended the ODE model discussed in Chapter 2 to a PDE model. The major difference is the spatial dependence of the model variables and controls and animal movements governed by diffusion. The optimal control analysis for controlling the spread among anthrax in wild animals modeled by a system of ODE/PDEs was completed to obtain existence and uniqueness of the solutions, as well as of the optimal controls. We presented the derivation of adjoint system and the characterization of optimal control that depend on coefficients in the objective functional as well as the state and adjoint variables.

Through the numerical results we were able to show that as in the case of non-diffusing populations, the application of optimal rates of vaccination and carcass disposal is a reasonable strategy to keep the density of infected animals and infected carcasses low with lower cost. The simulations results for the two different diffusion rates considered indicated that for smaller diffusion, the disease spreads quickly because the high concentration of susceptible animals implies longer contact time available for susceptibles to have contact

with infecteds and thus requires a longer use of the controls. For this latter case, the wave of infected animals barely reaches the boundary of the region in the time interval considered. Also, for both diffusion coefficients considered, the infection spreads quickly in the region where there is a higher concentration of susceptible animals. Finally, the results imply that the application of the controls should be more focused in the regions where initially infected animals and infected carcasses were observed. The simulations also illustrate some interesting effects of the diffusion coefficients in the disease spread and suggest the location where the control strategies should be focused.

More numerical simulations with various parameter combinations are needed to produce more realistic scenarios. Using a data set with detailed spatial and temporal features would be valuable. Also, numerical simulations in the two dimensional spatial case would be interesting to work on for the future.

Chapter 4

Modelling the Early Host-Pathogen Interaction in an Inhalational Anthrax Infection

4.1 Introduction

Inhalational anthrax is considered to be the most deadly form of anthrax infection. The infection usually initiates within a week after exposure to the spores, while in some cases, longer times on the order of months have been observed [49]. Without treatment the fatality rate of this disease is near 95% whereas immediate intervention of the disease progression can lower the fatality rate to about 50% [20]. People who work in places such as wool mills, slaughter house and tanneries may breathe in anthrax spores while working around infected animals or contaminated animal products [49]. Interestingly, however, one study estimated that workers in goat hair processing mills were estimated to be inhaling 600-1300 spores over an 8-hour shift yet without any ill consequences [10]. Additionally, a cumulative look among similar workers known to be repeatedly exposed to anthrax saw only 9 cases of the disease over 107 years [10]. Hence, there are clearly mechanisms of this disease that are not understood well enough to explain why in some cases exposure is fatal and in others it is not. Understanding the dynamics of the immune mechanisms involved in disease initiation

and progression is important to gain insight into this difference. Incorporating experimental work with mathematical modeling can provide a powerful means to do this.

Inhalational anthrax develops when the spores, deposited in the lung's alveoli, are engulfed by local phagocytic cells such as macrophages [27] and dendritic cells [7] and then transported to the nearby lymph nodes. The spores can germinate within these host cells either in the lung, or on the way to the lymph nodes [12]. Experimental work has confirmed that, while the spore form of anthrax is unable to be killed by these immune cells, the germinated bacterial form is highly susceptible [27, 32]. However, if the bacteria manage to survive the killing mechanisms of the immune cells, they can replicate quickly and produce toxins that cripple the body's immune response by various mechanisms [15]. Thus, inhalational anthrax may be initiated in the lung, but the primary battle ground when outgrowth occurs is in the draining mediastinal lymph nodes of the lung [11]. Severe respiratory distress is experienced by the infected host, followed by tissue damage, hemorrhage and multi-organ failure as a result of bacteria disseminating to the blood [20].

Prior modeling work related to immune processes in an anthrax infection has focused on estimating the disease incubation period of anthrax as well as rates for clearance of spores from the lung (mechanical and/or immune mediated) and germination of spores, which are all important aspects in disease progression. Work carried out by multiple investigators [2, 4, 24, 37, 55, 54] used various types of dose response models to estimate these entities. Some explicitly incorporated spore clearance and/or germination parameters and then estimated them from available dose response data. While these models provide a statistically based method to estimate these parameters, they lack detail of the complex immune mechanisms behind the processes and their dynamic nature.

A few dynamic mathematical models have been formulated that describe the mechanisms involved in pathogenesis of the early events in an inhalational anthrax infection. In the work of [42], a mathematical model is formulated that describes the interaction between the host macrophages and lethal factor (LF), a toxic component produced by Bacillus anthracis, in an inhalational anthrax infection. The paper focused on the effect of release of LT on macrophage activated protein kinase pathway (MAPK). In the work of [34], an ordinary differential equation model was constructed to study the effectiveness

of combination therapy of antibiotics and vaccination in a genetically diverse population and concluded that the combination therapy applied in the early phases of infection is helpful in averting shock and improving the survival. The model was built on the paradigm of infection leading to anthrax toxin-induced septic shock and did not focus on the early infection processes.

In [11], a two compartmental mathematical model consisting of ordinary differential equations was developed that included lung and lymph node components. The model explored the construct of a threshold deposited dose above which a fatal outcome is observed and included antibiotic treatment strategies to explore survival outcomes of an infected individual. The model considered early events in disease progression and investigated the relationship between the initial deposited dose and the length of time for spores to be phagocytosed, transported, and released as vegetative bacteria in the lymph node. The shorter that process is overall, the lower the threshold deposited dose needs to be in order to prove fatal. Some intracellular killing by host cells of germinated spores as well as some growth of bacteria possibly not killed by host cells was assumed to occur prior to release into the extracellular environment of the lymph nodes. However, that assumption was governed by a model parameter rather than with dynamic equation for intracellular anthrax components. In addition, an average number of intracellular spores per host cell was assumed rather than providing an equation that included extracellular and intracellular spores and unoccupied and occupied host cells. Thus, the initiation processes of phagocytosis by host cells and germination of intracellular anthrax spores were only modeled implicitly such that details about those processes could not be specifically explored with that model.

In [24], data from *in vivo* experimental studies in New Zealand White Rabbits was used to parameterize a linear two-compartment ordinary differential equations model to investigate bacterial dynamics and transport between the airways and lung tissue. The experimental data was initially used to estimate a physical clearance rate, an immune-killing clearance rate and a bacterial growth rate by assuming an exponential clearance of bacteria over time based on the net effect of these rates and by using select data sets which allowed the authors to isolate each parameter in a simplified equation in order to

estimate each. These parameter estimates were then used in the two-compartment bacterial transport model to determine the time frame for bacteria dynamics in each compartment which could then be compared to the experimental results. However, neither model used in that study explicitly modeled the host cell-spore interaction, but the authors did see a need to incorporate into the model a lag phase time from the time of inhalation of spores to the time of bacterial growth. From their data, they estimated this lag phase to be 12 hours and with a model lag time set to 7.7 hours the model exactly predicted the amount of bacteria at 36 hours post infection, one of the main data points in the study. While some of these prior studies include aspects of host-pathogen interaction and early disease events, they lacked the specific details regarding phagocytosis, germination and killing in the early stage of the disease, which appear to play an important role in disease progression and outcome.

In this present work, we develop a mathematical model to emulate an *in vitro* experimental protocol of the macrophage-spore interaction and use the data from the experiment to estimate model parameters [32]. We investigate early disease processes such as phagocytosis of spores by local macrophages, their germination within the macrophages and killing of the germinated spores by their respective host cells. The model uses ordinary differential equations to describe the dynamics of healthy and infected macrophages, extracellular and intracellular spores and newly germinated and vegetative bacterial populations. Incorporating the available data with the mathematical model provides a means to investigate the processes of phagocytosis, germination, and bacterial killing inside a macrophage and estimate the rates of these processes. As we will discuss below, our initial modeling efforts suggest that germinated spores progress through two bacterial stages, the newly-germinated and vegetative bacterial stage. The former stage is a fragile bacterial form, susceptible to macrophage killing and not yet capable of replicating. The latter form is more robust, however, this form is still susceptible to macrophage killing but can replicate.

The chapter is organized as follows: In section 4.2, we present a summary of the experimental protocol along with the dataset used for this work, the interpretation of the data and related assumptions for the modeling, and the development of two models. In section 4.3, parameter values for each model are estimated and numerical simulations are

shown and compared. We discuss the implication of our results in section 4.4 and include possible future directions.

4.2 Materials and Methods

In this section, we construct a mathematical model based on an *in vitro* experimental protocol as carried out in [32], use the experimental data to determine crucial model parameters, and use the model to suggest additional insights from the data. Below we recap the essential information regarding the experimental protocol and the associated data that was collected and then describe how this was used to construct and calibrate the mathematical model.

4.2.1 Summary of experimental protocol, dataset, and related assumptions

In the experimental work of [32], an *in vitro* experimental study was carried out to examine the macrophage-spore interaction. The experiment inoculated sets of 10^6 primary murine peritoneal macrophages obtained from Crl:CD-1 (ICR) BR (outbred) mice with varying doses of Sterne 34F2 mouse-virulent strain *Bacillus anthracis* spores for a 30 minute period. This strain is capable of germination and toxin production. The multiplicity of infection (MOI), or ratio of spores to macrophages in a given experiment, was examined for several quantities: 1:1, 1:2, 1:10 and 1:20. In other words, the number of macrophages remained constant across the MOIs examined at 10^6 while and the number of spores to which the macrophages were challenged were $10^6, 5 \times 10^5, 10^5$, and 5×10^4, respectively. Analogous experiments were performed using a germination-deficient strain of anthrax spores, $\triangle gerH$ in which germination is inhibited.

The 30 minute incubation period of spores with macrophages was followed by washing and incubation with an antibacterial agent, gentamicin, for an additional 30 minutes to ensure that no extracellular bacteria were present when the experiment continued. Then, in duplicate samples for each MOI, macrophages were lysed and the intracellular components counted with or without first being subjected to a heat treatment at 65^oC which is effective

in killing spores that have germinated into vegetative cells. In the heat treated cases, the number of viable intracellular components (i.e. spores) left over after heat treatment were counted in two duplicate samples for the $1, 3, 5$, or 24 hour time points. In the non-heat treated cases, the total number of intracellular components were also enumerated in duplicate samples for the $1, 3, 5$, or 24 hour time points and these are given in Table 4.1. For our modeling, we assume the total intracellular components are a combination of ungerminated spores, denoted as S_i, germinated spores, B_{ig}, and fully vegetative cells, B_i. Where specified, germinated spores and fully vegetative cells are sometimes considered as a single population, $B = B_{ig} + B_i$, with no differences between them.

Since the incubation period of macrophages with spores lasted for the first 30 minutes of the experiment after which washing occurred, we assume that no further phagocytosis occurs in the time period from 30 minutes to 1 hour into the experiment. However, from 30 minutes to 1 hour, while the additional gentamicin incubation period occurs, there may be intracellular events taking place such as spore germination and macrophage-induced killing of germinated spores. We note that this experimental data as well as previous reports [30, 53] demonstrate that macrophages are unable to kill the ungerminated spore form of anthrax. Thus, to estimate the number of intracellular (ungerminated) spores, S_i, at the 30 minute time point right after the end of the macrophage-spore incubation period, we take the total intracellular components measured at 1 hour in the non-heat treated samples that used the $\triangle gerH$ germination-deficient strain and assume that this amount is the number of spores present 30 minutes prior to the 1 hour measurement. This is done for each MOI. For instance, in Table 4.2 under the 30 minute column, the amount provided for each MOI is the average of counts from two duplicate samples in which total intracellular components were enumerated from non-heat treated samples that used the $\triangle gerH$ strain. The subsequent counts for S_i at $1, 3, 5$ and 24 hours given in the remaining columns of Table 4.2 for the different $MOIs$ are taken from the heat treated samples that used the virulent Sterne $34F$ strain, since the number of intracellular components left after heat treatment would be the intact spores that have not yet germinated. The table entries for each MOI provide averages of counts from two duplicate samples.

Table 4.1: For different MOI at $1, 3, 5$ and 24 hours after inoculation, counts are given for the total number of intracellular components (e.g. ungerminated spores, S_i and bacteria, B, where B may refer to a single population or sum of two separate populations with distinct properties distinguished as germinating spores, B_{ig}, and fully vegetative cells, Bi) are given. Spores at counts of $10^6, 5 \times 10^5, 10^5$ and 5×10^4, respectively, were initially incubated with 10^6 macrophages for 30 minutes after which, the medium was washed and 30 minutes of incubation with gentamicin took place. Then, at $1, 3, 5$, or 24 hours, the total number of intracellular (i.e. non-heated) components were counted for each MOI at each time point. Each number in the table represents the average of two duplicate experiments.

S_i	1 hr	3 hr	5 hr	24 hr
1 : 1	405000	295000	208500	280000
1 : 2	128000	78500	62500	49500
1 : 10	36500	26000	16750	5250
1 : 20	13900	8700	4850	1300

Table 4.2: The number of heat resistant spores, S_i, after application of heat treatment to the total intracellular components. Spores at counts of $10^6, 5 \times 10^5, 10^5$ *and* 5×10^4, respectively, were initially inoculated with 10^6 macrophages for 30 minutes. The medium was washed after 30 minutes and 30 minutes of incubation with gentamicin took place. Each sample was then heat treated at 65^oC to kill any germinated spores (i.e. ungerminated spores are heat-resistant) and the number of viable intracellular spores were counted in cell lysates at $1, 3, 5$ and 24 hours post inoculation. Each number in the table represents the average of two duplicate experiments. The data included in the column labeled 30 minutes is estimated from the count of the $\triangle gerH$ strain at 1 hour.

MOI	30 min	1 hr	3 hr	5 hr	24 hr
1 : 1	377500	200000	121500	138500	255000
1 : 2	139000	105000	11400	10250	29500
1 : 10	24500	27000	12000	9100	2750
1 : 20	13925	7900	6450	3100	300

To quantify the number of intracellular bacteria, at $1, 3, 5$, and 24 hours, we examine the number of intracellular components that are lost during heat treatment. In other words, we calculate the number of intracellular bacteria at the collection time points as the difference between the number of total intracellular components (Table 4.1) and the number of intracellular (ungerminated) spores that remain after heat treatment (Table 4.2). Thus using the data from Tables 4.1 and 4.2, the resulting counts for intracellular bacteria at $1, 3, 5$, and 24 hours are given in Table 4.3.

Table 4.3: The number of intracellular bacteria, B, at $1, 3, 5$ and 24 hours for different multiplicity of infection.

B_i	1 hr	3 hr	5 hr	24 hr
1 : 1	205000	173500	70000	25000
1 : 2	23000	67100	52250	20000
1 : 10	9500	14000	7650	2500
1 : 20	6000	2250	1750	1000

Since the available dataset does not provide data points before 1 hour, we estimate the number of intracellular spores, S_i, at 30 minutes as described above and assume that no germination or macrophage-induced killing occurs in the first 30 minutes of the experiment, during the macrophage-spore incubation period. This assumption is supported by the given dataset in that the counts of intracellular components at one hour in samples that used the germination deficient $\triangle gerH$ strain compared to samples that used the germination-proficient strain are very similar, indicating that even in one hour after the start of incubation the germination process does not appear to be a dominating process. In addition, other work supports this assumption [9, 44].

4.2.2 Development of Mathematical Models

Based on the experimental protocol followed in [32], we make the following assumptions in the development of the model, some of which were mentioned above to interpret the given data.

(a) Phagocytes (host cells) are unable to kill anthrax spores;

(b) Because the medium in which anthrax spores and macrophages are incubated is washed after 30 minutes (0.5 hr) of incubation, we assume that after 30 minutes of phagocytosis, extracellular spores are no longer present. Thus, phagocytosis effectively ceases;

(c) There is no difference between the rates of the phagocytosis process for healthy (unoccupied) versus infected (occupied) macrophages;

(d) Only intracellular spores can germinate. We consider two separate germination functions which may or may not depend on the average intracellular burden per occupied host cell (See Appendix A.2);

(e) The germination process for intracellular spores starts after the incubation period ends, i.e. it begins at 30 minutes;

(f) Either newly germinating bacilli are immediately able to replicate and are also susceptible to phagocytic killing or they are first susceptible to phagocytic killing before they mature to fully vegetative cells, capable of replicating (we consider each

assumption with two different models). In the latter assumption, germinated spores, B_{ig}, that survive phagocytic killing progress to becoming fully vegetative bacteria, B_i, and are assumed to still be susceptible to phagocytic-induced killing but can replicate. We consider two separate functional forms for killing that may or may not depend on the average intracellular burden per occupied host cell (See Appendix A.2) ;

(g) For bacterial growth, we assume exponential growth and do not consider a growth term that includes a carrying capacity (e.g. logistic growth) given the 24 hour time frame of the experiment which did not display outgrowth by this time for the macrophage type used;

The mathematical model we construct consists of two systems: one system for the first 30 minutes during which we assume there is only the process of phagocytosis and no spore germination (and therefore no bacterial growth and no phagocytic killing); and a second system for the processes of germination, phagocytic killing, and bacterial growth that occur after 30 minutes when phagocytosis ceases. For the second system, two alternative model formulations are considered.

We now describe an ordinary differential equation (ODE) model for events happening in the first 30 minutes. Based on the assumptions made above, only phagocytosis occurs during this period. This model consists of four components: macrophages that have not engulfed any spores, which we call healthy (or unoccupied) macrophages (P_h), macrophages that have engulfed spores, which we refer to as infected (or occupied) macrophages (P_i), extracellular spores (S_e) and intracellular spores (S_i). Also, we assume that an infected (i.e. already occupied) macrophage can engulf additional extracellular spores and assume the same rate for the phagocytosis process for each population, given by the rate constant k_1. Thus, the mathematical model describing the changes in these populations due to the phagocytosis process is given by equations (4.1) – (4.4).

$$\frac{dP_h}{dt} = -k_1 S_e P_h \tag{4.1}$$
$$\frac{dP_i}{dt} = k_1 S_e P_h \tag{4.2}$$
$$\frac{dS_e}{dt} = -k_1 S_e P_h - k_1 S_e P_i \tag{4.3}$$
$$\frac{dS_i}{dt} = k_1 S_e P_h + k_1 S_e P_i \tag{4.4}$$

with initial conditions,

$$P_h(0) = 10^6,\ P_i(0) = 0,\ S_e(0) = S_e^*,\ S_i(0) = 0.$$

In the experimental work [32], samples of 10^6 macrophages were inoculated with different numbers of spores for 30 minutes. Thus, the initial condition S_e^* given for $S_e(0)$ in system (4.1) − (4.4) denotes the initial spore load which is one of the following amounts (with corresponding MOI in parenthesis): $10^6(1:1)$, $5\times10^5(1:2)$, $10^5(1:10)$ and $5\times10^4(1:20)$. Equations (4.1) and (4.2) represent the rate of change of the healthy macrophage, P_h, and infected macrophages, P_i, due to phagocytosis and equations (4.3) and (4.4) represent the rate of change of the extracellular spores, S_e, and intracellular spores, S_i, spores due to the uptake of extracellular spores by both healthy and infected macrophages. This system approximates the dynamics of the first half hour of the *in vitro* experiment. We define a new system of equations to approximate the dynamics after this half hour period, wherein phagocytosis is assumed to cease and germination, replication and macrophage-induced killing events begin.

For the development of the equations that model events happening after 30 minutes (0.5 hour), we explored two different modeling assumptions regarding bacterial stages presented in assumption (f) above and compare the results. For each model, we consider two different functional forms for germination and killing processes. For the germination process, in the first case, germination depends simply on the population of intracellular spores and the population of infected macrophages harboring them, using mass action assumption. From assumption (d), since the germination happens only in the intracellular environment, if there are no infected macrophages then no spores can germinate. Similarly, the larger of either population of infected macrophages or spores, the more efficient germination will be.

Mathematically this can be described by a functional form S_iP_i. For second functional form of germination, we assume that the germination process depends on the average intracellular burden per infected macrophages such that the rate of germination is decreased by half when the average intracellular burden per infected macrophage is 5. The intracellular burden may consist of ungerminated or germinated spores or vegetative bacteria. Thus, in this case, the lower average intracellular burden per infected macrophage implies more efficient germination. We model this by using this functional form

$$S_i \frac{\frac{P_i}{S_i+\tilde{B}}}{\frac{P_i}{S_i+\tilde{B}}+C} = S_i \frac{P_i}{P_i + C(S_i+\tilde{B})}$$

where C is the half saturation constant assumed to be $\frac{1}{5}$ and $\tilde{B}$ is the total intracellular bacteria, $\tilde{B} = B$. Thus, for two bacterial stage model, we will have $\tilde{B} = B_{ig} + B_i$. For simplicity, we denote these two functional forms considered

$$G_1(S_i, P_i) = S_iP_i \tag{4.5}$$

$$G_2(S_i, P_i, \tilde{B}) = S_i \frac{P_i}{P_i + C(S_i+\tilde{B})} \tag{4.6}$$

In the same manner, the macrophage-induced killing is modeled by considering two functional forms similar in germination. The mass action functional form in killing means that the larger of either population of susceptible bacteria or infected macrophages the more effective intracellular killing will be; while the intracellular burden-dependent killing means that a higher average intracellular burden per infected macrophage, the less efficient macrophage killing. For simplicity, we denote these two functions by

$$F_1(B, P_i) = BP_i \tag{4.7}$$

$$F_2(S_i, P_i, B, \tilde{B}) = B \frac{P_i}{P_i + C(S_i+\tilde{B})} \tag{4.8}$$

where B is the number of bacteria in the corresponding bacterial stage compartment. For one bacterial stage model, B represents the total number of bacteria. So the functional forms for killing are exactly same as $(4.7) - (4.8)$ while in two bacterial stages model, B will be B_{ig} or B_i depending on which compartment the killing acts. For example, the functional

forms for killing for the newly germinated bacterial compartment, B_{ig}, in the two bacterial stage model are

$$F_1 = B_{ig}P_i$$
$$F_2 = B_{ig}\frac{P_i}{P_i + C(S_i + \tilde{B})},$$

and in the vegetative bacterial compartment, B_i, the functional forms for killing is

$$F_1 = B_iP_i$$
$$F_2 = B_i\frac{P_i}{P_i + C(S_i + \tilde{B})}.$$

The other variables have same meaning as in the functions for the germination process described above. Thus, using the above notation and denoting germination rate by g_i and killing rate by μ, we have that g_iG_r and μF_j for $j, r = 1, 2$, represent germination and killing processes in our model, respectively. To see the effect of saturation, let us consider an example. Suppose that each infected macrophage on average contain 10 intracellular components per P_i ($i.e,\ if\ \frac{S_i+B}{P_i} = 10$) then the killing rate term becomes

$$\mu F_2 = \mu B\frac{\frac{1}{10}}{\frac{1}{10} + 0.2} \approx \frac{1}{3}\mu B.$$

Hence, the maximum killing rate, μ, is reduced approximately by two thirds.

We now first discuss the model that describes events after 30 minutes ($t \geq 0.5hr$) which assumes one intracellular bacterial population, B. This population has a gain term due to newly germinated spores, a replication term, and a term representing a loss due to the effects of phagocytic killing. Figure 4.1 shows the interactions between the healthy macrophages (macrophages) and extracellular spores which become intracellular spores and later germinate into bacteria.

The mathematical model to describe these germination and killing processes with one bacterial stage is given by equations (4.9) and (4.10).

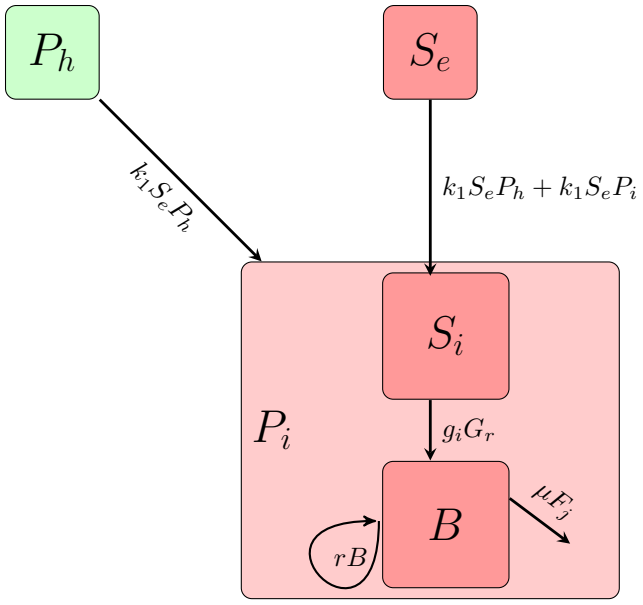

Figure 4.1: Systematic flow diagram of model (4.1) – (4.4) and (4.9) – (4.10). The solid lines represent progression to next cellular stage, e.g. from healthy/unoccupied macrophage, P_h, to infected/occupied macrophage, P_i. Also, the different functional forms considered for killing, F_j, and and germination, G_r, $j = \{1, 2\}$ are given in (4.5) – (4.8).

$$\frac{dS_i}{dt} = -g_i G_r \tag{4.9}$$

$$\frac{dB}{dt} = g_i G_r - \mu F_j + rB \tag{4.10}$$

with initial conditions,

$$P_h(0.5) = P_h^*, P_i(0.5) = P_i^*, S_i(0.5) = S_i^*, B(0.5) = 0$$

where F_j, G_r for j,r=1,2 will be chosen from (4.5) – (4.8).

Equation (4.9) represents the rate of change of intracellular spores, S_i, due to germination and equation (4.10) represents the rate of change of the intracellular bacterial population due to spore germination (with maximal rate g_i), macrophage-induced killing (with maximal rate μ), and replication (with rate r). Note that $\frac{1}{g_i}$ is the average time in model (4.9) – (4.10) that an engulfed spore takes to become a bacterium (first term in (4.10)), susceptible to macrophage-induced killing (2nd term in (4.10)) but also capable of

replicating (3rd term in (4.10)). Figure 4.1 depicts interactions between the healthy and infected macrophages with extracellular spores in the model with one bacterial population as modeled in equations (4.9) – (4.10).

Since the inoculation medium is washed after 30 minutes in the experiment, it is assumed that any extracellular spores are removed from the medium, meaning that there is no phagocytosis after 30 minutes (assumption (b) above). Thus, we set $k_1 = 0$ in the model (4.9) – (4.13) for $t \geq 0.5$ hour. This implies the rate of change of healthy and infected macrophages after the initial 30 minutes are zero, making P_h and P_i constants in system (4.9) – (4.10) or (4.11) – (4.13) , set to the value that each attained at $t = 0.5$ hour in the model system (4.1) – (4.4). Likewise, the population of S_e also no longer needs to be included in the dynamics of the system (4.9) – (4.10). Therefore, we do not track the dynamics of the variables P_h, P_i and S_e, since these populations are not changing after the initial 30 minutes of the experiment. We denote the 30 minute ending values produced from this model for the four populations of macrophages and spores with an asterisk: P_h^*, P_i^*, S_e^* and S_i^* and report all of these for completeness in Table 4.4. Lastly, based on assumptions (e) listed at the beginning of section 4.2.4, we assume the number of intracellular bacteria at 30 minutes ($t = 0.5$ hour) is zero, *i.e.* $B(0.5) = 0$, giving us the initial condition for B in (4.10). To provide a seamless timeline for the transition between models, the initial conditions for system (4.9) – (4.10) begin at 30 minutes after time zero of the experiment except for the extracellular spore population where we set $S_e(0.5) = 0$ since all extracellular spores are washed away after 30 minutes.

As will be discussed in the results, the system given by (4.9) – (4.10) with any combinations of the functional forms for the germination and killing processes do not match well with the available data. Thus, we formulated an alternative model for the dynamics for $t \geq 0.5$ hour which assumes two distinct intracellular bacterial populations as described previously: newly germinated bacteria, B_{ig}, and fully vegetative bacteria, B_i. This alternative model considered is given by equations (4.11) – (4.13).

Figure 4.2 illustrates interactions between the healthy and infected macrophages with extracellular spores in the model with two distinct bacterial stages inside an infected macrophage as modeled in the equations (4.1) – (4.4), (4.11) – (4.13).

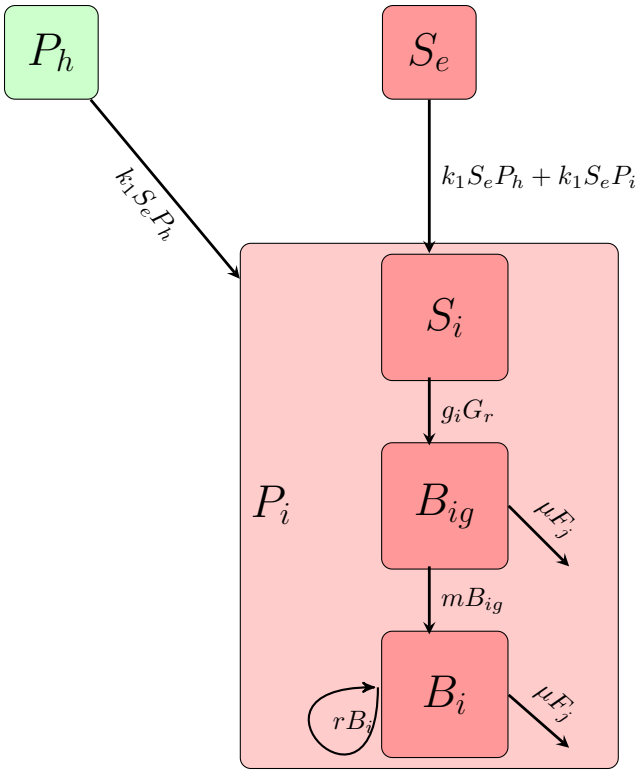

Figure 4.2: Systematic flow diagram of model (4.1) – (4.4) (the equations for the first half hour of the experiment) with model (4.11) – (4.13) (the equations for $t \geq 0.5hr$, which considers two separate bacterial stages). The solid lines represent progression to the next cellular stage. Also, the different functional forms considered for killing, F_j, and and germination, G_r, $j = 1, 2$ are given in (4.5) – (4.8).

$$\frac{dS_i}{dt} = -g_i G_r \tag{4.11}$$

$$\frac{dB_{ig}}{dt} = g_i G_r - \mu F_j - mB_{ig} \tag{4.12}$$

$$\frac{dB_i}{dt} = mB_{ig} + rB_i - \mu F_n \tag{4.13}$$

with initial conditions,

$$P_h(0.5) = P_h^*, P_i(0.5) = P_i^*, S_i(0.5) = S_i^*, B_{ig}(0.5) = 0, B_i(0.5) = 0$$

where G_r for $r = 1, 2$ are the functional forms for germination given in (4.5) – (4.6). Also, the functional forms for killing are F_j and F_n for $j, n = 1, 2$ in the corresponding bacterial

stages given by (4.7) − (4.8). For example, the functional form for mass action killing, F_1, is $\mu B_{ig} P_i$ in newly germinated spore compartment (i.e., equation 4.12) and $\mu B_i P_i$ in vegetative bacteria compartment (i.e., equation 4.13). Similarly, the intracellular burden dependent killing, F_2, is $\mu B_{ig} \frac{P_i}{P_i + C(S_i + B_{ig} + B_i)}$ in newly germinated spore compartment and $\mu B_i \frac{P_i}{P_i + C(S_i + B_{ig} + B_i)}$ in vegetative bacteria compartment.

Similar to the model (4.9) − (4.10) that included only one bacterial stage, equation (4.11) of this alternative model represents the rate of change in the intracellular spores, due to germination, as in equation (4.9). We assume that the population of newly germinating bacteria, B_{ig}, are susceptible to macrophage-induced killing since germination breaks down the protective exospore layers; however, we purpose they are not able to replicate in this stage considering that the germination process is not instantaneous and that replication processes may take some time to initiate while the spore is transitioning from an inert state. Thus, equation (4.12) describes the rate of change of the population of newly germinating bacteria, B_{ig}, due to a gain from the germinating spore population (first term) and losses due to macrophage-induced killing (second term) or to maturation into fully vegetative cells, B_i, at rate m (third term).

If these newly germinating bacteria survive macrophage-induced killing, they progress to becoming fully vegetative bacteria, B_i, at rate m and are now capable of replication. We assume that bacteria in the fully vegetative form are still susceptible to macrophage-induced killing, and include in equation (4.13) a similar terms presented in equation (4.12) representing macrophage-induced killing. Therefore, Equation (4.13) describes the rate of change of the fully vegetative intracellular bacteria population, B_i, due to a gain from the germinating population via maturation and a gain from replication, as well as the loss from macrophage-induced killing. Note that $\frac{1}{m}$ represents the average time it takes for a newly germinating bacterium, B_{ig}, to become a mature, fully vegetative bacterium, B_i. As in the one bacterial stage model, we explore the two bacterial stage model with various functional forms of germination and macrophage-induced killing in Appendix A.2, with selected results discussed in section 4.3.

4.3 Parameter Estimation

Since we have two uncoupled systems of ODEs to describe the dynamics before and after 30 minutes, we estimate the model parameters in two steps. First we estimate the parameter k_1, the rate governing the phagocytosis process in system (4.1) – (4.4). We then use the model with this estimated parameter value to find the values of state variables at 30 minutes (0.5 hour) and use these later as initial conditions for the respective populations in system (4.9) – (4.10) or in system (4.11) – (4.13) as described previously. Next, the parameters appearing in system (4.9) – (4.10) or, alternatively in system (4.11) – (4.13) and that are not set will be estimated by minimizing the relative error defined as the sum of the squares errors between the given data points for both experimental bacterial population (Table 4.3) as well as experimental spore population (Table 4.2) and the output of the model divided by the sum of the squares of data. To perform this optimization, we use MATLAB's global optimization toolbox and, in particular, the *multistart* algorithm which uses several uniformly distributed starting points around which a local optimization solver, $fmincon$, is called. Thus, at each of the starting guesses for an estimate of a model parameter value, the local solver $fmincon$ finds local optima representing the best fit of the model to the data. This is performed numerous times via the *multistart* algorithm which allows a more thorough search for a global minimum. For more information on this, see the Global Optimization Toolbox [31].

4.3.1 Estimation of phagocytosis rate k_1

First, we estimate the value in each MOI of the parameter k_1, the rate that macrophage phagocytose spores. Since experimental data prior to 30 minutes is not available, we estimate k_1 in each MOI by using the respective MOI initial conditions and the corresponding data for intracellular spore counts at 30 minutes after incubation, given in Table 4.2. Column 2 in Table 4.4 shows the estimated values for the phagocytosis rate for each of the different MOI scenarios. Columns 3, 4 and 5 of Table 4.4 show respectively, the model output for the number of healthy macrophages, P_h^*, infected macrophages, P_i^*, intracellular spores,S_i^*, made via the estimation of k_1 to match the intracellular spore count data from Table 4.2), and extracellular spores, S_e^*, present at the end of 30 minutes of

the simulation using model (4.1) − (4.4) with the corresponding k_1 value for each MOI. Based on the models output for the number of infected macrophages at the end of the 30 minute incubation period, we also calculate (in the last column in Table 4.4) the average intracellular burden per infected macrophage: the number of intracellular spores at the end of 30 minutes divided by the number of infected macrophages at the same endpoint of the simulation: $\frac{S_i^*}{P_h^*}$. An asterisk superscript is used to denote values of the given variable at the end of this 30 minutes period.

Table 4.4: The best fit parameter value for the phagocytosis rate k_1 and the model approximated values of the state variables P_h, P_i, S_i, and S_e at the end of 30 minutes (denoted with asterisks) for multiplicity of infection $1:1,\ 1:2,\ 1:10,\ 1:20$. Data in Table 4.2 were used to estimate the parameter value k_1. The intracellular burden at 30 minutes $\frac{S_i^*}{P_i^*}$ is presented in column 6.

MOI	k_1	P_h^*	P_i^*	S_i^*	S_e^*	$\frac{S_i^*}{P_i^*}$
$1:1$	9.4803×10^{-7}	685593	314406	377500	622499	1.2
$1:2$	6.5146×10^{-7}	870227	129772	13900	360999	1.071
$1:10$	5.6205×10^{-7}	975796	24203	24500	75499	1.012
$1:20$	6.5280×10^{-7}	986171	13828	13925	36074	1.007

From Table 4.4, we see that as the initial number of extracellular spores incubated with the initial one million macrophages increases from 5×10^4 in the last row to 10^6 in the first row of $MOIs$, the average number of engulfed spores per infected macrophage at 30 minutes also increases according to the model (last column of Table 4.4). These ratios could be considered the effective or actual $MOIs$ suggested by the model. When the initial experimental MOI is $1:1$, the number of spores per infected macrophage (or the effective MOI) is approximately 1.2 at 30 minutes while this number is less (≈ 1.0) for the MOI of $1:20$. The examination of the experimental results presented in Kang et al. showed that more bacterial killing occurred in the $1:20$ case than in any of the other MOI cases. Our model suggests that a possible explanation is that the $1:20$ experimental MOI, has an effective MOI, as we have defined it here, that is lower than the other MOIs indicating a comparatively smaller per macrophage burden. In fact, the experimental $1:20$ MOI has an effective MOI much closer to a true $1:1$ ratio compared to the effective MOI of the experimental $1:1$ MOI which is slightly higher, indicating a greater per macrophage burden that can decreases killing efficiency as assumed in our model equations.

4.3.2 Estimation of remaining parameters

Next we estimate the germination rate, g_i, killing rate, μ, and the growth rate, r. As set before, the saturation parameter C is still taken 0.2. We consider two different models: one bacterial stage as given by equations $(4.9) - (4.10)$ versus the two bacterial stages as given by equations $(4.11) - (4.13)$. In both stages, the initial values of the variables P_h, P_i and S_i are the values at the end of 30 minutes from the system $(4.1) - (4.4)$ given in Table 4.4. Note that in the case where two bacterial stages are modeled, estimation of 4 parameters is needed: germination rate, g_i, killing rate, μ, the growth rate, r and the maturation rate, m. Since we have a limited amount of data points, estimating all four parameters with these data can lead to overfitting the data. Thus, we fix the value of the maturation rate parameter, m, and estimate the remaining three parameters. Several values of a fixed maturation rate are investigated. Also, Appendix A.2 presents some of the discussions for models $(4.9) - (4.10)$ as well as $(4.11) - (4.13)$ with different combinations of functional forms for killing, F_j and germination, G_r (see $(4.5) - (4.8)$) including parameter estimation and numerical simulations.

Estimating Parameters in One Bacterial Stage Model

We now present the estimates of the parameter values for the model $(4.9) - (4.10)$ that considers a single bacterial stage model with functional forms for germination given by (4.5) and killing given by (4.8). The results from other functional forms are presented in Appendix A.2. We pick this combination of functional forms for germination and killing because of the smallest relative error for most of the MOIs compared to other functional forms. Tables 4.5 summarizes the estimated parameter values of spore germination rate, g_i, phagocytic killing rate, μ, and the bacterial growth rate, r, for different MOIs acquired from fitting model $(4.9) - (4.10)$ to the experimental data for total bacterial population, B, given in Table 4.3 and total spore and bacterial population, S_i given in tables 4.2 at $1, 3, 5$, and 24 hr time points. Also, given is the total number of bacteria that are killed inside their host cells within the $0.5 - 24$ hour experimental period in each MOI; that is, we calculate

$$\int_{0.5}^{24} \mu B \frac{P_i}{P_i + C(S_i + B)} dt$$

for each MOI. This quantity along with the relative errors

$$RE = \frac{\sum(model - data)^2}{\sum(data)^2}$$

of estimation are provided in the last two columns of each of the table, respectively. Model fits to this data are displayed in Figure 4.3.

Table 4.5: The estimated model parameter values (columns 2,3,4) for the model (4.9) – (4.10) with simple germination, $g_i G_1$, and intracellular burden dependent killing, μF_2, by fitting the spore and bacterial populations from Table 4.2 and Table 4.3. The total number of bacteria killed in [0.5,24] hours period is presented in the 5th column and the error of estimation is shown in column 6. Each graph represent the quantities for different initial spore loads (MOI).

MOI	g_i	μ	r	# of B killed	RE
$1:1$	1.5313×10^{-6}	2.0398	1.3424	1.4805×10^{6}	0.8465
$1:2$	4.8649×10^{-6}	0.3661	0.0010	1.3936×10^{5}	0.1646
$1:10$	1.1122×10^{-5}	1.3296	0.9900	2.1403×10^{5}	0.3779
$1:20$	5.7934×10^{-4}	5.5895	3.9900	6.7551×10^{4}	0.4367

From Table 4.5, we observe the increasing pattern for germination rates for decreasing initial spore loads (MOIs) and no such patterns for killing and replication rates. However, The killing rate and the replication rates are highest for MOI 1:20. Also in Appendix A.2, we have presented the parameters estimated by using only the experimental bacterial data and the model (4.9) – (4.10) as well as the model with with other functional forms for germination and killing. One of the observations we made from the parameters and numerical simulations for one bacterial stage model (4.9) – (4.10) with varying functional forms for germination and killing is that the fits of this model to the experimental bacterial and spore datasets, particularly at 24 hours, is quite poor for all MOIs. Thus, this led us to consider the development of the alternate model given by equations (4.11) – (4.13).

In model (4.9) – (4.10), the start of germination of a spore and its ability to replicate can occur simultaneously along with phagocytic killing. However, the germination process that a spore must undergo before it is viable to replicate is not instantaneous even though it might be quick compared to other events. As the spore breaks down its protective exospore layers in response to appropriate germinants to transform into a vegetative bacterium, it is also becoming more vulnerable to the killing mechanisms of its host cell. Thus, we developed model (4.11) – (4.13) to separate the bacterial populations into those that are germinating and those that are fully vegetative and capable of replication, as explained in Section 4.2.

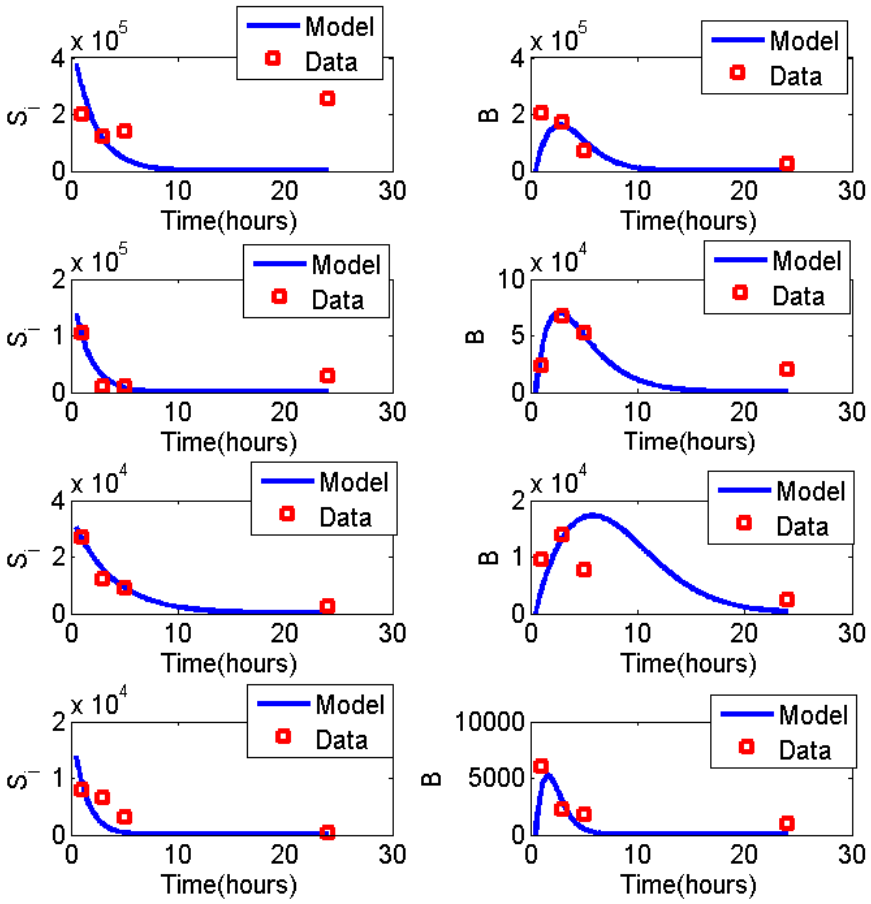

Figure 4.3: Numerical results showing the model fit with estimated parameters from Table 4.5 to the experimental data from Tables 4.2 and 4.3. The two graphs in each row represent the model fit to the experimental data (red squares) for spore and bacterial populations for MOIs 1:1 through 1:20. Here, model (4.9) – (4.10) is considered with simple germination ($g_i G_1$) and intracellular burden-dependent killing (μF_2).

Therefore, in the next section, we find the best fit parameters for the model (4.11) – (4.13) that incorporates these two distinct bacterial stages: newly germinating bacteria, B_{ig}, and the mature vegetative bacteria, B_i.

Estimating Parameters in Two Bacterial Stage Model

Equations (4.11) – (4.13) contain four parameters: germination rate, g_i, killing rate, μ, maturation rate, m and the replication rate, r. Due to the distinct bacterial stages considered in this model, the maturation rate is the average rate a germinated spore becomes

a fully vegetative replicating bacteria and thus, $\frac{1}{m}$ represents the average time (in hours) that a newly germinated spore, B_{ig} takes to become a fully vegetative forms capable of replicating, B_i. The concept that there is a delay that germinating spores experience before maturing into fully vegetative bacteria capable of replicating is neither theoretically nor empirically well-established. Thus, we present results for the following fixed average maturation durations: 2.5, 5 and 10 hours, giving $m = 0.4, 0.2, 0.1$, respectively.

Each value of m corresponds respectively to Cases $I - III$ below. In each case, the optimization scheme discussed above is used to acquire the respective best fit values for the parameters of model $(4.11) - (4.13)$ to the experimental data for experimental bacterial populations given in Table 4.3 as well as the experimental spore populations given in Table 4.2. The parameter estimates are then displayed in 2nd, 3rd, and 4th columns of tables (cf. Tables 4.6 - 4.8) followed by corresponding simulation results (cf. Figures 4.4 - 4.6). The total number of bacteria that are killed inside their host cells within the $0.5 - 24$ hour experimental period (as was done in the one bacterial stage case) together with the relative errors of estimation are provided in the last two columns of these tables (cf. Tables 4.6 - 4.8). The figures all display the model output for the total bacterial population which is the sum of two separate bacterial populations, B_{ig} and B_i and also the model output for the spore populations. Each of the four rows in Figures 4.4, 4.5 and 4.6 corresponds to one of the four $MOIs$: $1:1, 1:2, 1:10$, and $1:20$, respectively.

Case I: Two bacterial stage model with $m = 0.4$

For a value of $m = 0.4$ the average time of maturation is 2.5 hours. Table 4.6 provides the parameters estimated using bacterial population data from Table 4.3 and spore population data from Table 4.2. Figure 4.4 shows the model output and corresponding experimental data as discussed above.

From Table 4.6, we observe that the germination rate, g_i, is increasing with decreasing initial spore loads. The effective germination in low initial spore challenge which results to low intracellular burden per infected macrophage (see table 4.4) makes sense as less intracellular burden may provide more space to germinate. The other two parameters μ and r do not show a clear dependence in initial spore load (MOIs). However, for MOI

Table 4.6: Estimated values of spore germination rate, gi, phagocytic killing rate, μ, and the bacterial growth rate, r, for different $MOIs$, assuming a maturation rate of germinating spores as $m = 0.4$. Model (4.11) – (4.13) with germination, $g_i G_1$, killing, μF_2 where $F_2 = B_{ig}\frac{P_i}{P_i+C(S_i+B_{ig}+B_i)}$ in equation (4.12) and $F_2 = \mu B_i\frac{P_i}{P_i+C(S_i+B_{ig}+B_i)}$ in equation (4.13) was used with the experimental bacterial data from Table 4.3 and spore from Table 4.3 to acquire these parameter estimates. The last two columns respectively show for each MOI the calculation of total intracellular bacteria $B = B_{ig} + B_i$ that were killed over the $0.5 - 24$ hours and the the relative errors of the estimates.

MOI	g_i	μ	r	# of B killed	RE
1 : 1	4.5680×10^{-6}	0.4872	0.0001	3.7754×10^{5}	0.7166
1 : 2	5.1980×10^{-6}	0.7419	0.6509	6.3136×10^{5}	0.1133
1 : 10	1.1704×10^{-5}	0.1648	0.0003	2.8760×10^{4}	0.2863
1 : 20	5.9443×10^{-4}	1.0490	0.0013	1.3923×10^{4}	0.4452

1 : 20, the estimated phagocytic killing rate value is the highest in all $MOIs$. Also the error is maximum for MOI 1:1 due to the mismatch of model and data for spore populations. All the error estimates are smaller than those in the one bacterial stage model (Case I).

From Figure 4.4, we see that for $MOIs$ 1 : 1 through 1 : 10, the model fits the experimental bacterial data well for first 5 hours. For the spore populations, the model fits the data well for $MOIs$ 1:2 through 1:10. But the 24 hour data points do not fit for the both bacterial and spore population for almost all $MOIs$.

Case II: Two bacterial stage model with $m = 0.2$

Case II considers a value of m which corresponds to an average time of maturation to be 5 hours. Table 4.7 show the best fit parameter estimates for the model $(4.11) - (4.13)$ where parameters are estimated by taking experimental bacterial population from Table 4.3 and spore populations from Table 4.2. As in the previous case, the columns 2, 3 and 4 are the estimated parameter values and column 5 and 6 represent the number of bacteria killed in $0.5 - 24$ hours period and the relative error of estimation respectively. The corresponding numerical results are presented in Figure 4.5 for each $MOIs$ where each row represent model prediction and experimental data for bacterial and spore populations in each $MOIs$.

From Table 4.7, we observe the increasing behaviors of the germination rates for decreasing initial spore loads. Also for the other two parameters μ and r, the values are increasing with decreasing initial spore loads except for MOI 1:10. The relative errors are smaller than the one bacterial stage case as well as two bacterial case with $m = 0.4$. Also as

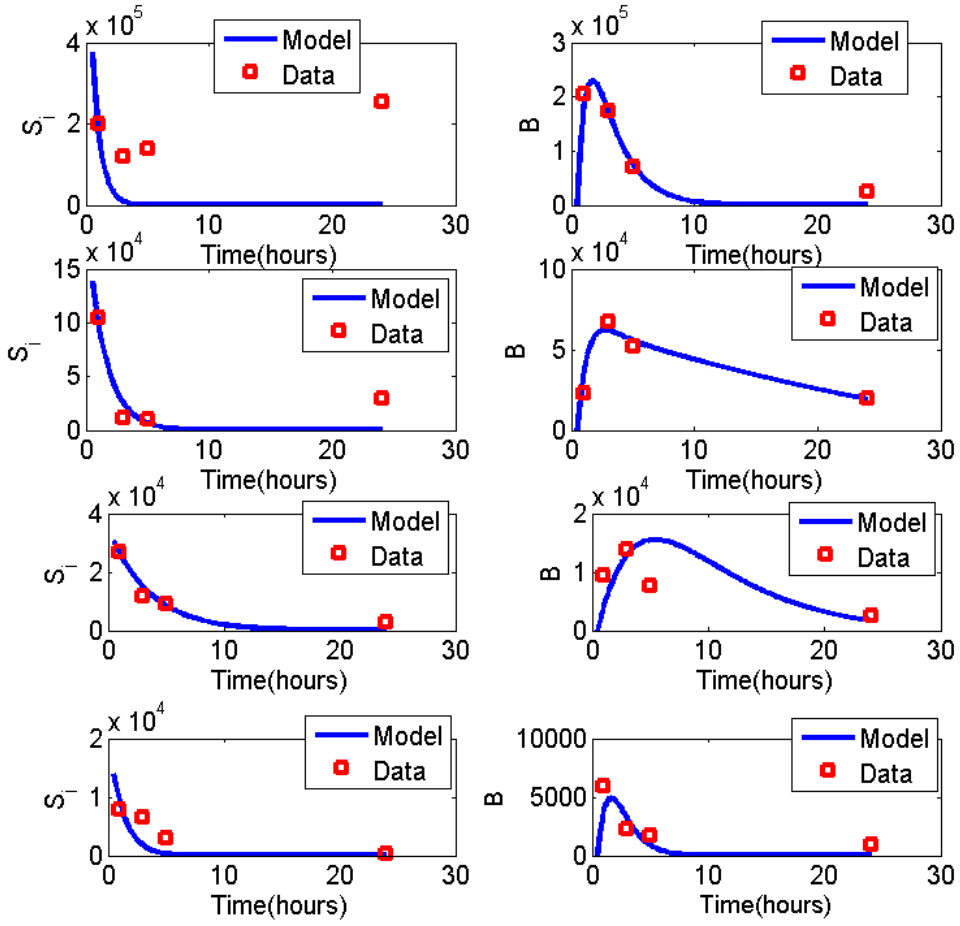

Figure 4.4: Numerical results showing the model fit with estimated parameters from Table 4.6 to the experimental bacterial data from Table 4.3 and spore data from the Table 4.2 assuming the maturation rate $m = 0.4$. The two graphs in each row represent the model fit to the experimental data (red squares) for Spore and bacterial populations for MOIs 1:1 through 1:20. Here model (4.11) – (4.13) is considered with simple germination, $g_i G_1$, and intracellular burden dependent killing, μF_2, where $F_2 = B_{ig} \frac{P_i}{P_i + C(S_i + B_{ig} + B_i)}$ in equation (4.12) and $F_2 = B_g \frac{P_i}{P_i + C(S_i + B_{ig} + B_i)}$ in equation (4.13).

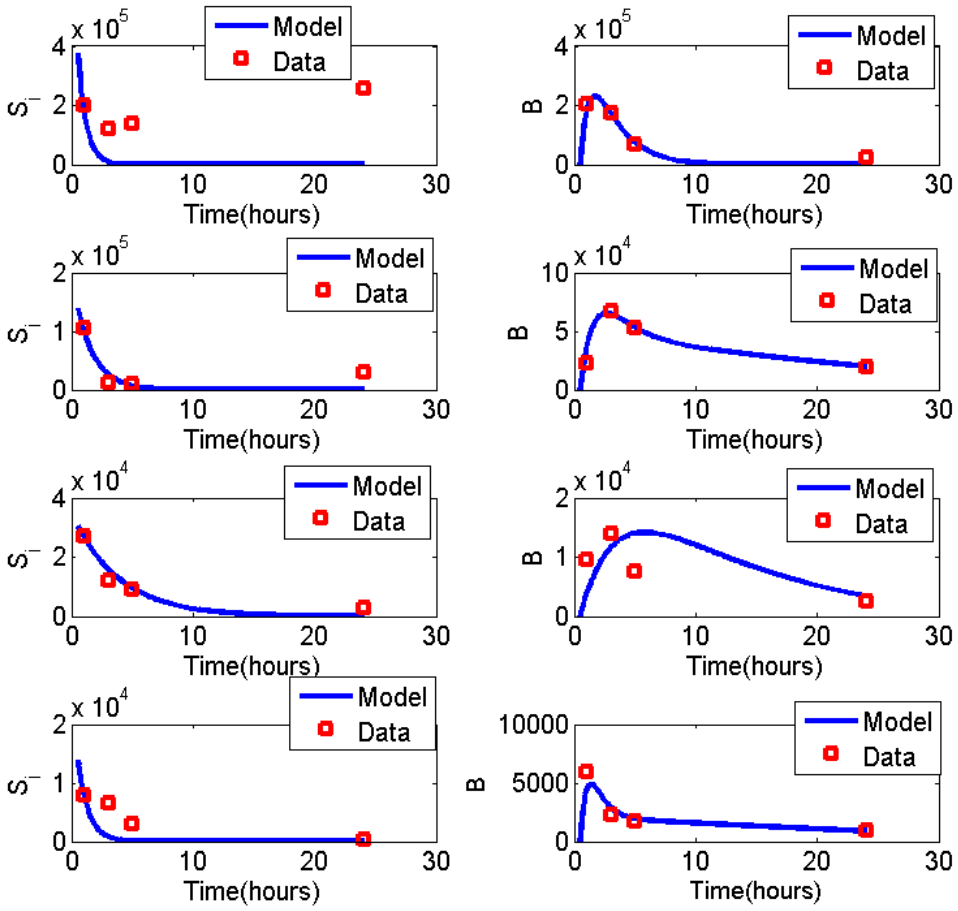

Figure 4.5: Numerical results showing the model fit with estimated parameters from Table 4.6 to the experimental bacterial data from Table 4.3 and spore data from the Table 4.2 assuming the maturation rate $m = 0.2$. The two graphs in each row represent the model fit to the experimental data (red squares) for Spore and bacterial populations for MOIs 1:1 through 1:20. Here, model (4.11) – (4.13) is considered with simple germination, $g_i G_1$, and intracellular burden dependent killing, μF_2, where $F_2 = B_{ig} \frac{P_i}{P_i + C(S_i + B_{ig} + B_i)}$ in equation (4.12) and $F_2 = B_g \frac{P_i}{P_i + C(S_i + B_{ig} + B_i)}$ in equation (4.13).

Table 4.7: Estimated values of spore germination rate,gi, phagocytic killing rate, μ, and the bacterial growth rate, r, for different $MOIs$, assuming a maturation rate of germinating spores of $m = 0.2$. Model (4.11) – (4.13) with germination, $g_i G_1$, killing, μF_2, where $F_2 = B_{ig}\frac{P_i}{P_i+C(S_i+B_{ig}+B_i)}$ in equation (4.12) and $F_2 = \mu B_i\frac{P_i}{P_i+C(S_i+B_{ig}+B_i)}$ in equation (4.13) was used with the experimental bacterial data from Table 4.3 and spore from Table 4.3 to acquire these parameter estimates. The last two columns respectively show for each MOI the calculation of total intracellular bacteria $B = B_{ig} + B_i$ that were killed over the $0.5 - 24$ hours and the relative errors of the estimates.

MOI	g_i	μ	r	# of B killed	RE
1 : 1	4.5689×10^{-6}	0.4874	0.0010	3.7782×10^{5}	0.7166
1 : 2	5.0744×10^{-6}	0.5454	0.4817	4.2830×10^{5}	0.1121
1 : 10	1.0707×10^{-5}	0.2372	0.1290	4.4482×10^{4}	0.2598
1 : 20	8.1434×10^{-5}	1.5758	1.5078	6.0407×10^{4}	0.4326

in the previous case, the highest parameter values are observed in MOI 1:20. The higher values of all the parameters are for smaller intracellular burden makes sense as the spore may have better environment to germinate and later replicate for the survived bacteria and it may be easier for infected macrophage to handle smaller burden. For bacterial populations, the model fits the data fairly well as observed in Figure 4.5 and similar fits are observed for spore population compared to the $m = 0.4$ case.

Case III: Two bacterial stage model with $m = 0.1$

Case III examines the last value presented here of $m = 0.1$ for an average time of maturation of 10 hours. Table 4.8 show the best fit parameter estimates for the model $(4.11) - (4.13)$ where parameters are estimated by taking experimental bacterial population from Table 4.3 and spore populations from Table 4.2 . As in the previous cases, the columns 2, 3 and 4 of Table 4.8 are the estimated parameter values and column 5 and 6 represent the number of bacteria killed in $0.5 - 24$ hours period and the relative error respectively. The corresponding numerical results are presented in Figures 4.6 for each $MOIs$.

From Table 4.8, we observe that the germination rate, g_i, and the replication rates, r, show the increasing pattern with decreasing initial spore load and the killing rate, μ, shows similar values for $MOIs$ 1:1 and 1:2 and follows the increasing trend with decreasing initial spore loads. As in the previous cases the highest values of all parameters are observed in the lowest initial spore loads. The relative errors in this case seems to be comparable to the $m = 0.2$ case. The model fits the bacterial data fairly well as observed in Figure 4.6

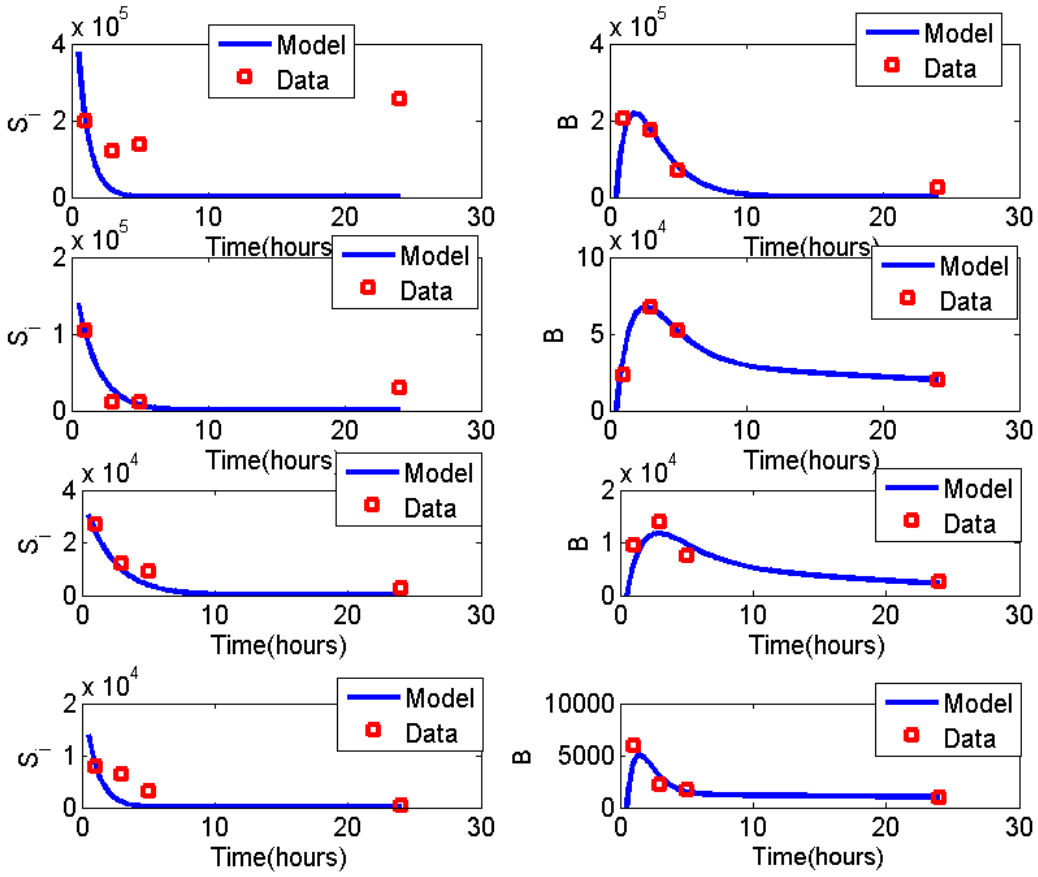

Figure 4.6: Numerical results showing the model fit with estimated parameters from Table 4.6 to the experimental bacterial data from Table 4.3 and spore data from the Table 4.2 assuming the maturation rate $m = 0.1$. The two graphs in each row represent the model fit to the experimental data (red squares) for Spore and bacterial populations for MOIs 1:1 through 1:20. Here, model (4.11) – (4.13) is considered with simple germination, $g_i G_1$, and intracellular burden dependent killing, μF_2, where $F_2 = B_{ig} \frac{P_i}{P_i + C(S_i + B_{ig} + B_i)}$ in equation (4.12) and $F_2 = B_g \frac{P_i}{P_i + C(S_i + B_{ig} + B_i)}$ in equation (4.13).

Table 4.8: Estimated values of spore germination rate,gi, phagocytic killing rate, μ, and the bacterial growth rate, r, for different $MOIs$, assuming a maturation rate of germinating spores of $m = 0.1$. Model (4.11) − (4.13) with germination, $g_i G_1$, killing, μF_2, where $F_2 = B_{ig}\frac{P_i}{P_i+C(S_i+B_{ig}+B_i)}$ in equation (4.12) and $F_2 = \mu B_i\frac{P_i}{P_i+C(S_i+B_{ig}+B_i)}$ in equation (4.13) was used with the experimental bacterial data from Table 4.3 and spore from Table 4.3 to acquire these parameter estimates. The last two columns respectively show for each MOI the calculation of total intracellular bacteria $B = B_{ig} + B_i$ that were killed over the $0.5 - 24$ hours and the relative errors of the estimates.

MOI	g_i	μ	r	# of B killed	RE
$1:1$	3.8715×10^{-6}	0.4873	0.0004	3.7762×10^{5}	0.7223
$1:2$	4.9935×10^{-6}	0.4590	0.4220	3.2871×10^{5}	0.1128
$1:10$	1.8867×10^{-5}	0.5616	0.4947	6.5722×10^{4}	0.1198
$1:20$	7.4532×10^{-5}	1.3108	1.2791	4.4425×10^{4}	0.4167

and the spore data fit is similar to the previous cases for $m = 0.4$ and $m = 0.2$. From these results and results from Appendix A.2, we can see that the model fits the data better for smaller values of m.

In results from additional simulations not shown here, we note that when we ignored phagocytic killing of fully vegetative bacteria, the m-values required to achieve acceptable model fits to the data implied very long and possibly unreasonable average maturation durations of $30 - 100$ hours ($i.e. m \in \{0.033, 0.02, 0.01\}$). Also, If the maturation rate is larger than $m = 0.4$, the proposed model does not fit the experimental data well (results not shown), although it fits much better than when we considered system (4.9) − (4.10) which only included one bacterial stage. If the estimated values found above for the parameters given a particular value of m are not considered to be feasible average rates for these processes, then a modified model would need to be considered in order to account for other aspects of these processes. For instance, fully germinated spores may still not be able to replicate immediately after germination is complete as is assumed in model (4.11) − (4.13) but, instead, there may be an additional delay before replication which is not presently accounted for.

4.4 Conclusion and Discussion

Our work developed a novel mathematical model of the dynamics of a host pathogen interaction based on an *in vitro* experiment with anthrax. We first purposed a model that considered a single bacterial stage and then a second model which included two bacterial

stages. The main distinction between one stage verses to bacterial stage model were that the two bacterial stages model consists of newly germinated spores which are not able to to replicate and vegetative bacteria that are able to replicate. While all bacteria in the one bacterial stage model are hemogeneous in terms of replication. In both models we considered two different functional forms for spore germination and macrophage killing events: simple mass action functional form and intracellular burden-dependent functional form. Our results after fitting the various model types to the available experimental data show that a one bacterial stage model with any combination of the functional forms for spore germination and macrophage killing did not describe the data well. This model fit the first 5 hour data but did not fit the 24 hour data point. The two bacterial stage model using any combination of functional forms for germination and macrophage killing fits the experimental data better. Also, estimating parameters using bacterial only data gave the nearly perfect fit for the model and experimental data for two bacterial stages model. This suggest that replication of the vegetative bacteria does not simultaneously occur with the initiation of germination. We purpose that the newly germinated spores are susceptible to macrophage-induced killing but can not yet replicate and that it takes a sufficient amount of time for the germinating spores to become ready and able to replicate; thus effectively defining two distinct bacterial stages. From the two bacterial stage model, we see that the killing rate tend to increase for lower initial spore loads. Our numerical simulation suggested that newly germinated bacteria takes about 5 hours or longer to become fully vegetative bacteria. The variation of models using different functional forms for germination and macrophage-induced killing suggested that the model output is not significantly different among the different functional forms considered.

We were able to find a model variation that fit the S_i and B data fairly well. We note that the model fits with the spore data were not very accurate for some of the MOIs and had the higher error size. Another hypothesis that could be explored is to consider that a spore does not instantaneously germinate when phagocytosed. A second spore variable could be considered much like the two bacterial bacterial stages. Perhaps, during incubation, some spores get stuck to the macrophage but not yet internalized. If the medium is washed these spores may still retain their position but still unable to germinate. At one hour when cell

are lysed and spores are counted, they would be counted among the intracellular CFU. In the later time points these may have been fully phagocytosed and now in an appropriate environment to begin germination.

Bibliography

[1] P. Apps. Smithers' mammals of southern africa: A field guide. *Struik Publishers*, Third edition, 2000. 18, 19

[2] T.A. Bartrand, M.H. Weir, and C.N. Haas. Dose-response models for inhalation of bacillus anthracis spores: interspecies comparisons. *Risk Analysis*, 28:1115–1124, 2008. 78

[3] S.E. Bellan, P.C.B. Turnbull, W. Beyer, and W.M. Getz. Effects of experimental exclusion of scavengers from carcasses of anthrax-infected herbivores on *bacillus anthracis* sporulation, survival and distribution. *Applied and Environmental Microbiology*, 79(12):3756–3761, 2013. 17, 18, 19

[4] R. Brookmeyer, E. Johnson, and S. Barry. Modelling the incubation period of anthrax. *Statistics in Medicine*, 24(4):531–542, 2005. 78

[5] L. Busch. Bison herd suffers worst anthrax outbreak on record. *Northern News Services Online,*
$http://www.nnsl.com/frames/newspapers/2012-08/aug13\_12bs.html$, 2012. 1, 4

[6] S.B. Clegg, P.C. Turnbull, C.M. Foggin, and P.M. Lindeque. Massive outbreak of anthrex in wildlife in the malilangwe wildlife reserve, zimbabwe. *The Veterinary Record*, 160(4):113–118, 2007. 5, 8, 17, 18, 19, 21, 25, 30

[7] A. Cleret, A. Quesnel-Hellmann, A. Vallon-Eberhard, B. Verrier, S. Jung, D. Vidal, J. Mathieu, and J. N. Tournier. Lung dendritic cells rapidly mediate anthrax spore entry through the pulmonary route. *Journal of Immunology*, 178(12):7994–8001, 2007. 3, 78

[8] Texas Animal Health Commission. Anthrax confirmed in eadwards county deer, $http://www.ttha.com/ttha/news/2014/09/08/anthrax-confirmed-in-edwards-county-deer$. 2014. 1

[9] J.P. Corre, A. Piris-Gimenez, M. Moya-Nilges, G. Jouvion, A. Fouet, I.J. Glomski, M. Mock, J.C. Sirard, and P.L. Goossens. In vivo germination of bacillus anthracis spores during murine cutaneous infection. *Journal of Infectious Disease*, 207(3):450–457, 2013. 84

[10] C.M. Dahlgren, B.L, H.M. Decker, S.W. Freed, C.R. Phillips, and P.S. Brachman. *bacillus anthracis* aerosols in goat hair processing mills. *American Journal of Hygine*, 72:34–31, 1960. 77

[11] J. Day, A. Friedman, and L.S. Schlesinger. Modeling the host response to inhalation anthrax. *Theoritical Biology*, 276:199–208, 2011. 3, 78, 79

[12] T.C. Dixon, A.A. Fadl, T.M. Koehler, J.A. Swanson, and P.C. Hanna. Early *bacillus anthracis – macrophage* interactiona: intracellular survival and escape. *Cellular Microbiology*, 2(6):453–463, 2000. 3, 78

[13] D.C. Dragon and R.P. Rennie. The ecology of anthrax spores: Tough but not invincible. *Canadian Veterinary Journal*, 36:295–301, 1995. 4

[14] P. Van Den Driessche and J. Watmough. Reproduction number and sub-threshold endemic equilibria for compartmental models of disease transmission. *Mathematical Bioscience*, 180:29–41, 2002. 10, 12

[15] R L. During, W.Li, B. Hao, J.M. Koenig, D.S. Stephens, C.P. Quinnand, and F.S. Southwick. Anthrax lethal toxin paralyzes neutrophil acting based motility. *Journal of Infectious Disease*, 192:837–845, 2005. 78

[16] L.C. Evans. *Partial Differential Equations*, volume 19. American Mathematical Society, Reading, Massachusetts, 1998. 35, 36

[17] A. Fasanella, D. Galante, G. Garofolo, and M. Hugh Jones. Anthrax under valued zoonosis. *Veterinary Microbiology*, 140:318–331, 2010. 3

[18] E.M. Fevre, B.M. de C. Bronsvoort, K.A. Hamilton, and S. Cleaveland. Animal movements and the spread of infectious diseases. 14(3):125–131, 2006. 29

[19] K.R. Fister, S. Lenhart, and J.S. McNally. Optimizing chemotherapy in an HIV model. 32:1–12, 1998. 16, 22

[20] Center for Disease Control and Prevention. Inhalational anthrax, *http* : *//www.cdc.gov/anthrax/types/inhalation.html*. 2013. 1, 2, 77, 78

[21] A. Friedman and A-A. Yakubu. Anthrax epizootic and migration: Persistence or extinction. *Mathematical Bioscience*, 241(1):137–144, 2013. 7, 8, 30

[22] P.R. Furniss and B.D. Hahn. A mathematical model of an anthrax epizootic in the kruger national park. *Applied Math Modeling*, 5(3):130–136, 1981. 8

[23] R. Grunow, L. Verbeek, D. Jacob, T. Holzmann, G. Birkenfeld, D. Wiens, L. Von Eichel-Streiberand G. Grass, and U. Reischl. Injection anthrax–a new outbreak in heroin users. *Deutsches Arzteblatt International*, 109(49):843–848, 2012. 2

[24] B. Gutting. Deterministic models of inhalational anthrax in new zealand white rabbits. *Biosecurity Bioterrorism*, 12(1):29–41, 2014. 78, 79

[25] W.K. Hackbusch. A numerical method for solving parabolic equations with opposite orientations. 20:229–240, 1978. 22

[26] B.D. Hahn and P.R. Furniss. A deterministic model of and anthrax epizootic: Threshold results. *Ecological Modelling*, 20(2-3):233–241, 1983. 7

[27] P.C. Hanna, D. Acosta, and R.J. Collier. On the role of macrophages in anthrax. *Microbiology*, 90:10198–10201, 1993. 3, 78

[28] L. Hartfield. Bad year for anthrax outbreaks in us livestock. *Center for Infectious Disease Research and Policy (CIDRAP), University of Minnesota, http* : *//www.cidrap.umn.edu/news* − *perspective/2005/08/bad* − *year* − *anthrax* − *outbreaks* − *us* − *livestock*, 2005. 1

[29] Anna Cavalli-Bjrkman Hellstrm. The secret life of *bacillus anthracis*. *Sveriges lantbruksuniversitet*, 17:1—15, 2013. 3, 4

[30] H. Hu, Q. Sa, T.M Koehler, A.I. Aronson, and D. Jhou. Inactivation of *bacillus anthracis* spores in murine primary macrophages. *Cellular Microbiology*, 8:1634–1642, 2006. 82

[31] The MathWorks Inc. *Global optimization toolbox user's guide*. Release 2015a, 2015. 18, 93

[32] T.J. Kang, M.J. Fenton, M.A. Weiner, B. Subhendu S. Hibbs, L. Baillie, and A.S. Cross. Mourine macrophages kill the vegetative form of *bacillus anthracis*. *Infection and Immunity*, 73(11):7495–7501, 2005. 78, 80, 81, 84, 86

[33] J.E. Kirby. Anthrax lethal toxin induces human endothelial cell apoptosis. *Infection and Immunity*, 72:430–439, 2004. 3

[34] R. Kumar, , C.C. Chow, J.D. Bartels, G. Clermont, and Y. Vodovotz. A mathematical simulation of the inflammatory response to anthrax infection. *Shock*, 29(1):104–111, 2008. 78

[35] S. Lenhart and J. T. Workman. *Optimal Control Applied to Biological Models*. Chapman and Hall/CRC, 1998. 22

[36] D.L. Lukes. *Differential equations: classical to controlled*, volume 162. 14

[37] A. Mayer-Scholl. A review of the interaction of *bacillus anthracis* with cells of the innate immune response. *Berl Munch Tierarztl Wochenschr*, 119(5-6):216—221, 2006. 78

[38] J.S. Nishi, D.C Dragon, B.T. Elkinand, J. Mitchell, T.R. Ellsworthand, and M.E. Hugh-Jones. Emergency response planning for anthrax outbreaks in bison herds of northern canada. *Annals of the New York Academy of Sciences*, 969:245—250, 2002. 5

[39] Department of Agriculture Forestry Fisheries. Department of Agriculture Forestry and Fisheries, Republic of South Africa, Agricultural Development Institute, *http : //gadi.agric.za/articles/furstenburg_d/kudu.php*. 2015. 18, 19

[40] Ministry of Environment and Republic of Namibia Tourism. Species management plan: Roan antelope, sable antelope and tsessebe, *http : //www.nnf.org.na/rarespecies/mammals/rare_library_docs/rst_smp.pdf*. 2003. 18, 19

[41] L.S. Pontryagin, R.V. Gamkrelize, V.G. Boltyanskii, and E.F. Mishchenko. *The Mathematical Theory of Optimal Processes*. Wiley, New York, 1962. 15

[42] P.J. Robinson, E.J. Fleming, E.C. Hack, D.J. Schneider, and J.M. Gearhart. *Biologically Based Modeling Of Anthrax Infection: Modulation Of Macrophage MAPK Signaling Pathway By Lethal Toxin*, volume 8. J Med CBR Def, 2010. 78

[43] S. Salsa, F. Vegni, A. Zaretti, and P. Zunino. *Primer on PDEs. Models, Methods, Simulations*. Springer, Italia, 2013. 35

[44] P. Sanz, L.D. Teel, F. Alem, H.M. Carvalho, S.C. Darnell, and A. D. O'Brien. Detection of bacillus anthracis spore germination in vivo by bioluminescence imaging. *Infection and Immunity*, 76(3):1036—1047, 2008. 84

[45] A.H. Seydack, C.C. Grant, I.P. Smit, W.J. Vermeulen, J. Baard, and N. Zambatis. Large herbivore population performance and climate in a south african semi-arid savanna. *KOEDOE*, 54(1):1—20, 2012. 18, 19

[46] S.V. Shadomy and T.L. Smith. Anthrax. *Journal of the American Veterinary Medical Association*, 233:63—72, 2008. 2

[47] J. Simon. Compact sets in the space $l^p(0, t, b)$. *Annali di Mathematica pura ed applicata (IV)*, CXLVI:65—96, 1987. 49, 55

[48] R. Thompson. Anthrax outbreak abating. *Northern News Services Online, http : //www.nnsl.com/frames/newspapers/2012 − 08/aug16_12BIS.html*, 2012. 1

[49] P.C.B. Turnbill. *Anthrax in animals and humans*. WHO Press, Fourth edition, Geneva., 2013. 1, 2, 3, 4, 5, 18, 19, 25, 29, 30, 77

[50] U.S. Food and Drug Administration . *Anthrax.* *http : //www.fda.gov/BiologicsBloodVaccines/Vaccines/ucm*061751.*htm*. U.S. Food and Drug Administration, 2015. 2

[51] V.De Vos. The ecology of anthrax in the Kruger National Park, South Africa. *Koedoe*, 68:19–23, 1990. 4

[52] V.De Vos, G.L. Rooyen, and J.J. Kloppers. Anthrax immunizations of free ranging roan antelope hippotragus equinus in the Kruger National Park. *Koedoe*, 16(1):11–25, 1973. 5, 18, 19

[53] S. Welkos, A. Friedlander, S. Weeks, S. Little, and I. Mendelson. *in vitro* characterisation of the phagocytosis and fate of anthrax spores in macrophages and the effects of anti-pa antibody. *Journal of Medical Microbiology*, 51(10):821–831, 2002. 82

[54] D.A. Wilkening. Sverdlovsk revisited: modeling human inhalation anthrax. *Proc National Academy of Science U S A*, 103(20):7589–7594, 2006. 78

[55] D.A. Wilkening. Modeling the incubation period of inhalational anthrax. *Medical Decision Making*, 28(4):593–605, 2008. 78

Appendix

Appendix A

A.1 Proof of Claim II (page 39)

Claim: $\bar{S}, \bar{I}, \bar{V}$ are bounded from above.

Proof of the claim: Since $||s^0(x)||_{L^\infty} \leq \frac{M}{2}$, let $w(x,t) = (\bar{S} - \frac{M}{2})^+ = \max\{(\bar{S} - \frac{M}{2}), 0\}$ multiply the inequality (3.18) by $w(x,t)$ and integrate over Ω. Then as in Claim I, we get

$$\int_\Omega \frac{\partial \bar{S}}{\partial t} w dx + d\int_\Omega \nabla \bar{S} \cdot \nabla w dx + \int_\Omega (\lambda - r\frac{(h_1+h_3)}{K}e^{\lambda t} + \theta_c h_4 e^{\lambda t} + \theta_i h_2 e^{\lambda t} + u_1)\bar{S} w dx \leq 0$$

$$\frac{1}{2}\frac{\partial}{\partial t}\int_\Omega w^2 dx + d\int_\Omega |\nabla w|^2 dx + \int_\Omega (\lambda - r\frac{(h_1+h_3)}{K}e^{\lambda t} + \theta_c h_4 e^{\lambda t} + \theta_i h_2 e^{\lambda t} + u_1) w^2 dx$$

$$\leq -\int_\Omega (\lambda - r\frac{(h_1+h_3)}{K}e^{\lambda t} + \theta_c h_4 e^{\lambda t} + \theta_i h_2 e^{\lambda t} + u_1) w K_1 dx$$

Choose λ big and T small enough s.t. $\forall t \in (0,T)$, $\lambda \geq r\frac{(h_1+h_3)}{K}e^{\lambda t} + \theta_c h_4 e^{\lambda t} + \theta_i h_2 e^{\lambda t} + u_1$

Then we get

$$\frac{1}{2}\frac{\partial}{\partial t}\int_\Omega w^2 dx + d\int_\Omega |\nabla w|^2 dx + \int_\Omega (\lambda - r\frac{(h_1+h_3)}{K}e^{\lambda t} + \theta_c h_4 e^{\lambda t} + \theta_i h_2 e^{\lambda t} + u_1) w^2 dx \leq 0$$

implying

$$\frac{\partial}{\partial t}\int_\Omega w^2 dx \leq 0$$

Integrating over 0 to t; where $t \in (0,T)$, we get

$$\int_\Omega w^2(x,t) dx \leq \int_\Omega w^2(x,0) dx \tag{A.1}$$

Since $w(x,0) = 0$ ($\because$ $w(x,0) = max\{\bar{S}(x,0) - \frac{M}{2}, 0\} = max\{s^0(x) - \frac{M}{2}, 0\}$) and $w(x,t) \geq 0$, then using (3.19) we get , $w(x,t) = 0$.

This implies from the definition of $w(x,t)$ that $\bar{S} - K_1 \leq 0$.

Thus, $\bar{S}$ is bounded above by K_1. Similarly we can show that $\bar{I}$ and $\bar{S}$ are bounded above.

A.2 Comparison of different functional forms in host-pathogen interaction models

Here we present the parameter values and corresponding numerical simulations of one bacterial model (4.9) – (4.10) and two bacterial stage models (4.11) – (4.13) for different functional forms for germination and killing processes. The case with combination of simple germination $G_1 = S_i P_i$ and intracellular burden dependent phagocyte killing $F_2 = B\frac{P_i}{P_i + C(S_i + B)}$ was presented in Section 4.3.2. Here we present the other possible combinations of F_j and G_j for $j = 1, 2$. Note that for each model, the parameters are estimated by fitting both spore and bacterial populations simultaneously. In the two bacterial stage model, several values of the parameter m are examined since this parameter was not estimated using experimental data.

A.2.1 One bacterial stage

Case 1: Simple germination and killing

(a) We consider model (4.9) – (4.10) with $G_1 = S_i P_i$ and $F_1 = BP_i$.

(b) The estimated parameters, the number of bacteria killed intracellularly and the relative error are presented in Table A.1. The simulation results for this case is presented in Figure A.1. From Table A.1, we see that all three parameters, the germination rates (g_i), killing rates (μ) and the replication rate (r) increase with decreased initial spore loads. Also from Figure A.1, we see that our model fits

Table A.1: Estimated model parameter values (columns 2,3,4) for model (4.9) – (4.10) with simple germination, $g_i G_1$, and simple killing, μF_1, fit to both bacterial and spore population simultaneously (Table 4.3 and Table 4.2). The total number of bacteria killed in [0.5,24] hours period is presented in the 5th column and the error of estimation is shown in column 6. Each row represent the quantities for different initial spore loads (MOI).

MOI	g_i	μ	r	# of B killed	SRE
$1:1$	3.6178×10^{-6}	2.5338×10^{-6}	0.3730	7.0984×10^{5}	0.7301
$1:2$	4.8937×10^{-6}	7.4362×10^{-6}	0.6479	4.2254×10^{5}	0.1632
$1:10$	1.5748×10^{-5}	7.3958×10^{-5}	0.8411	1.3106×10^{5}	0.1740
$1:20$	4.0516×10^{-5}	1.2832×10^{-4}	0.9816	3.1177×10^{4}	0.4707

both of the spore and the bacterial data will for first 5 hours and do not fit the 24 hour data points for all initial spore loads.

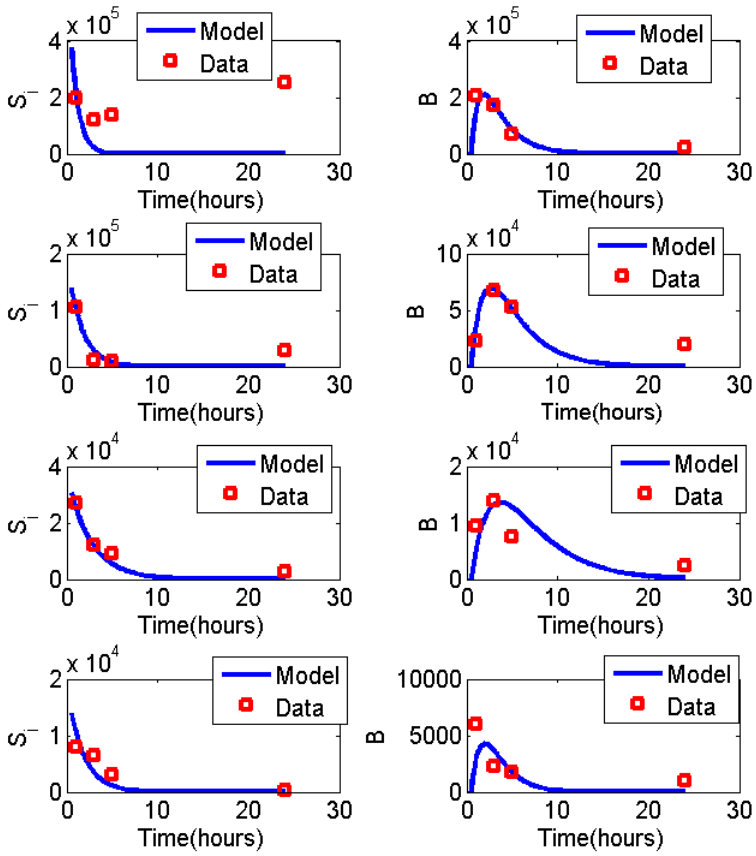

Figure A.1: Numerical results showing the model fit with estimated parameters from Table A.1 to the experimental data from Tables 4.2 and 4.3. The two graphs in each row represent the model fit to the experimental data (red squares) for spore and bacterial populations for MOIs 1:1 through 1:20. Here, model (4.9) – (4.10) is considered with simple germination, $g_i G_1$, and simple killing, μF_1.

Case 2: Intracellular burden dependent germination and simple killing

(a) We consider model (4.9) – (4.10) with $G_2 = S_i \frac{P_i}{P_i + C(S_i + B)}$ and $F_1 = BP_i$.

(b) The estimated parameters, the number of bacteria killed intracellularly and the relative error are presented in Table A.2. The simulation results for this case is presented in Figure A.2.

Table A.2: Estimated model parameter values (columns 3,4,5) for model (4.9) – (4.10) with intracellular burden dependent germination, $g_i G_2$, and simple killing, μF_1, fit to both bacterial and spore population simultaneously (Table 4.3 and Table 4.2). The total number of bacteria killed in [0.5,24] hours period is presented in the 5th column and the error of estimation is shown in column 6. Each row represent the quantities for different initial spore loads (MOI).

MOI	g_i	μ	r	# of B killed	SRE
$1:1$	1.0226	4.7811×10^{-6}	1.0810	7.0984×10^{5}	0.7760
$1:2$	0.7617	1.1825×10^{-5}	1.2128	4.2254×10^{5}	0.1613
$1:10$	0.5565	5.2573×10^{-5}	0.8747	1.3106×10^{5}	0.1332
$1:20$	1.0122	7.9144×10^{-5}	0.1706	3.1177×10^{4}	0.4704

From Table A.2, we see that the killing rates, μ, increases with decreased initial spore loads while the other two parameters, the germination rates, g_i, and the replication rate, r, do not show any specific trend for decreased initial spore loads. Also from Figure A.2, we see that our model fits both of the spore and the bacterial data will for first 5 hours and do not fit the 24 hour data points for all initial spore loads.

Case 3: Both germination and killing depend on intracellular burden

(a) We consider model (4.9) – (4.10) with $G_2 = S_i \frac{P_i}{P_i + C(S_i + B)}$ and $F_2 = B \frac{P_i}{P_i + C(S_i + B)}$.

(b) The estimated parameters, the number of bacteria killed intracellularly and the relative error are presented in Table A.3. The simulation results for this case is presented in Figure A.3

From Table A.3, we see that non of the three parameters, killing rates, μ, the germination rates, g_i, and the replication rate, r, show any specific trend for decreased initial spore loads. Also from Figure A.3, we see that our model fits

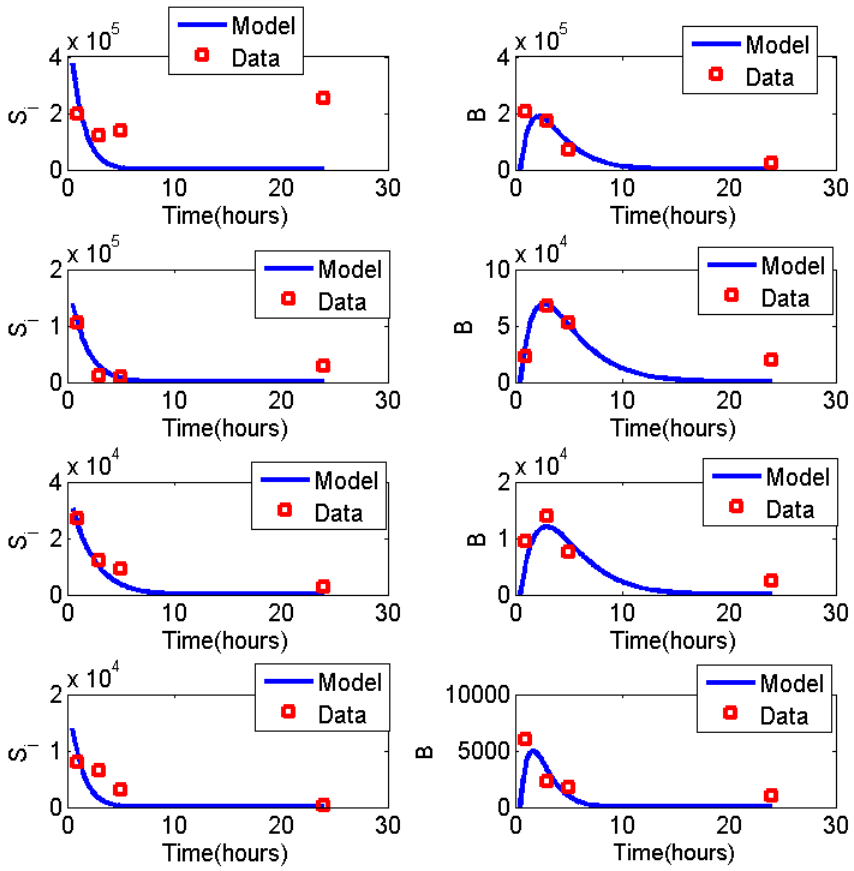

Figure A.2: Numerical results showing the model fit with estimated parameters from Table A.2 to the experimental data from Tables 4.2 and 4.3. The two graphs in each row represent the model fit to the experimental data (red squares) for spore and bacterial populations for MOIs 1:1 through 1:20. Here, model (4.9) – (4.10) is considered with intracellular dependent germination, $g_i G_2$, and simple killing, μF_1.

Table A.3: Estimated model parameter values (columns 2,3,4) for model (4.9) – (4.10) with intracellular burden dependent germination, $g_i G_2$ and killing, μF_2, fit to both bacterial and spore population simultaneously (Table 4.3 and Table 4.2). The total number of bacteria killed in [0.5,24] hours period is presented in the 5th column and the error of estimation is shown in column 6. Each row represent the quantities for different initial spore loads (MOI).

MOI	g_i	μ	r	# of B killed	SRE
1 : 1	1.0607	1.9492	1.266	1.4270×10^6	0.7282
1 : 2	0.7576	0.3717	0.0010	1.3937×10^5	0.1814
1 : 10	0.5253	4.0312	2.9	2.1483×10^5	0.1172
1 : 20	1.0231	5.9	4.37	7.9874×10^4	0.4466

both of the spore and the bacterial data will for first 5 hours and do not fit the 24 hour data points for all initial spore loads.

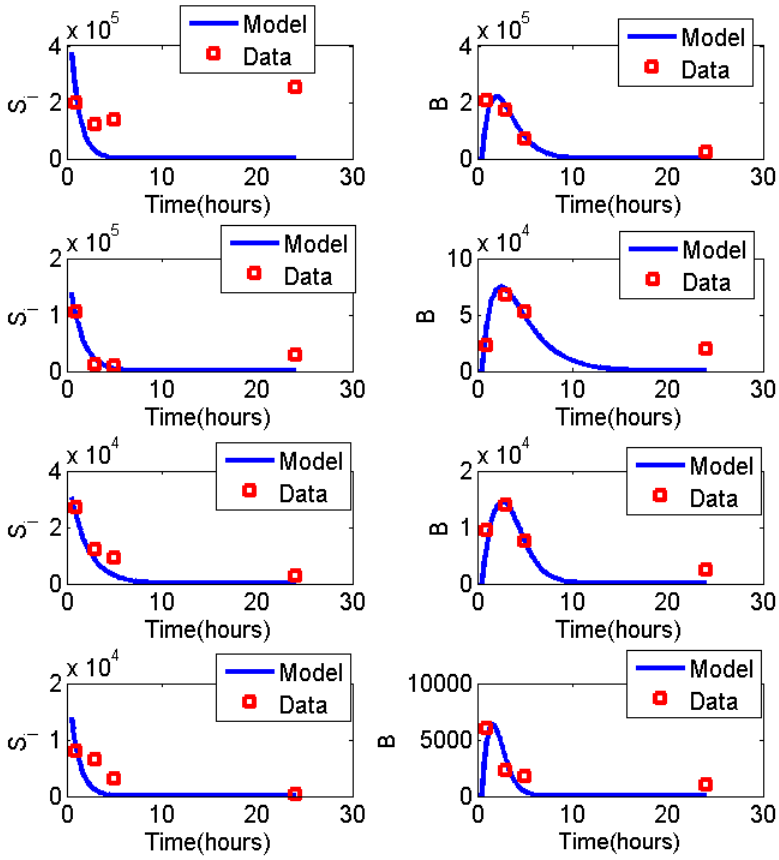

Figure A.3: Numerical results showing the model fit with estimated parameters from Table A.3 to the experimental data from Tables 4.2 and 4.3. The two graphs in each row represent the model fit to the experimental data (red squares) for spore and bacterial populations for MOIs 1:1 through 1:20. Here, model (4.9) – (4.10) is considered with intracellular burden dependent germination, $g_i G_2$, and killing, μF_2.

A.2.2 Two bacterial stages for $m = 0.1$

Case 1: Simple germination and killing

(a) We consider model (4.11) – (4.13) with $G_1 = S_i P_i$, $F_1 = B_{ig} P_i$ in equation (4.12) and $F_1 = B_i P_i$ in equation (4.13).

(b) The estimated parameters, the number of bacteria killed intracellularly and the relative error are presented in Table A.4. The simulation results for this case is presented in Figure A.4 From Table A.4, we see that all three parameters, the germination rates, g_i, killing rates, μ, and the replication rate, r, increase with

Table A.4: Estimated model parameter values (columns 2,3,4) for the model (4.11) – (4.13) with simple germination, g_iG_1, and simple killing, μF_1, assuming $m = 0.1$ where $F_1 = B_{ig}P_i$ in (4.12) and $F_1 = B_iP_i$ in (4.13) fit to both bacterial and spore population simultaneously (Table 4.3 and Table 4.2) . The total number of bacteria killed in [0.5,24] hours period is presented in the 5th column and the error of estimation is shown in column 6. Each row represent the quantities for different initial spore loads (MOI).

MOI	g_i	μ	r	# of B killed	SRE
$1:1$	3.6334×10^{-6}	1.3499×10^{-6}	0.0100	3.7928×10^{5}	0.7298
$1:2$	4.9765×10^{-6}	2.9703×10^{-6}	0.3680	2.9537×10^{5}	0.1126
$1:10$	1.8846×10^{-5}	1.8830×10^{-5}	0.4101	5.7117×10^{4}	0.1209
$1:20$	7.4631×10^{-5}	8.1685×10^{-5}	1.1238	3.8904×10^{4}	0.4213

decreased initial spore loads. Also from Figure A.4, we see that our model fits both of the spore and the bacterial data better compared to the single bacterial stage model for all initial spore loads.

Case 2: Intracellular burden dependent germination and simple killing

(a) We consider model (4.11) – (4.13) with $G_2 = S_i\frac{P_i}{P_i+C(S_i+B_{ig}+B_i)}$, $F_1 = B_{ig}P_i$ in equation (4.12) and $F_1 = B_iP_i$ in equation (4.13).

(b) The estimated parameters, the number of bacteria killed intracellularly and the relative error are presented in Table A.5. The simulation results for this case is presented in Figure A.5 From Table A.5, we see that the killing rates, μ, increase

Table A.5: Estimated model parameter values (columns 2,3,4) for model (4.11) – (4.13) with intracellular burden dependent germination, g_iG_2, and simple killing, μF_1, assuming $m = 0.1$, where where $F_1 = B_{ig}P_i$ in equation (4.12) and $F_1 = B_iP_i$, fit to both bacterial and spore population simultaneously (Table 4.3 and Table 4.2). The total number of bacteria killed in [0.5,24] hours period is presented in the 5th column and the error of estimation is shown in column 6. Each row represent the quantities for different initial spore loads (MOI).

MOI	g_i	μ	r	# of B killed	SRE
$1:1$	1.3296	1.3993×10^{-6}	0.0100	3.7930×10^{5}	0.7418
$1:2$	0.7773	2.9563×10^{-5}	0.3756	3.1303×10^{5}	0.1126
$1:10$	0.5567	1.9193×10^{-5}	0.4198	5.7684×10^{4}	0.1279
$1:20$	1.3780	6.1337×10^{-5}	0.1194	1.4166×10^{4}	0.4775

with decreased initial spore load and the germination rate, g_i, and the replication rate, r, do not show any dependence on the initial spore loads. Also from Figure A.5, we see that our model fits both of the spore and the bacterial data better compared to the single bacterial stage model for all initial spore loads.

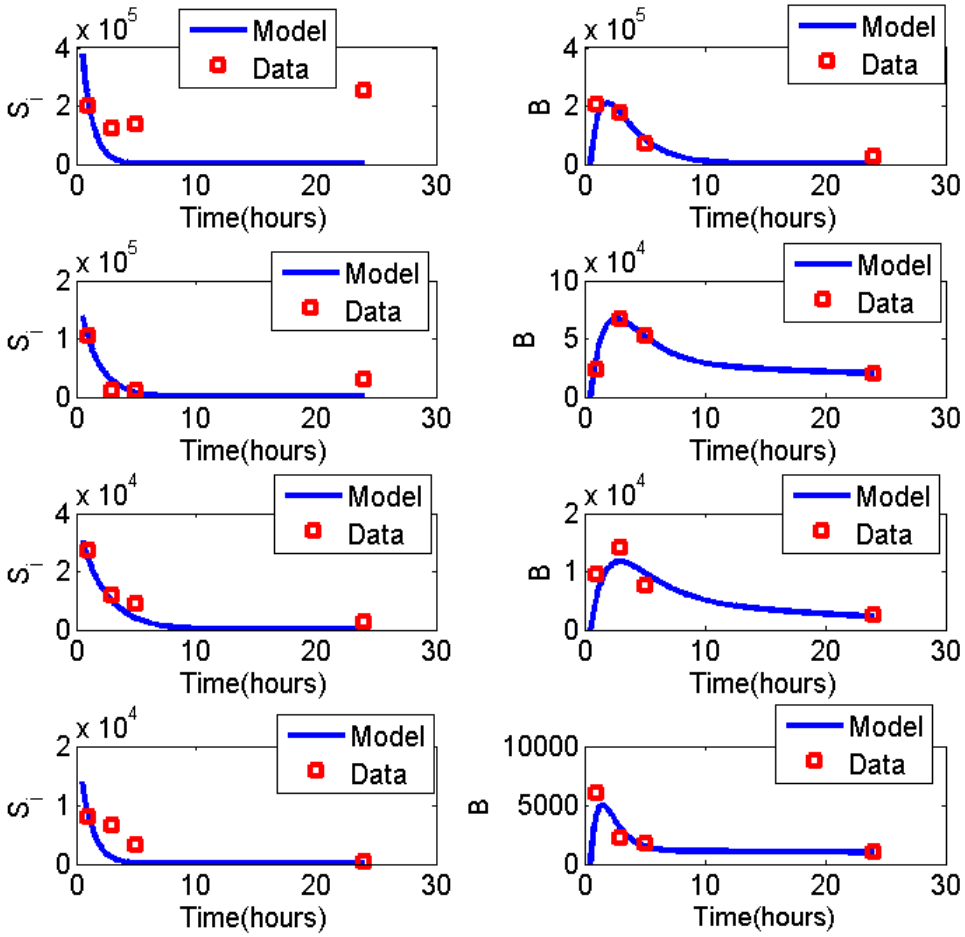

Figure A.4: Numerical results showing the model fit with estimated parameters from Table A.4 to the experimental bacterial data from Table 4.3 and spore data from the Table 4.2 assuming the maturation rate $m = 0.1$. The two graphs in each row represent the model fit to the experimental data (red squares) for spore and bacterial populations for MOIs 1:1 through 1:20. Here model (4.11) – (4.13) is considered with simple germination, $g_i G_1$, and simple killing, μF_1, where $F_1 = B_{ig} P_i$ in equation (4.12) and $F_1 = B_i P_i$ in equation (4.13).

Case 3: Both germination and killing depend on intracellular burden

(a) We consider model (4.11)−(4.13) with $G_2 = S_i \frac{P_i}{P_i + C(S_i + B_{ig} + B_i)}$, $F_2 = B_{ig} \frac{P_i}{P_i + C(S_i + B_{ig} + B_i)}$ in equation (4.12) and $F_2 = B_i \frac{P_i}{P_i + C(S_i + B_{ig} + B_i)}$ in equation (4.13).

(b) The estimated parameters, the number of bacteria killed intracellularly and the relative error are presented in Table A.6. The simulation results for this case is presented in Figure A.6

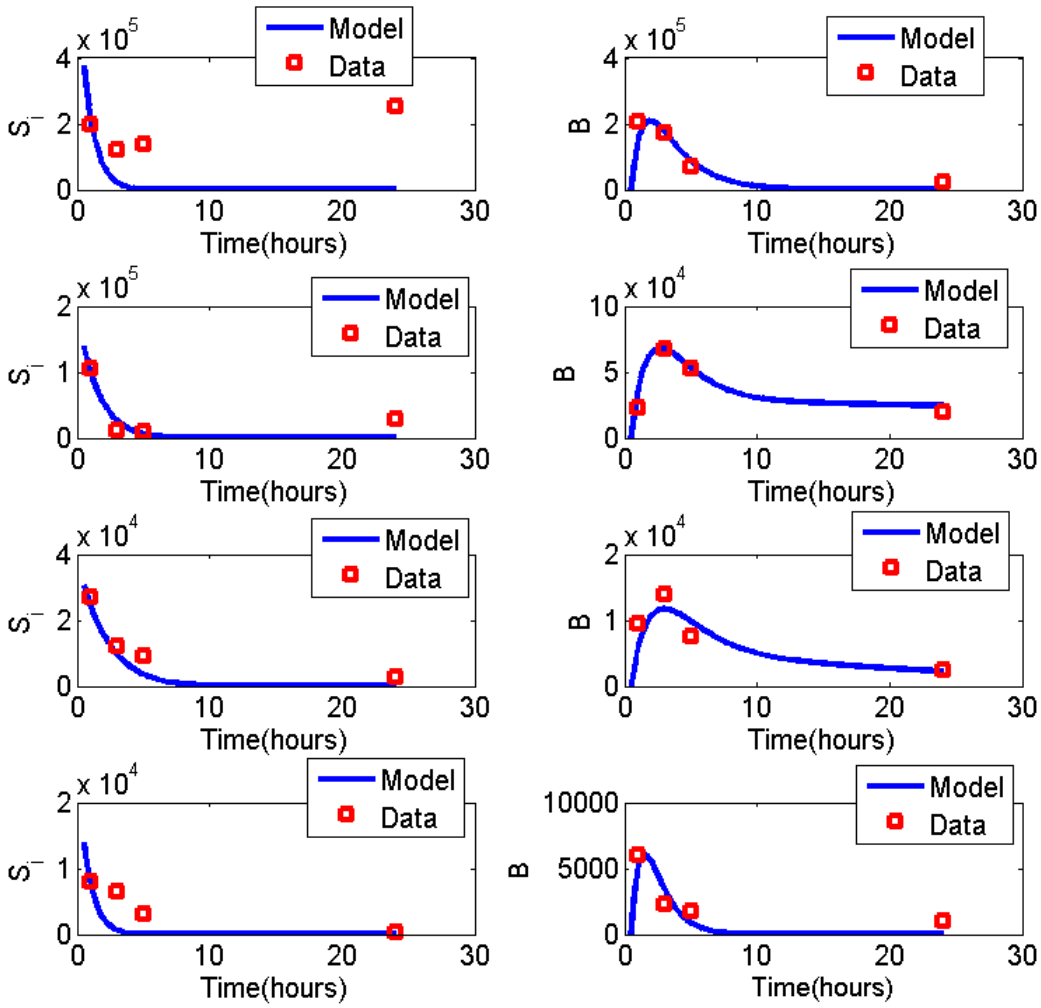

Figure A.5: Numerical results showing the model fit with estimated parameters from Table A.5 to the experimental bacterial data from Table 4.3 and spore data from the Table 4.2 assuming the maturation rate $m = 0.1$. The two graphs in each row represent the model fit to the experimental data (red squares) for spore and bacterial populations for MOIs 1:1 through 1:20. Here model (4.11) – (4.13) is considered with intracellular dependent germination, $g_i G_2$, and simple killing, μF_1, where $F_1 = B_{ig} P_i$ in equation (4.12) and $F_1 = B_i P_i$ in equation (4.13).

From Table A.6, we see that the killing rate, μ, and the replication rate, r, increase with decreased initial spore load and the germination rate, g_i, do not show any dependence on the initial spore loads. Also from Figure A.6, we see that our model fits both of the spore and the bacterial data better compared to the single bacterial stage model for all initial spore loads.

Table A.6: Estimated model parameter values (columns 2,3,4) for the model (4.11) – (4.13) with intracellular burden dependent germination, g_iG_2, and killing, μF_2,, where $F_2 = B_{ig}\frac{P_i}{P_i+C(S_i+B_{ig}+B_i)}$ in equation (4.12) and $F_2 = B_i\frac{P_i}{P_i+C(S_i+B_{ig}+B_i)}$ in equation (4.13) assuming $m = 0.1$, fit to both bacterial and spore population simultaneously (Table 4.3 and Table 4.2). The total number of bacteria killed in [0.5,24] hours period is presented in the 5th column and the error of estimation is shown in column 6. Each row represent the quantities for different initial spore loads (MOI).

MOI	g_i	μ	r	# of B killed	SRE
$1:1$	1.1111	0.4864	00100	3.7918×10^5	0.7616
$1:2$	0.7741	0.4673	0.4309	3.3203×10^5	0.1100
$1:10$	0.5572	0.5721	0.5062	6.6429×10^4	0.1268
$1:20$	1.0651	1.3006	1.2698	4.4806×10^4	0.4423

A.2.3 Two bacterial stages for $m = 0.2$

Case 1: Simple germination and killing

(a) We consider model (4.11) – (4.13) with $G_1 = S_iP_i$, $F_1 = B_{ig}P_i$ in equation (4.12) and $F_1 = B_iP_i$ in equation (4.13).

(b) The estimated parameters, the number of bacteria killed intracellularly and the relative error are presented in Table A.7. The simulation results for this case is presented in Figure A.7

Table A.7: Estimated model parameter values (columns 2,3,4) for the model (4.11) – (4.13) with simple germination, g_iG_1, and simple killing, μF_1, assuming $m = 0.1$, where $F_1 = B_{ig}P_i$ in (4.12) and $F_1 = B_iP_i$ in (4.13), fit to both bacterial and spore population simultaneously (Table 4.3 and Table 4.2). The total number of bacteria killed in [0.5,24] hours period is presented in the 5th column and the error of estimation is shown in column 6. Each row represent the quantities for different initial spore loads (MOI).

MOI	g_i	μ	r	# of B killed	SRE
$1:1$	1.6298×10^{-6}	1.1435×10^{-6}	0.1062	4.3228×10^5	0.8737
$1:2$	5.0683×10^{-6}	3.4216×10^{-6}	0.4062	3.6770×10^5	0.1120
$1:10$	1.8737×10^{-5}	1.6199×10^{-5}	0.00054	3.0497×10^5	0.1276
$1:20$	8.0364×10^{-5}	9.5111×10^{-5}	1.2831	5.0136×10^4	0.4329

From Table A.7, we see that the killing rates, μ, and the germination rate, g_i, increase with decreased initial spore load but the replication rate, r, does not show any dependence on the initial spore loads. Also from Figure A.7, we see that our model fits both of the spore and the bacterial data better compared to the single bacterial stage model for all initial spore loads.

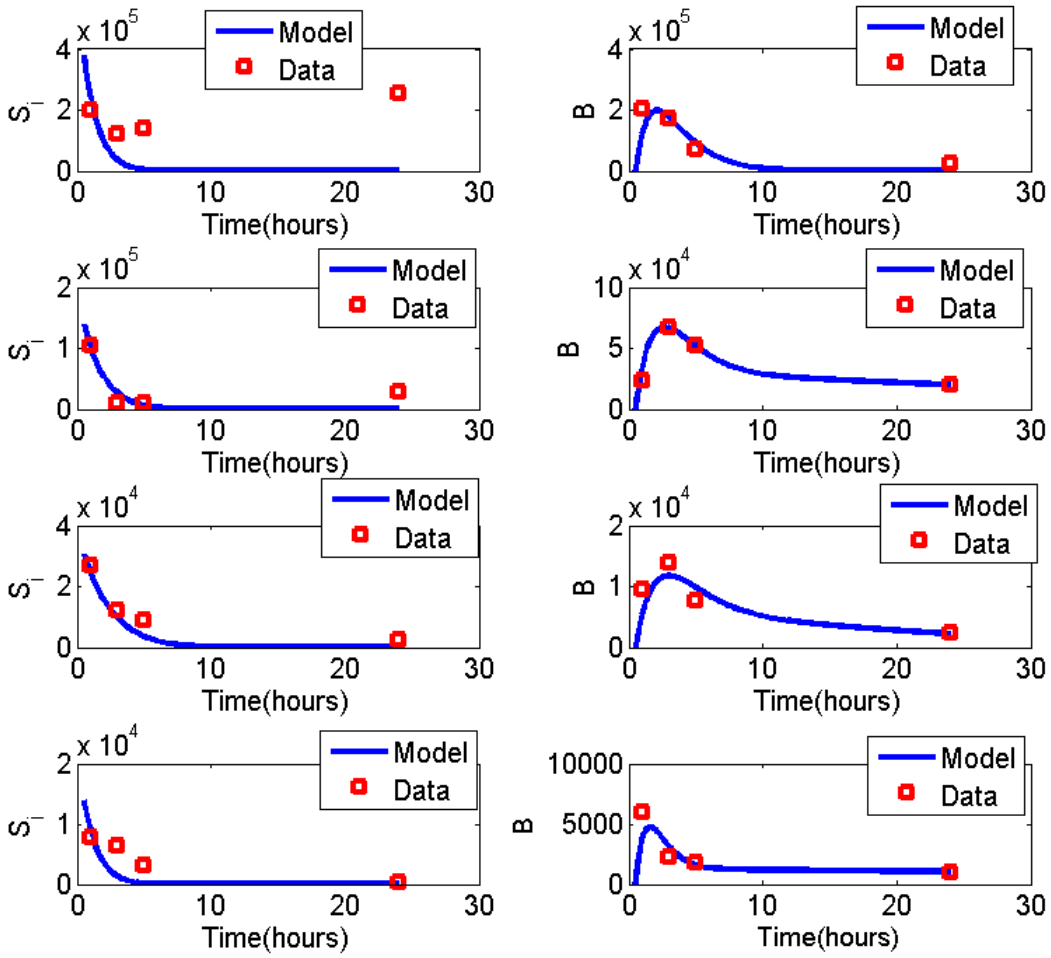

Figure A.6: Numerical results showing the model fit with estimated parameters from Table A.6 to the experimental bacterial data from Table 4.3 and spore data from the Table 4.2 assuming the maturation rate $m = 0.1$. The two graphs in each row represent the model fit to the experimental data (red squares) for spore and bacterial populations for MOIs 1:1 through 1:20. Here model (4.11) – (4.13) is considered with intracellular dependent germination, $g_i G_2$, and killing, μF_2, where $F_2 = B_{ig}\frac{P_i}{P_i+C(S_i+B_{ig}+B_i)}$ in equation (4.12) and $F_2 = B_i\frac{P_i}{P_i+C(S_i+B_{ig}+B_i)}$ in equation (4.13)

Case 2: Intracellular burden dependent germination and simple killing

(a) We consider model (4.11) – (4.13) with $G_2 = S_i\frac{P_i}{P_i+C(S_i+B_{ig}+B_i)}$, $F_1 = B_{ig}P_i$ in equation (4.12) and $F_1 = B_iP_i$ in equation (4.13).

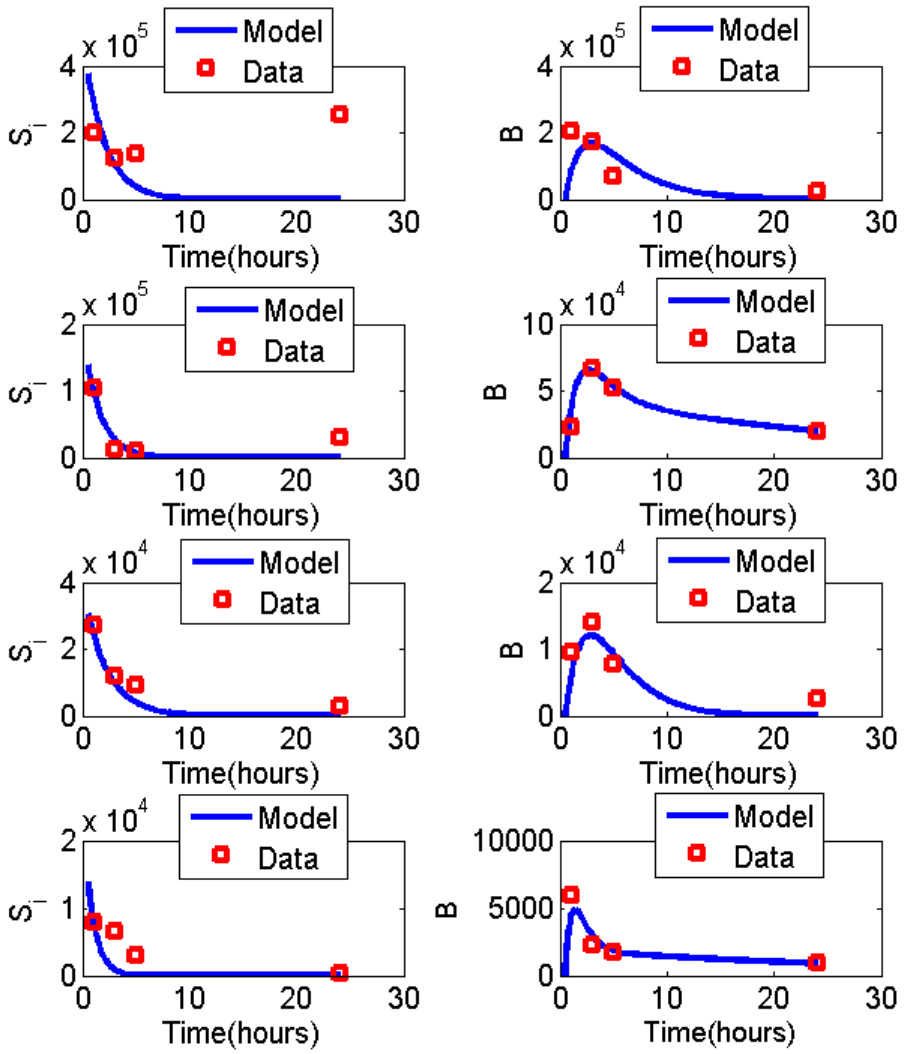

Figure A.7: Numerical results showing the model fit with estimated parameters from Table A.7 to the experimental bacterial data from Table 4.3 and spore data from the Table 4.2 assuming the maturation rate $m = 0.2$. The two graphs in each row represent the model fit to the experimental data (red squares) for Spore and bacterial populations for MOIs 1:1 through 1:20. Here model (4.11) – (4.13) is considered with simple germination, $g_i G_1$, and simple killing, μF_1, where $F_1 = B_{ig} P_i$ in equation (4.12) and $F_1 = B_i P_i$ in equation (4.13).

(b) The estimated parameters, the number of bacteria killed intracellularly and the relative error are presented in Table A.8. The simulation results for this case is presented in Figure A.8

Table A.8: Estimated model parameter values (columns 2,3,4) for the model (4.11) – (4.13) with intracellular burden dependent germination, $g_i G_2$, and simple killing, μF_1, where $F_1 = B_{ig} P_i$ in equation (4.12) and $F_1 = B_i P_i$ in equation (4.13) assuming $m = 0.2$, fit to both bacterial and spore population simultaneously (Table 4.3 and Table 4.2). The total number of bacteria killed in [0.5,24] hours period is presented in the 5th column and the error of estimation is shown in column 6. Each row represent the quantities for different initial spore loads (MOI).

MOI	g_i	μ	r	# of B killed	SRE
$1:1$	1.4345	1.3406×10^{-6}	0.0006	3.7771×10^{5}	0.7343
$1:2$	0.7888	3.5220×10^{-5}	0.4209	3.7593×10^{5}	0.1085
$1:10$	0.5533	1.6547×10^{-5}	0.0005	3.0501×10^{5}	0.1346
$1:20$	1.1723	9.5407×10^{-5}	1.2884	5.0506×10^{4}	0.4566

From Table A.8, we see that only the killing rates (μ) increases with decreased initial spore loads but the replication rate (r) and the germination rate (g_i) do not show any dependence on the initial spore loads. Also from Figure A.8, we see that our model fits both of the spore and the bacterial data better compared to the single bacterial stage model for all initial spore loads.

Case 3: Both germination and killing depend on intracellular burden

(a) We consider model (4.11)−(4.13) with $G_2 = S_i \frac{P_i}{P_i + C(S_i + B_{ig} + B_i)}$, $F_2 = B_{ig} \frac{P_i}{P_i + C(S_i + B_{ig} + B_i)}$ in equation (4.12) and $F_2 = B_i \frac{P_i}{P_i + C(S_i + B_{ig} + B_i)}$ in equation (4.13).

(b) The estimated parameters, the number of bacteria killed intracellularly and the relative error are presented in Table A.9. The simulation results for this case is presented in Figure A.9

From Table A.9, we see that the killing rates, μ, and the replication rate, r, increase with decreased initial spore load but the germination rate, g_i, does not show any dependence on the initial spore loads. Also from Figure A.9, we see that our model fits both of the spore and the bacterial data better compared to the single bacterial stage model for all initial spore loads.

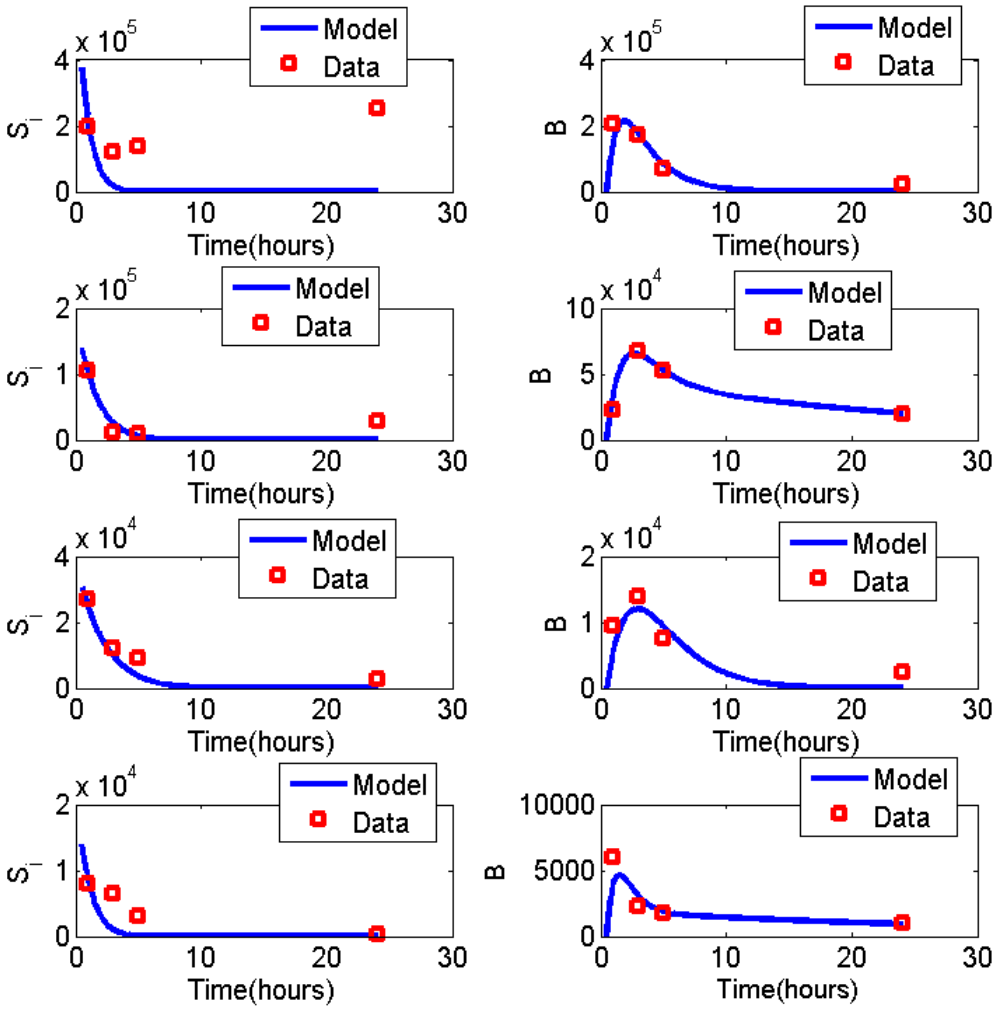

Figure A.8: Numerical results showing the model fit with estimated parameters from Table A.8 to the experimental bacterial data from Table 4.3 and spore data from the Table 4.2 assuming the maturation rate $m = 0.2$. The two graphs in each row represent the model fit to the experimental data (red squares) for Spore and bacterial populations for MOIs 1:1 through 1:20. Here model $(4.11) - (4.13)$ is considered with intracellular burden dependent germination, $g_i G_2$, and simple killing, μF_1, where $F_1 = B_{ig} P_i$ in equation (4.12) and $F_1 = B_i P_i$ in equation (4.13).

Table A.9: Estimated model parameter values (columns 2,3,4) for the model (4.11) – (4.13) with intracellular burden dependent germination, $g_i G_2$, and killing, $\mu B F_2$, where $F_2 = B_{ig}\frac{P_i}{P_i+C(S_i+B_{ig}+B_i)}$ in equation (4.12) and $F_2 = B_g\frac{P_i}{P_i+C(S_i+B_{ig}+B_i)}$ in equation (4.13), fit to both bacterial and spore population simultaneously (Table 4.3 and Table 4.2). The total number of bacteria killed in [0.5,24] hours period is presented in the 5th column and the error of estimation is shown in column 6. Each row represent the quantities for different initial spore loads (MOI).

MOI	g_i	μ	r	# of B killed	SRE
1 : 1	1.4125	0.4852	0.0010	3.7782×10^6	0.7332
1 : 2	0.7845	0.5574	0.4943	4.3471×10^5	0.1085
1 : 10	0.5536	0.6581	0.5570	8.2322×10^5	0.1383
1 : 20	1.1775	1.4700	0.4037	1.4674×10^4	0.5031

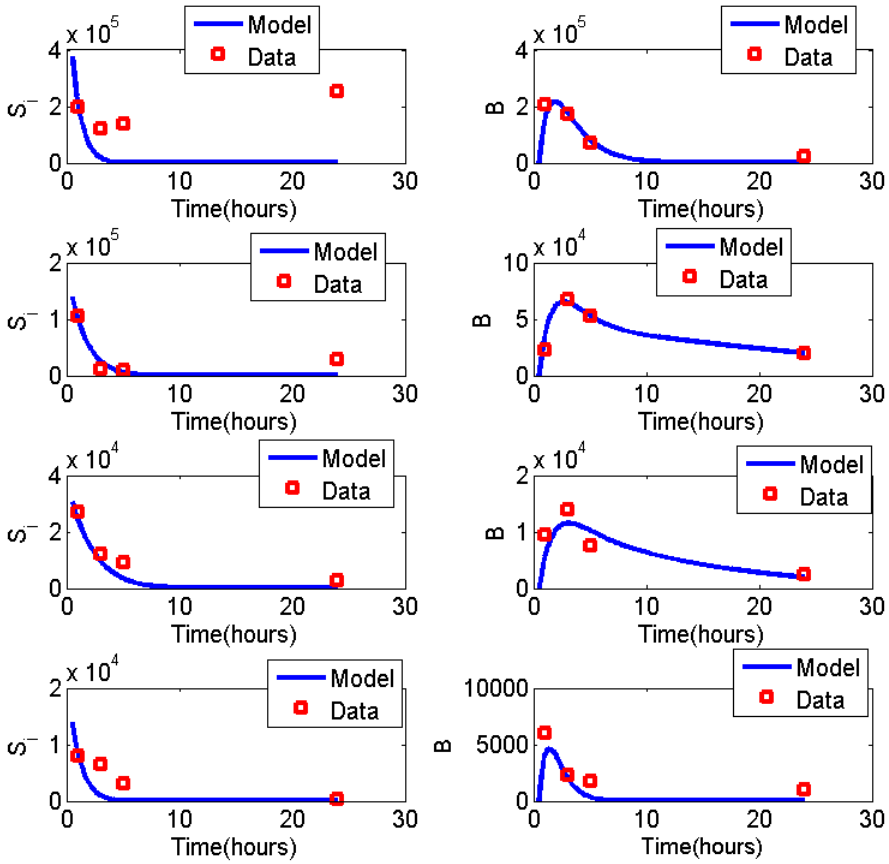

Figure A.9: Numerical results showing the model fit with estimated parameters from Table A.9 to the experimental bacterial data from Table 4.3 and spore data from the Table 4.2 assuming the maturation rate $m = 0.2$. The two graphs in each row represent the model fit to the experimental data (red squares) for Spore and bacterial populations for MOIs 1:1 through 1:20. Here model (4.11) – (4.13) is considered with intracellular burden dependent germination, $g_i G_2$, and simple killing, μF_1, where $F_2 = B_{ig}\frac{P_i}{P_i+C(S_i+B_{ig}+B_i)}$ in equation (4.12) and $F_2 = B_g\frac{P_i}{P_i+C(S_i+B_{ig}+B_i)}$ in equation (4.13).

A.3 Numerical Approximation Scheme for Spatio-temporal Anthrax Outbreak Model:

We present the numerical techniques applied in Section 3.5. We consider one spatial dimension $\Omega = [0, 1]$ in the time interval $[0, 1]$. Then our system (3.1)-(3.4) has the form

$$\begin{aligned}
\frac{\partial s}{\partial t} &= d\frac{\partial^2 s}{\partial x^2} + rn(1 - \frac{n}{K}) - \theta_c sc - \theta_i si - u_1 s \\
\frac{\partial i}{\partial t} &= d_1\frac{\partial^2 i}{\partial x^2} + \theta_c sc + \theta_i si - \gamma i \\
\frac{\partial v}{\partial t} &= d\frac{\partial^2 v}{\partial x^2} + u_1 s \\
\frac{dc}{dt} &= \gamma i - \alpha(s + i + v)c - (p + u_2)c \\
&\text{where } n = s + v
\end{aligned}$$

with Initial and boundary conditions,

$$\begin{aligned}
&s(x, 0) = s^0(x), i(x, 0) = i^0(x), v(x, 0) = v^0(x), c(x, 0) = c^0(x), x \in \Omega, \\
&s(x, t) = i(x, t) = v(x, t) = 0; \qquad (x, t) \in \partial\Omega \times [0, T],
\end{aligned}$$

Also the Adjoint system (3.43) is

$$\begin{aligned}
-(\lambda_1)_t - d(\triangle\lambda_1) + m_{11}\lambda_1 + m_{21}\lambda_2 + m_{31}\lambda_3 + m_{41}\lambda_4 &= B_1 u_1 \\
-(\lambda_2)_t - d_1(\triangle\lambda_2) + m_{12}\lambda_1 + m_{22}\lambda_2 + m_{32}\lambda_3 + m_{42}\lambda_4 &= B_1 u_1 + A_1 \\
-(\lambda_3)_t - d(\triangle\lambda_3) + m_{13}\lambda_1 + m_{23}\lambda_2 + m_{33}\lambda_3 + m_{43}\lambda_4 &= 0 \\
-(\lambda_4)_t + m_{14}\lambda_1 + m_{24}\lambda_2 + m_{34}\lambda_3 + m_{44}\lambda_4 &= A_2 + B_2 u_2
\end{aligned}$$

with $\lambda_i(x, T) = 0$ *for* $i = 1, 2, 3, 4$ for $x \in \Omega$ (final time conditions) and $\lambda_i(x, t) = 0$ for $i = 1, 2, 3$ on $\partial\Omega \times (0, T)$, where matrix M^τ is the transpose of matrix

$M = m_{ij}$ for $i, j = 1, 2, 3, 4$ given by

$$\begin{aligned}
m_{11} =& - r + \frac{2r}{K}(s + v) + \theta_c c + \theta_i i + u_1, m_{12} = \theta_i s, m_{13} = -r + \frac{2r}{K}(s + v), \\
& m_{14} = \theta_c s. \\
m_{21} =& - \theta_c c - \theta_i i, m_{22} = -\theta_i s + \gamma, m_{23} = 0, m_{24} = -\theta_c s. \\
m_{31} =& - u_1, m_{32} = 0, m_{33} = 0, m_{34} = 0 \\
m_{41} =& \alpha c, m_{42} = -\gamma + \alpha c, m_{43} = \alpha c, m_{44} = \alpha(s + i + v) + (u_2 + p)
\end{aligned}$$

A.3.1 Numerical Method

To solve the optimality system numerically, we used backward-forward sweep iterative method. We used finite difference scheme to approximate the derivative terms in our system. For the time derivative of state variables, forward difference method is applied and for the spatial second order derivatives, we used the central difference. Also for the adjoint system, we used backward difference for the time derivative because we have the finite time condition for adjoint variables and central difference scheme is used for the spatial second derivative. For example:

$$\frac{\partial s(x,t)}{\partial t} \approx \frac{s(x, t + \delta t) - s(x,t)}{\delta t}$$

and

$$\frac{\partial^2 s(x,t)}{\partial x^2} \approx \frac{s(x + \delta x, t) - 2s(x,t) + s(x - \delta x, t)}{(\delta x)^2}.$$

Similarly,

$$\frac{\partial \lambda(x,t)}{\partial t} \approx \frac{\lambda(x, t - \delta t) - \lambda(x,t)}{\delta t}$$

and

$$\frac{\partial^2 \lambda(x,t)}{\partial x^2} \approx \frac{\lambda(x + \delta x, t) - 2\lambda(x,t) + \lambda(x - \delta x, t)}{(\delta x)^2}$$

where δx is the increment in space variable and δt is the increment in time. Then the discretized form of the state system is

$$\begin{aligned} S_i^{j+1} &= S_i^j + \frac{d(\delta t)}{(\delta x)^2}\big[S_{i-1}^j + S_{i+1}^j - 2S_i^j\big] \\ &\quad + r(\delta t)(S_i^j + V_i^j) - \frac{r}{K}(\delta t)[(S_i^j + V_i^j)^2] \\ &\quad - (\delta t)\theta_i S_i^j I_i^j - (\delta t)\theta_c S_i^j C_i^j - (\delta t)(u_1)_i^j S_i^j; \end{aligned} \tag{A.2}$$

$$\begin{aligned} I_i^{j+1} &= I_i^j + \frac{d_1(\delta t)}{(\delta x)^2}\big[I_{i-1}^j + I_{i+1}^j - 2I_i^j\big] \\ &\quad + (\delta t)\theta_i S_i^j I_i^j + (\delta t)\theta_c S_i^j C_i^j - (\delta t)\gamma I_i^j; \end{aligned} \tag{A.3}$$

$$V_i^{j+1} = V_i^j + \frac{d(\delta t)}{(\delta x)^2}\big[V_{i-1}^j + V_{i+1}^j - 2V_i^j\big] + (\delta t)(u_1)_i^j S_i^j; \tag{A.4}$$

$$\begin{aligned} C_i^{j+1} &= C_i^j + (\delta t)\gamma I_i^j - (\delta t)\alpha\big[S_i^j + I_i^j + V_i^j\big]C_i^j \\ &\quad - (\delta t)[p + (u_2)_i^j]C_i^j \end{aligned} \tag{A.5}$$

where S_i^j denote the value of variable S at space $x = i$ and time $t = j$. For the adjoint system we have,

$$\begin{aligned} (\lambda_1)_i^{j-1} &= (\lambda_1)_i^j + \frac{d(\delta t)}{(\delta x)^2}\big[(\lambda_1)_{i+1}^j - 2(\lambda_1)_i^j + (\lambda_1)_{i-1}^j\big] \\ &\quad - (\delta t)\big[-r + \frac{2r}{K}(S_i^j + V_i^j) + \theta_c C_i^j + \theta_i I_i^j + (u_1)_i^{j-1}\big](\lambda_1)_i^j \\ &\quad - (\delta t)\big[-\theta_c C_i^j - \theta_i I_i^j\big](\lambda_2)_i^j - (\delta t)[-(u_1)_i^{j-1}](\lambda_3)_i^j \\ &\quad - (\delta t)\big[\alpha C_i^j\big](\lambda_4)_i^j + (\delta t)B_1(u_1)_i^{j-1}; \end{aligned} \tag{A.6}$$

$$\begin{aligned} (\lambda_2)_i^{j-1} &= (\lambda_2)_i^j + \frac{d_1(\delta t)}{(\delta x)^2}\big[(\lambda_2)_{i+1}^j - 2(\lambda_2)_i^j + (\lambda_2)_{i-1}^j\big] \\ &\quad - (\delta t)\big[\theta_i S_i^j\big](\lambda_1)_i^j - (\delta t)\big[-\theta_i S_i^j + \gamma\big](\lambda_2)_i^j \\ &\quad - (\delta t)\big[-\gamma + \alpha C_i^j\big](\lambda_4)_i^j + (\delta t)[A_1 + B_1(u_1)_i^{j-1}]; \end{aligned} \tag{A.7}$$

$$\begin{aligned} (\lambda_3)_i^{j-1} &= (\lambda_3)_i^j + \frac{d(\delta t)}{(\delta x)^2}[(\lambda_3)_{i+1}^j - 2(\lambda_3)_i^j + (\lambda_3)_{i-1}^j] \\ &\quad - (\delta t)\big[-r + \frac{2r}{K}\big(S_i^j + V_i^j\big)\big)\big](\lambda_1)_i^j - (\delta t)\big[\alpha C_i^j\big](\lambda_4)_i^j; \end{aligned} \tag{A.8}$$

$$(\lambda_4)_i^{j-1} = (\lambda_4)_i^j - (\delta t)\big[\theta_c S_i^j\big](\lambda_1)_i^j - (\delta t)\big[-\theta_c S_i^j\big](\lambda_2)_i^j$$
$$- (\delta t)\big[\alpha(S_i^j + I_i^j + V_i^j) + (u_2)_i^j + p\big](\lambda_4)_i^j + (\delta t)(A_2 + B_2(u_2)_i^{j-1}). \qquad \text{(A.9)}$$

Starting with the initial guesses for controls and given initial values for state variables, the state system $(A.2) - (A.5)$ are solved forward in time. Then the state values and controls are used to solve the adjoint system $(A.6) - (A.9)$ backward in time. Next, we update the controls using the values of state and adjoint functions. Then we check for convergence and continue the iteration until convergence criterion is meet. In the simulation we choose $\delta t = 0.01$, and $\delta x = 0.1$.

Vita

Buddhi Raj Pantha was born in Ghansikuwa Village Development Committee -03, Tanahun District, Gandaki Zone Nepal, on April 10, 1978. He is the younger son of Krishna Prasad Pantha and Maiya Devi Pantha. He started his studies at Shree Siddheshowri Secondary School, Kamalbari and went to Shree Nirmal Secondary School, Damauli of Tanahun District where he graduated with grade 10. He graduated from Prithwi Narayan Campus, Pokhara with his high school diploma in 1996. He received his Bachelor of Mathematics in Education in 2000 and Masters of Science in Mathematics in 2003 from Tribhuvan University. In July 2003, Buddhi joined Pinnacle College as a mathematics faculty where he taught for 5 years.

In August 2008, Buddhi came to the United States to pursue his further studies in Mathematics. He graduated from Western Illinois University with Masters of Science in Mathematics in May 2010. In the Fall of 2010, Buddhi joined the University fo Tennessee as a graduate student where he was supported by Graduate Teaching Associate from fall 2010 to Summer 2015. He was awarded a Graduate Research Fellowship from the National Institute of Mathematical and Biological Synthesis, which supported his graduate studies from August 2015-July 2016. Buddhi graduated in August 2016 with his P.hD. in Mathematics with a concentration in Mathematical Ecology.

Buddhi Pantha will continue his work in mathematical biology and teaching mathematics as an Assistant Professor of Mathematics in the Department of Mathematics at Abraham Baldwin Agricultural College, Georgia.